ABSTRACT

LIU, YUEYING. Analytical Physics Based AlGaN/GaN HFET Large Signal Model and Nonlinearity Analysis with Nonlinear Source Resistance. (Under the direction of Dr. Robert J. Trew and Dr. Griff L. Bilbro).

In this work the impact of nonlinear source resistance and RF channel breakdown on AlGaN/GaN HFETs RF and linearity performance were studied. AlGaN/GaN HFETs are well known strong candidates for high power devices due to superior material properties of the nitrides, such as high electric field to achieve electron saturation velocity and high mobility. Practical amplifiers, however, do not demonstrate the good RF linearity performance predicted from fundamental semiconductor materials properties. In particular, it has been demonstrated that a nonlinear source resistance is generated in these devices due to the onset of space-charge limited (SCL) transport in the gate-source region. It has been demonstrated that the nonlinear source resistance modulation degrades the linearity of the device, even under modest RF drive conditions.

RF Breakdown has been found to be a major factor that limits a FET's performance under large signal operating conditions. For AlGaN/GaN HFETs, breakdown could happen both in the channel and on the surface. The lower critical

value for channel breakdown determines that it dominates in the breakdown process and contributes most in the device's operation.

In this work a physics based large signal FET model was modified to include the nonlinear source resistance effect and RF channel breakdown. The model was further modified to include multi-tone and wide-band signal simulation capability to study the device's linearity performance.

The goal of this work is to understand the physical mechanisms that determine the device's RF and linearity performance and provide the optimization options of improving these effects effectively and efficiently. The physical mechanisms were able to be quantified and determined based on the study using the analytical physics based model. It allows the development and optimization of a power amplifier before the device is fabricated. The physical device model used in this work permits determination of the nonlinear distortion under large signal operation as a function of bias, device physical parameters such as structural dimensions, doping, etc, and circuit tuning conditions.

Analytical Physics Based AlGaN/GaN HFET Large Signal Model and Nonlinearity Analysis with Nonlinear Source Resistance

by
Yueying Liu

A dissertation submitted to the Graduate Faculty of
North Carolina State University
In partial fulfillment of the
Requirements for the degree of
Doctor of Philosophy

Electrical Engineering

Raleigh, North Carolina

May 12th, 2009

APPROVED BY:

Dr. Robert J. Trew Committee Chair	Dr. Griff L. Bilbro Committee Co-Chair
Dr. Doug Barlage	Dr. C.T. Kelley

DEDICATION

I dedicate this work to my father in heaven...

BIOGRAPHY

Yueying Liu was born in Beijing, China in Oct. 1978. She went to Yibin Yizhong, in Sichuan, China during her high school years 1993-1996. She attended Beijing University of Aeronautics and Astronautics in 1996, where she graduated with a Bachelor of Science degree in Mechanical Engineering and Automation. Then she went to Shanghai Institute of Microsystem and Information Technology, Chinese Academy of Sciences, and graduated with a Master of Science degree in Microelectronics in 2003. Later in August of the same year, she started her study toward Ph.D degree in North Carolina State University after Dr. Robert. J. Trew and Dr. Griff. L. Bilbro. Her research focuses on nonlinear and large-signal modeling of AlGaN/GaN HFET devices. Her research interests include nonlinear source resistance modulation, breakdown mechanism, RF & nonlinearity impact of nonlinear source resistance and III-V group semiconductor devices modeling. Yueying Liu had a device modeling intern experience at RF Micro Devices, Greensboro, NC in 2007.

ACKNOWLEDGMENTS

I want to extend my most sincere appreciation and gratitude to Dr. Trew for his constant encouragement, inspiration, support, guidance and belief in me during my PhD study at NC State Univ. The great experience of working with Dr. Trew would benefit me throughout my career and life. I have learned from Dr. Trew both from his profound knowledge and rich research experience, and also his righteousness and integrity as a person. Dr. Trew, as many times as I have said “thank you”, is still not enough to express my appreciation and respect to you. You have everything that one would want in an advisor!

I would also like to thank Dr. Bilbro for the support I have received. Dr. Bilbro has been inspired me with many great ideas during my research work. He has been a wonderful advisor!

Special thanks to my committee member, Dr. Barlage and Dr. Kelley, who have been extremely helpful both in my research and inside their classes.

I also want to thank Dr. Zhilin Li from Mathematic Department for the constructive advice and helping me solve the numerical problem for wide band signal simulation.

I appreciate the help from my colleagues and friends, Weiwei Kuang, Hong Yin, Danqiong Hou, and Ryan Schimizzi for all the beneficial discussion.

Finally, I am deeply indebted to my parents, Qimin Liu and Zufang Wen, my husband, Sanchau Wong and my daughter, Sophia W. Wong for your patience, support and unconditional love!

TABLE OF CONTENTS

LIST OF TABLES

LIST OF FIGURES

CHAPTER 1

1.1 Introduction

The power amplifier (PA) is the most important component in PCS (Personal Communications Service) and cellular base station designs. Within the design of third generation (3G) wide-band Code Division Multiple Access (WCDMA) cellular technology, the microwave power amplifier contributes most of the cost and power consumption in the overall BTS (Base Transceiver Station). Since the power amplifier operates at a much higher power level than other cellular components, the efficiency of the power amplifier greatly determines the handset operating time. The design of a power amplifier usually focuses on the achievement of finding an optimum point to compromise and balance between efficiency and linearity. A high efficiency is preferred for a long battery operating time and to avoid the overheating problem. A good linear device guarantees the quality of signal during transmission. Unfortunately the two metrics are conflict with each other. The satisfaction of one metric usually means that the other one has to be sacrificed. In order to meet with both requirements, some linearization technique has to be used for a PA with good linearity and reasonable efficiency.

The design requirement of PA changes dramatically along with the evolution of cellular base station designs. Fig. 1.1 is the diagram for single carrier multi amplifier and multicarrier single amplifier BTS architecture [1].

The first generation analog system used single carrier BTS architecture, where each RF carrier was amplified and combined before propagation to the antenna. In another words, the amount of carrier determines how many amplifiers need to be used. The greater than 50% efficiency available from a class C amplifier suffices for both linearity and power consumption requirements.

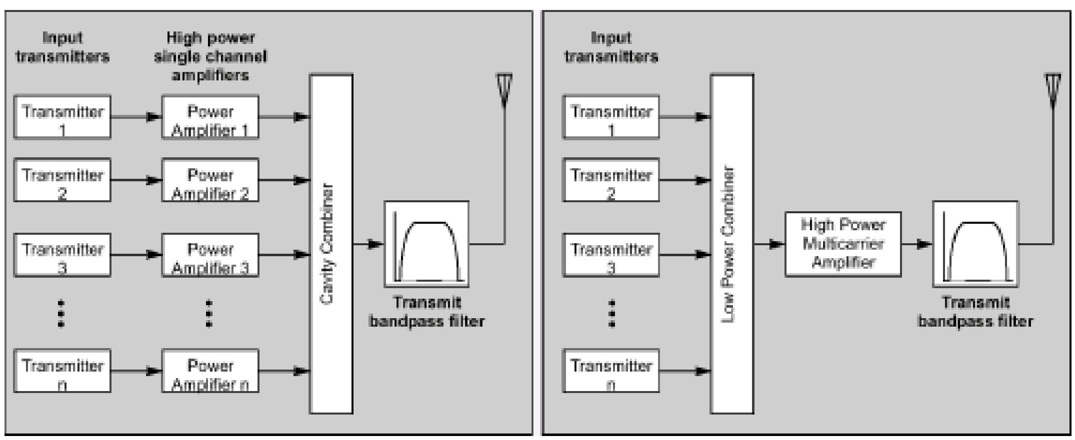

Fig. 1.1 Comparison between Single Carrier Multi Amplifier and MultiCarrier Single Amplifier Base station Architectures [1]

With data traffic increasing exponentially and enormous growth of subscribers, digital modulation schemes were introduced and are now dominate. The advantage of digital modulation is the increase in spectral efficiency, which transmits the maximum amount of data with minimum amount of spectrum. The disadvantage is the non-constant RF amplitude envelopes. To guarantee a good transmission with high quality digital modulated signal, the system must offer a distortion-free or low distortion transmission, which means a class C amplifier can not be employed in this case. A Class-AB amplifier with lower efficiency but offering higher linearity is preferred. To achieve a better efficiency, the information-bearing RF carrier is combined at low power level with only one amplifier being used. This brings out a multi carrier pre-amplification combining architecture for 3rd generation systems. The new BTS architecture put a much more stringent requirement of power, linearity and efficiency on the PA. The combination of multiple RF carriers with variable envelope increases the peak average ratio or crest factor of the composite waveform. The PA is often operated with several dBm back off from the peak Power-added Efficiency (PAE) condition in order to accommodate the signal peaks. However, operating the amplifier in under back-off conditions leads to very inefficient operation, typically less than 10%. Therefore other circuit linearization techniques such as feed forward, digital predistortion, and waveshaping need to be used to ensure the linear performance of the system. The PA is required to handle a much higher power level and needs to render a much better efficiency in order to achieve the operation time goal.

The primary goal of developing new RF power amplifier technology or Multicarrier PA (MCPA) is to achieve high linearity to satisfy the 3GPP requirements and optimum efficiency to reduce the power consumption of base station.

AlGaN/GaN HFET microwave power amplifiers are of interest for use in base station transmitters for cellular systems at S- and C-band and for radar transmitters at X through Ka band. These amplifiers can produce RF output power an order of magnitude greater than Si and GaAs-based devices, while maintaining high power added efficiency. A field-plate HFET when biased at a Vds=120V has produced over 30 W/mm RF power density at S-band [2], and 10.55 W/mm at 40 GHz with a drain bias of Vds=30V [3]. Recently, it has also been shown that these devices can achieve very low microwave noise figures (NF = 0.4 dB at 2 GHz) [4]. Based upon theoretical material parameters arguments, the nitride-based devices also have inherent advantages for linear operation. These results imply that AlGaN HFET's are strong candidate for transmitter and receiver high dynamic range modules for various communication systems.

AlGaN/GaN HFETs are well known strong candidates for high power devices due to its high breakdown field (3MV/cm), high thermal conductivity (1.3

W • $cm^{-1}C$), high peak velocity ($>3\times10^7$ $cm^{-1}s$), high saturation velocity ($>1.5\times10^7$ $cm^{-1}s$), and high sheet charge density (1×10^{13} cm^{-2}). AlGaN/GaN HFETs are also predicted to have good linearity due to favorable material properties, such as high electric field to achieve electron saturation velocity and high mobility. Practical amplifiers, however, do not demonstrate the good linearity performance predicted from fundamental semiconductor materials properties. Circuit linearization techniques, such as digital predistortion, feedforward linearization, envelope elimination and restoration, are generally employed to achieve linear performance. These techniques require additional circuitry design and complex digital signal processing work, and also increase the overall complexity and cost.

In particular, it has been demonstrated that a nonlinear source resistance is generated in these devices due to the onset of space-charge limited (SCL) transport in the gate-source region [5-7]. The nonlinear source resistance is generated when the magnitude of the channel current exceeds the threshold for space-charge limited current. Once this occurs, the resistivity of the conducting channel increases rapidly, and the source resistance can increase in magnitude by up to an order of magnitude, with resulting degradation in linearity and RF performance.

The nonlinear source resistance degrades the RF gain and PAE of the HFET, and also limits the linearity and dynamic range of the amplifier. In this work, these effects are investigated. The work makes use of an advanced large-signal RF device/circuit simulator [8] that includes a physics-based device model.

Most device models used for nonlinearity simulation are either based on equivalent circuit methods [9], or make use of Volterra-series analysis techniques [10]. These models require extensive device characterization and calibration with experimental data before they can be used and are not suitable for investigation of device parameter optimization for specific application. The physical device model used in this work permits determination of the nonlinear distortion under large signal operation as a function of bias, device physical parameters such as structural dimensions, doping, etc, and circuit tuning conditions. In this work the model has been modified for multi-frequency operation and the determination of linearity characteristics of the device. The physics based model provides a more accurate description of device nonlinearities such as channel breakdown, gate leakage current and nonlinear source resistance. It allows the development and optimization of amplifier RF performance before the device is fabricated. In addition, physical phenomena that affect the device linearity performance can be determined and quantified.

1.2 Thesis Outline

The goal of this work is to develop a physics based large signal model that represents the DC&RF behavior of AlGaN/GaN HFETs, and then use the developed model to study the impact of physical mechanism on device's RF and linearity performance.

Chapter 2 discusses the physics origin behind nonlinear source resistance and RF channel breakdown. It was also demonstrated that the limitation of RF performance due to these effects. Some unusal behaviors of AlGaN/GaN HFETs due to the existence of these effects are compared in respect to normal FETs.

Chapter 3 explains the implementation of nonlinear source resistance and RF breakdown in the large signal physics based model. The process of incorporation of both mechanisms in physics based model is shown in this chapter. The impact of these effects on device RF performance is illustrated both through measured data and simulation results.

Chapter 4 analyzes the nonlinearity of AlGaN/GaN HFETs under the impact of nonlinear source resistance and other physical mechanism. Power amplifier's IMD behavior with source resistance modulation is studied by changing the threshold current and linear resistance value. A polynomial model was developed to study the

AM-AM and AM-PM conversion with source resistance modulation. The device nonlinearity is studied with one-tone, two-tone, multi-tone and wide band signal condition.

REFERENCES

[1] Andrew Wright, Oliver Nesper, "Multi-Carrier WCDMAS Basestation Design Considerations-Amplifier Linearization and Crest Factor Control", PMC2021396, Issue1, August, 2002.

[2] Y-F Wu, A. Saxler, M. Moore, R.P. Smith, S. Sheppard, P.M. Chavarkar, T. Wisleder, U.K. Mishra, and P.Parikh, "30-W/mm GaN HEMTs by Field Plate Optimization," *IEEE Electron Dev. Lett.*, vol. 25, pp. 117-119, Nov. 2004.

[3] T. Palacios, et. al., "High-Power AlGaN/GaN HEMTs for Ka-Band Applications," *IEEE Electron Dev. Lett*., vol. 26, pp. 781-783, Nov. 2005.

[4] Yutaka Hirose, Yoshito Ikeda, Motonori Ishii, Tomohiro Murata, Kaoru Inoue, Tsuyoshi Tanaka, etc. "Low Noise and Low Distortion Performances of an AlGaN/GaN HFET," *IEICE TRANSACTIONS on Electronics*, Vol.E86-C No.10 pp.2058-2064

[5] R.J. Trew, Y. Liu, G.L. Bilbro, W.W. Kuang, R. Vetury, and J.B. Shealy, "Nonlinear Source Resistance in High Voltage Microwave AlGaN/GaN HFET's," *IEEE Trans.Microwave Theory and Tech*., vol. 54, pp. 2061-2067, May 2006

[6] R.J. Trew, “Modeling and limitations of AlGaN/GaN HFETs,” in *Int. Semicond. Device Res. Symp.*, Dec. 5–7, 2001, pp. 432–435.

[7] R.J.Trew, “SiC and GaN transistors: Is there one winner for microwave power applications?,” *Proc. IEEE*, vol. 90, no. 6, pp. 1032–1047, Jun. 2002.

[8] T.A. Winslow and R.J. Trew, "Principles of Large-Signal MESFET Operation," *IEEE Trans. Microwave Theory Tech.*, vol. 42, pp.935-942, June 1994.

[9] Pedro M. Cabral, Jose C. Pedro, Nuno B. Carvalho, “Nonlinear device model of microwave power GaN HEMTs for high power-amplifier design,” *IEEE Trans. Microwave Theory & Tech.,* vol. 52, no. 11, pp. 2585-2592, November 2004.

[10] Syed S. Islam, A. F. M. Anwar, “Large-signal modeling of GaN FET and nonlinearity analysis using volterra series,” *2002 IEEE MTT-S Int. Microwave Symp. Dig.,* vol. 1, pp. 267-270, June 2002.

CHAPTER 2

2.1 Physical Mechanisms that Limit AlGaN/GaN RF Performance

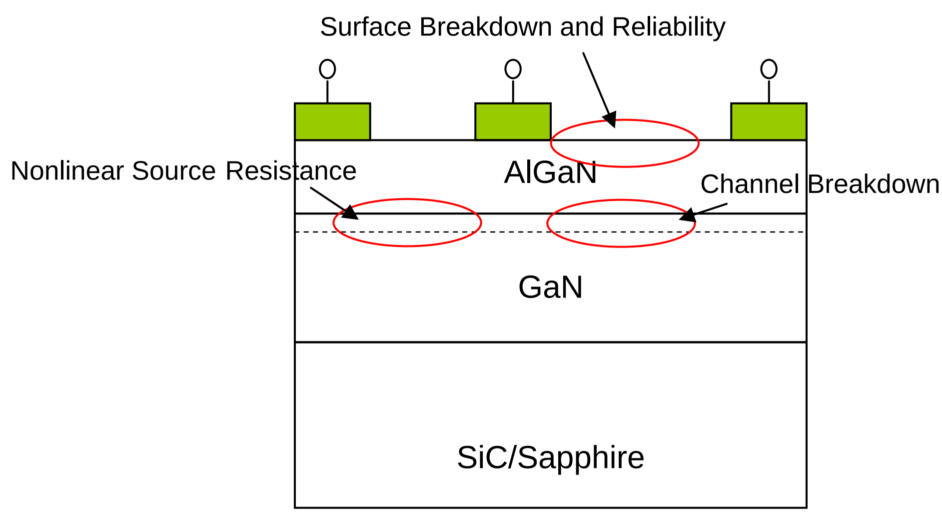

Fig. 2.1 AlGaN/GaN HFET cross section and physical mechanisms in corresponding regions.

The AlGaN/GaN HEMT power amplifier has been a very prospective competitor in front-end module base station application, due to its superior material property and high sheet charge density (1×10^{13} /cm^2) coming from the large polarization field. The good RF performance of these devices are expected in GaN due to optimum material properties, such as high critical electric field for breakdown

(3×10^6 V/cm), high peak velocity (3×10^7 cm/s) and high saturation velocity (1.5×10^7 cm/s), high mobility (1500 cm^2/sec•V), and good thermal conductivity (1.3 W $cm^{-1}C^{-1}$).

AlGaN/GaN HFET amplifiers usually operate under extreme conditions such as high voltage, high current, and high temperature. Second order physical effects are significant in such cases and play a very important role in determining device's behavior under these conditions. Breakdown, nonlinear source resistance, and gate leakage current are three main mechanisms that are significant for these devices. They are the major contributors in limiting devices performance.

Fig. 2.1 plots the AlGaN/GaN device structure with the corresponding physical mechanisms. Surface breakdown can occur at the surface of the AlGaN layer on the drain side due to high magnitude electric field at the gate edge. When the electric field at gate edge is large enough, the electrons on the gate metal at the gate side gain sufficient energy to permit tunnel injection into electronic states in the semiconductor at the surface. The electrons could either be trapped by surface states and stay on the surface becoming surface charge or be transmitted by a trap-to-trap hopping mechanism along the surface under the influence of the drain-to-gate electric field. This mechanism produces a gate leakage current and is a factor in device reliability.

RF channel breakdown occurs in the 2DEG channel at the drain region. Electron ionization in the conducting channel causes electron and hole pairs to be generated when the electric field in the conducting channel reaches the critical value. RF channel breakdown has been found to be a major factor that limits the device RF performance.

Nonlinear source resistance in the source access region also affects the RF performance of the device, particularly linearity. This phenomenon occurs when the drain current reaches the threshold current value to achieve Space Charge Limited (SCL) current effects. When SCL current occurs, the source resistance increases rapidly with additional increases in current magnitude. Nonlinear source resistance has been found especially important in AlGaN/GaN devices due to the lack of background doping in conducting channel, which would provide an electric field that would resist the onset of SCL current. The nitride devices are prone to SCL effects since they are generally operated under high RF power conditions where the device experiences high magnitude RF operating current and voltage. Source resistance modulation limits the device's performance by introducing nonlinearity and suppression of saturation current. The nonlinear source resistance effect, RF channel breakdown, and surface breakdown and hopping are the three major contributors that limit device RF performance.

2.2 Nonlinear Source Resistance

The AlGaN/GaN heterostructures is of interest for HFET devices due to the extremely high velocity and high mobility of electrons confined in the two-dimensional electron gas (2DEG) conducting channel of the HFET. Compared with GaAs, the GaN material has a wider bandgap and a larger effective mass, which ironically implies a lower mobility. However due to higher intervalley energy separation and the large energy of optical phonons, bulk GaN has a higher mobility under high electric fields than GaAs. The steady state and pulse IV measured electron transport are shown in Fig.2.2.

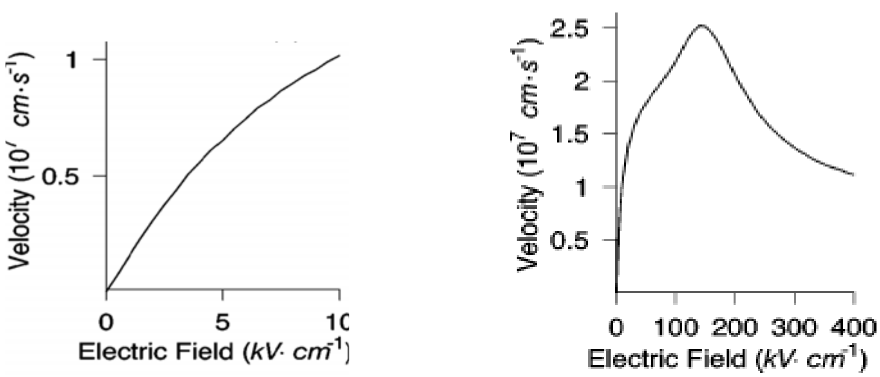

Fig. 2.2 Monte Carlo study of electron transport in the GaN/Al0.37Ga0.63N structure [1].

Recently many researchers have noticed an early "quasi-saturation" [2] phenomenon at very low electric fields (10-25 kV/cm) in the HFET source access region. This effect introduces a source resistance modulation effect at high current driving condition and degrades the transconductance when the device enters into open channel operation. There are several possible explanations to this effect,

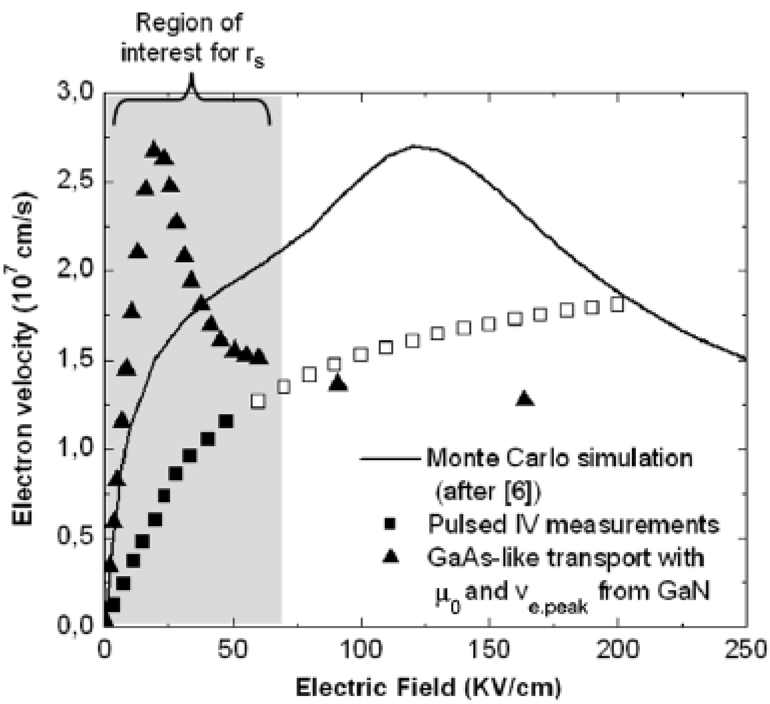

Fig. 2.3 Electron velocity vs electric field profile in AlGaN/GaN structures for different transport models used during the ATLAS simulations. [2]

1. Self heating.

2. Rough interface scattering

3. Non-equilibrium phonon emission and absorption.

4. Space-Charge-Limited effect

The first three mechanisms are not the main factors according to previous research results. First, there is no obvious improvement in electron transport at low field when, for example, low thermal conductivity sapphire substrates are replaced with high thermal conductivity SiC. This indicates that self-heating is not the reason causing velocity pre-saturation. Second, interface scattering affects charge transport and the degradation of transconductance still exists under increased drain-source voltage where interface scattering is limited, while keeping the 2DEG concentration constant. As electrons move faster under higher electric field, the probability of being scattered by surface roughness is decreased. This factor is proved to be insignificant in the pre-saturation effect. It was assumed that non-equilibrium phonon was the main reason causing this pre-saturation. Many simulations using ensemble Monte Carlo methods [2, 4] have been reported to verify this model. It was observed that the little "hump" in electron transport plot [3], originating from longititude optical phonon scattering at low field, is related to transconductance drops at high current. According to the results, hot optical phonon did cause a suppression of transconductance at high current drive [3]. However, compared to the pulsed IV measured velocity-field curve, the simulation mobility and velocity are still overestimated [2].

Space-charge-limited current has been reported to be a significant factor in the onset of the nonlinear source resistance [5]. The SCL effect appears in the device's operation when the conducting current is increased to a critical threshold current value. A detail analysis of current transport in a bulk GaN semiconductor using Atlas, a 2-D device simulator, has verified the existence of the SCL effect and nonlinear resistance under high current injection operation [6]. A numerical model that includes nonlinear source resistance accurately repeats experimental dc IV data on practical devices as the bias varies from pinch off to open channel [6] conditions.

The nonlinear source resistance effect plays a very important role in AlGaN/GaN HFET device operation. The direct result of this effect is the degradation of gm at high current drive conditions as shown in Fig. 2.4.

The degradation of gm due to nonlinear source resistance is amplified by gm due to a negative feedback from output to input by source resistance. The extrinsic transconductance is degraded from the intrinsic value by a factor of 1+Rs*gm. The resulting transconductance is written as:

$$gm = \frac{gm0}{1 + gm0 \cdot Nlrss} \qquad (2.1)$$

From load line point of view, nonlinear source resistance degrades PA's RF performance by limiting the maximum current value and introducing nonlinearity at the output through negative feedback. The load lines in Fig. 2.5 show the result when the device operates at saturation condition. The SCL effect increases the nonlinear source resistance and forces the RF dynamic load line, when plotted on the I-V plane to rotate counterclockwise. The maximum current the device is permitted to achieve is suppressed by this behavior. The rule of thumb is that the maximum power the amplifier delivers is determined by the maximum current through the devices and the maximum RF voltage, which is limited to the device breakdown voltage. Reduction of the saturation current by the nonlinear source resistance reduces the output power. Also the nonlinear source resistance increases becomes significant when the devices is operating in the high current region. The device linearity is degraded rapidly by the source resistance under high power operation, which is very important and needs to be considered during PA design.

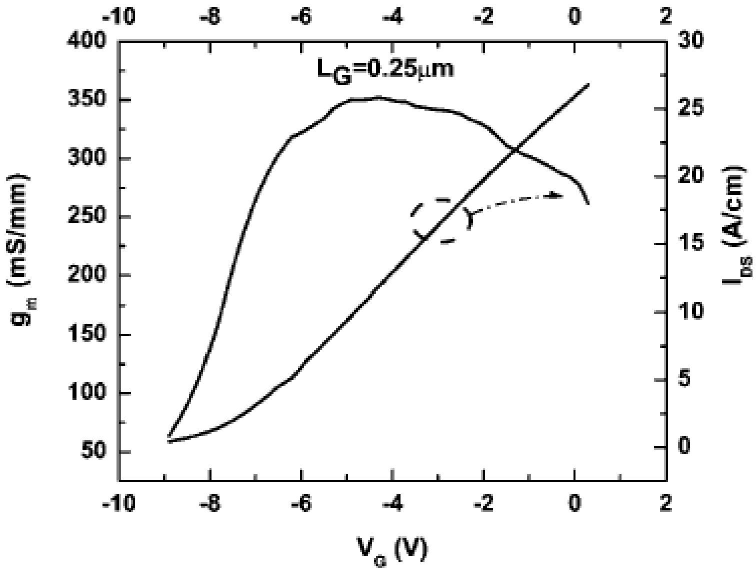

Fig. 2.4 Variation of gm and Id with gate bias for Lg = 0.25μm. Lsg = 0.65μm. [3]

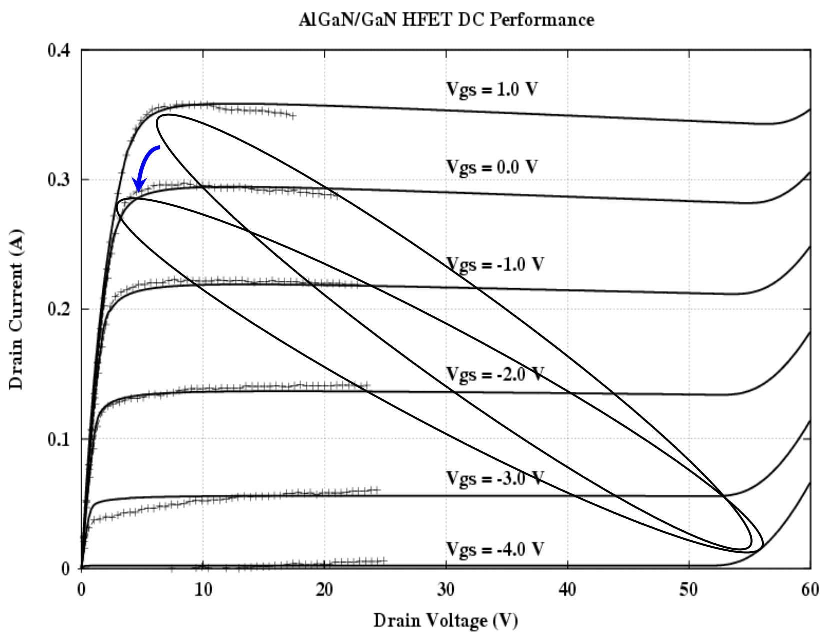

Fig.2.5 Load line analysis for AlGaN/GaN HFET device with and without nonlinear source resistance.

2.2.1 Nonlinear Source Resistance Analytical Model

Space charge limited current effect directly comes from fundamental physics. It starts from Poisson's equation:

$$\varepsilon \frac{\partial E}{\partial x} = Nd - n \qquad \varepsilon \frac{\partial E}{\partial x} = -\delta n \tag{2.2}$$

As current increases, a large number of electrons are injected into the conducting channel from the source contact. The injected electrons suppress the electric field at source access region and increase the resistivity of the material in the gate-source region. A threshold value exists for this effect. The SCL is turned on when current reaches the threshold value and the source resistance becomes nonlinear. The critical current to turn on this effect is approximately on the order of Jsat = q*nss*vsat, where q is elementary charge, nss is carrier concentration in the 2DEG, and vsat is electron saturation velocity for GaN . Substitute nss=1.0×10^{13} /cm^2, vsat = 1.5×10^{7} cm/s into equation. Jsat = 24 A/cm.

It has been reported that the channel breakdown is the main mechanism that limits the RF performance [5]. When avalanche breakdown occurs in the conducting channel under the gate electrode on the drain side, both holes and electrons are generated. Generated electrons are quickly swept through the 2DEG by the channel electric field and collected by the drain, where they enhance the drain current. The generated hole on the other hand will drift back to the source access region. The holes move very slowly due to their low mobility, and most of them recombine with the high density of electrons in the conducting channel in the source access region. The decrease in electron density from this recombination process will further decrease the threshold for the onset of SCL conditions. Usually the SCL current effect occurs at a much smaller current value than the value predicted from q*nss*vsat, especially when device is operated at high power level.

A first order model for nonlinear source resistance can be developed by assuming a small constant electric field at the source access region and $\beta = 1$ in the Caughey and Thomas expression [7] for electric field dependent mobility expression.

Starting with the current equation

$$J = qnv \tag{2.3}$$

Substitute $v = \dfrac{\mu E}{1 + \dfrac{E}{Esat}}$ into above the equation and rearrange,

$$J + J\frac{E}{Esat} = \sigma \cdot E \tag{2.4}$$

where $\sigma = qn\mu$, is conductivity

Multiply cross section area on both sides

$$Id + Id\frac{Vrss}{Vsat} = \sigma \cdot E \cdot A \tag{2.5}$$

Assume the change of electric field at the source access region is relatively small, therefore $E \cdot L = Vrss$, where Vrss is the voltage drop across the source resistance, $Esat \cdot L = Vsat$

As $rss = \frac{1}{\sigma} \cdot \frac{L}{A}$, and $\sigma \cdot A = \frac{L}{rss}$, eqn. (2.5) is modified as:

$$Id + Id\frac{Vrss}{Vsat} = \frac{Vrss}{rss} \tag{2.6}$$

Solve for Vrss:

$$Vrss = \frac{Id \cdot rss}{1d - \frac{I}{Isc}} \tag{2.7}$$

where $Isat = q \cdot n \cdot Vsat \cdot A$

We could write the equation for nonlinear source resistance

$$Nlrss = \frac{Vrss}{Id} = \frac{rss}{1 - \frac{Id}{Isc}} \tag{2.8}$$

As this equation shows, the source resistance is determined by the linear term rss, the SCL threshold Isc, and the drain current Id. When the drain current is small compared to Isc, the denominator is close to unity, and source resistance is a linear component with value determined by rss. When current increases to a value comparable to Isc, the denominator is less than 1, and the source resistance is becoming nonlinear with its value larger than the linear term rss. Simulation shows at modest drive condition, the nonlinear source resistance value could double or even triple the original value at small signal.

2.2.2 Nonlinear Drain Resistance

The SCL effect also occurs at the drain access region, which leads to a nonlinear drain resistance. After the same analysis, the analytical equation of nonlinear drain resistance yields:

$$Nlrdd = \frac{rdd}{1 - \dfrac{Id}{Isat, drain}} \tag{2.9}$$

However, since drain resistance is at the output in series with the load. Its impact is easily absorbed by the larger load resistance, and the nonlinear drain resistance has only minor effect upon the RF operation of the device. On a DC IV plot, the nonlinear drain resistance affects the slope of the IV characteristic in the linear region, as well as the transition between the linear and saturation regions, but does not introduce much impact upon device operation.

2.3 RF Channel Breakdown

It has been recognized that avalanche breakdown is a leading physical mechanism that limit PA's RF performance, since it determines the maximum drain voltage devices could be developed during the RF cycle [8]. A physics based large signal model [9] has been used to study the FETs behavior under large-signal RF conditions. In this model the avalanche breakdown is assumed to occur on the semiconductor surface, consistent with experimental observations. RF breakdown was found to be the main factor limiting RF performance of the device. An analytic model for RF breakdown was reported and was modified for the work reported in this thesis.

Two different breakdown mechanisms have been observed in FET devices. One signature to identify them is the breakdown voltage variation with temperature. However contradictory temperature coefficient has been found for breakdown voltage in AlGaN/GaN HFETs. Breakdown occurring on the surface originates from electron tunneling from the gate electrode, which is characterized with a negative temperature coefficient. Breakdown initiated in the channel is due to the avalanche ionization, which exhibits a positive temperature coefficient.

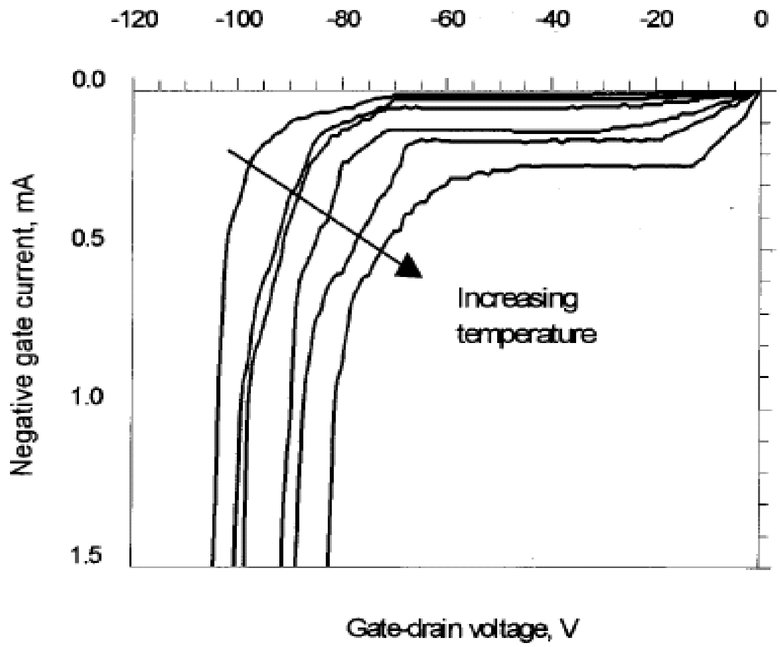

Fig. 2.6 Negative gate leakage current, Ig, vs the gate-drain voltage as a function of the temperature. The curves were measured at 20, 70, 100, 130, 160, and 200°C. [11]

The electric field at the gate edge on the drain side could be high enough to cause electron tunneling from gate electrode onto the surface on the drain side. The electron tunneling from the gate could either be trapped and stay on the surface, becoming surface charge, or drift toward drain electrode through a hopping mechanism [10]. Electron hopping along the surface causes surface leakage from gate to drain. Surface charges deplete the 2DEG in the channel, and leads to current collapse in devices IV response. Surface charge and gate leakage are two mechanisms that have been found to affect AlGaN/GaN HFETs reliability.

Electron tunneling from the gate is not controllable when the electric field at the gate edge is increased to a critical value. A two terminal test, which connects the gate and drain, while leaving the source floating, and measuring the gate current, Ig, versus the gate-drain voltage, Vgd, is often used to measure the breakdown voltage. During the test, the devices are measured at a deeply pinched off condition and the breakdown voltage measured is usually called Off State Breakdown Voltage. Fig. 2.6 shows the typical results from a two-terminal test [11]. The leakage current is due to the electron hopping transport mechanism, and is very sensitive to temperature. The leakage current magnitude increases with temperature and measured data show the electrons trapped electrons on the surface have activation energy of about Ea~210meV [11]. The negative temperature coefficient of the breakdown voltage is a signature of electron tunneling.

Another breakdown mechanism can be measured through a three-terminal test. The three electrodes are connected in a way that the device is normally operated or turned off, and drain current is measured when Vds increases. The device could be either turned on or off during the test. The three-terminal breakdown is correlated with electron avalanche ionization in the channel. As the electrons in the 2DEG gain enough energy due to sufficient high electric field, the carriers are ionized and electron-hole pairs are generated. Fig. 2.7 shows measured results of the temperature variation of a three terminal test for breakdown voltage. The positive temperature coefficient of the breakdown voltage signifies that the breakdown is being initiated by impact ionization.

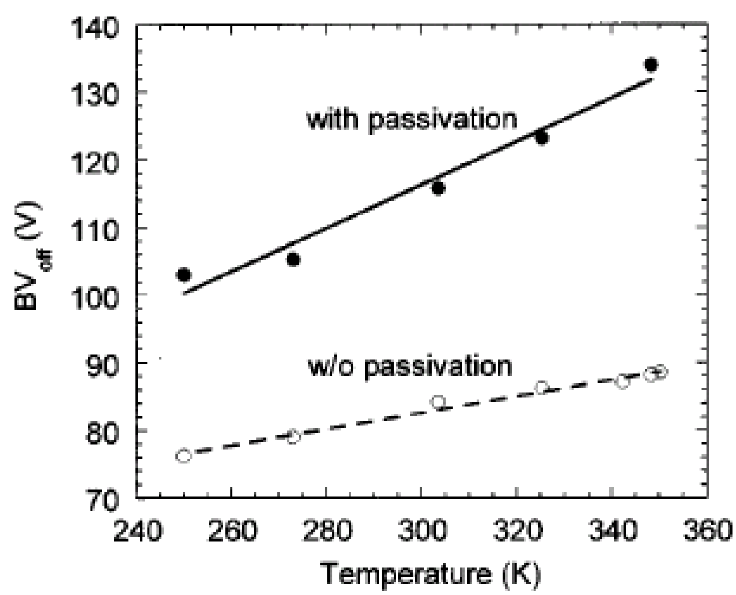

Fig. 2.7 Temperature dependency of channel breakdown voltage. [12]

To differentiate between the two breakdown mechanisms, the one that occurs on the surface is called gate breakdown, and the other one that occurs in the channel is called channel breakdown. Both mechanisms can occur during the large-signal RF operation of an FET. The mechanism with the lower threshold will dominate in any given situation. For the GaAs MESFET, the breakdown mechanism that dominates is generally correlated with gate current and electric field at gate edge on the surface [9]. Gate-drain breakdown in GaAs FETs correlates well with gate tunnel leakage and surface breakdown. However for AlGaN/GaN HFETs, this is usually not the case, and channel breakdown is found to have the lower threshold, and therefore dominates large-signal RF performance. Gate leakage occurs, but gate breakdown is not generally observed to occur, except under extreme operating conditions.

Fig. 2.8 shows measured Ids and Igd as a function of Vds for AlGaN/GaN transistors from the same wafer. The gate current and drain current are measured when the device is pinch off and Vds varies from zero to 40V. The finite and negative gate current is the leakage current from gate to drain and is due to electron hopping conduction along the surface. The gate breakdown shown as a rapid increase in gate current is never observed in the measurement. Vds is on the order of 60-70V to demonstrate the gate breakdown

On the other hand, the drain current in the measurement does show device breakdown in the conducting channel. As indicated, the RF channel breakdown voltage has a significantly lower value than gate breakdown, and some of the devices begin to demonstrate breakdown at drain voltages as low as 30V.

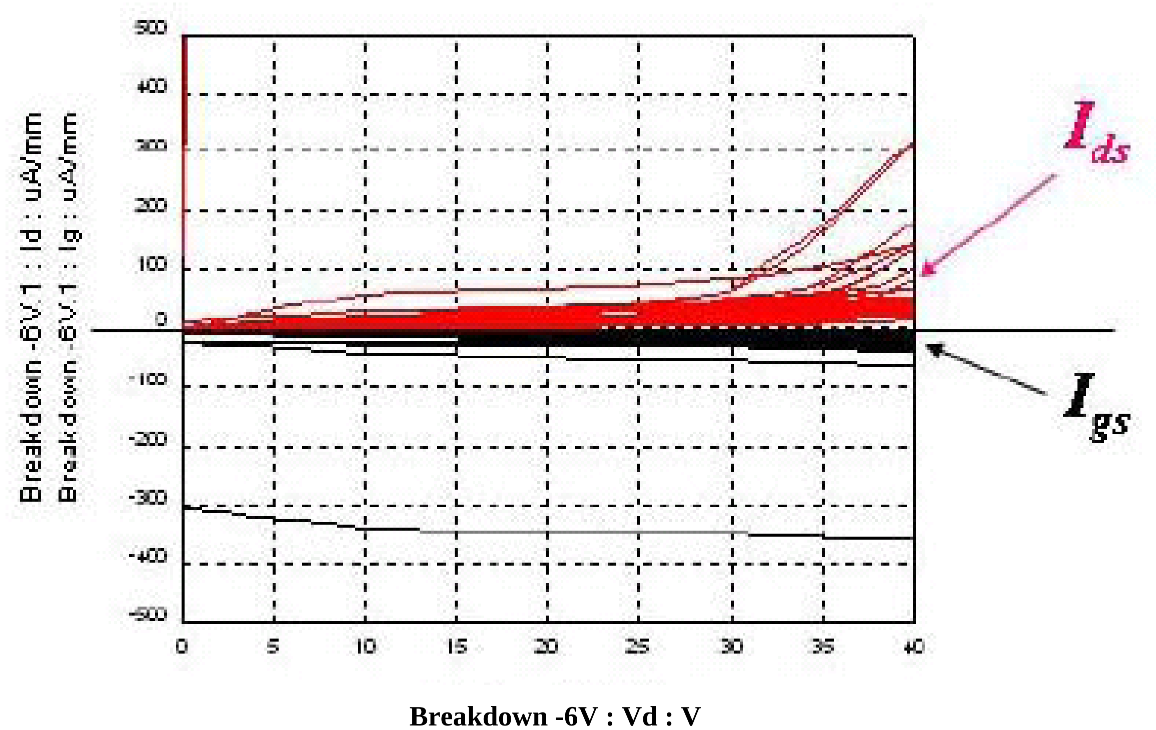

Fig. 2.8 Measured Id and Ig as a function of Vds for selected AlGaN/GaN HFET's from the same wafer. [7]

The lower magnitude of the breakdown voltage for RF channel breakdown means that for AlGaN/GaN devices, RF channel breakdown is the dominate mechanism that limits device performance. Gate breakdown and gate leakage current affect device reliability, but do not have significant affects upon RF performance.

A possible explanation for the high breakdown voltage on the surface for AlGaN/GaN HFET devices is due to the existence of surface states. As electrons tunneling from the gate either enter into the surface being trapped by surface states or contribute to the gate leakage current through hopping conduction toward the drain electrode. Both mechanisms decrease the negative charges at the gate region, and lower the electric field at gate edge. The gate breakdown voltage for AlGaN/GaN HFETs is much higher than devices without or with less surface states. This is the reason that GaAs MESFET's RF large signal behavior is dominated by gate breakdown and AlGaN/GaN HFET is dominated by channel breakdown.

Fig. 2.9 illustrates how the RF channel breakdown limits device performance. When the electric field in the channel reaches critical value, sufficient to cause electron impact ionization, electron-hole pairs are generated. The electrons move toward the drain, enhancing the channel current and causing a self-biasing effect. The holes drift back to the source. The holes move very slowly and have a high probability of recombining with the high density of channel electrons in the gate-source region.

The recombination process reduces the 2DEG concentration and enhances the SCL effect by lowering the SCL threshold value. The nonlinear source resistance effect is affected by the RF channel breakdown and ionization degree in the device.

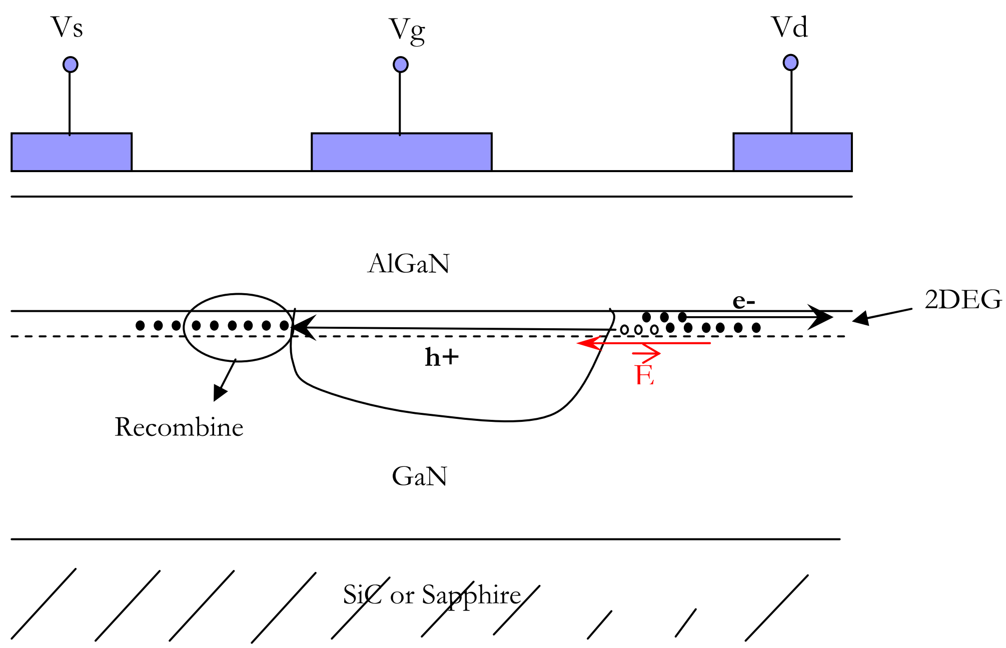

Fig. 2.9 Cross-Section of AlGaN/GaN HFETs at RF channel breakdown.

Under classical theory the input capacitance Cgs for a GaAs MESFET will increase with input power, driving the device to a lower input impedance state. This phenomenon occurs because of the thinner depletion region beneath the gate at higher input voltage, consistent with high RF power drive. However, as shown in Fig. 2.10, the opposite behavior is observed for AlGaN/GaN devices, where the input capacitance is observed to decrease as power increases.

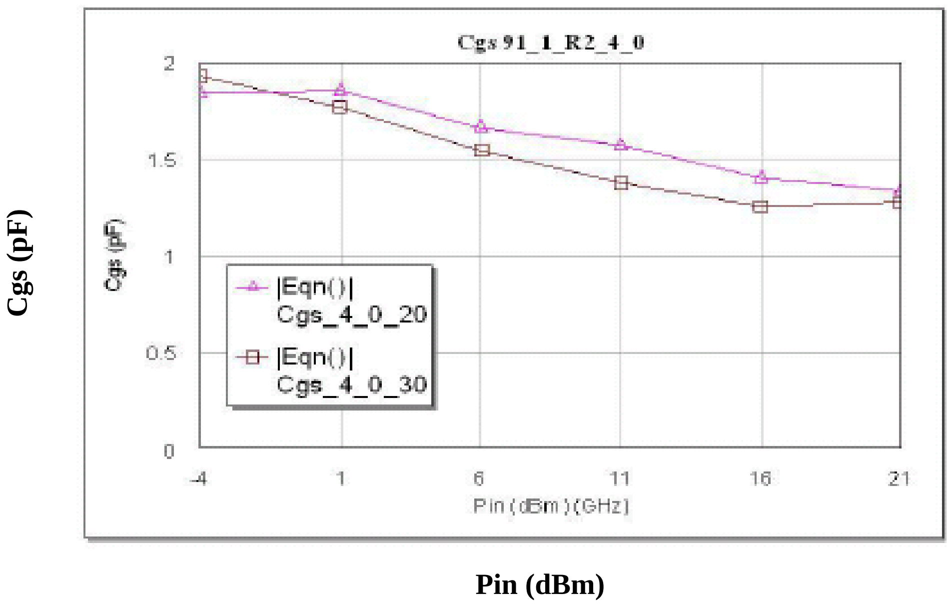

Fig. 2.10 Measured Cgs as a function of input power drive. [13]

The decrease of Cgs at high power is a nonlinear source resistance result. The extrinsic capacitance can be written as:

$$Cgs = \frac{Cgs0}{1 + Cgs0 \cdot Nlrss} \tag{2.10}$$

The intrinsic $Cgs0$ increases with power as normal FETs behave. As it is compensated by the degradation of nonlinear source resistance, the result of extrinsic Cgs decreases when power increases as the experimental results show. Electron ionization increases hole generation in the channel when power increases, which reduces the input capacitance. The recombination of holes at high power drive contributes to the reduction of Cgs.

Normal FETs operates at a much lower power and lower current level than GaN FET devices. The inherent background doping in the channel also makes SCL less easy to produce in these devices.

2.4 Summary

The inherent superior material quality enables AlGaN/GaN devices operate under extreme conditions, which introduce second order physical mechanisms such as RF channel breakdown, nonlinear source resistance and surface electron hopping conduction. Different from surface breakdown observed in normal FET like GaAs MESFET, the RF channel breakdown is initiated by electron ionization in the conduction channel. It is separated from the gate surface by AlGaN buffer layer. The positive temperature coefficient has verified that the origin of breakdown is avalanche ionization. The higher critical field for gate breakdown determines that RF channel breakdown dominates the breakdown process and contributes most in limiting devices performance.

Nonlinear source resistance originates from SCL effect when conduction current reaches the threshold current value. This effect degrades devices performance by suppression transconductance and introduces nonlinearity. The lack of background doping and high current operation make this effect very important in AlGaN/GaN power amplifiers. The nonlinear source resistance magnitude can significantly increase under even modest power drive conditions. The nonlinear source resistance is found to limit the devices gain, output power, and also linearity behavior.

Nonlinear source resistance is affected by the degree of electron ionization in the 2DEG channel. The increase of hole generated by electron ionization recombines with electrons when they drift back to source access region. The threshold current value for SCL effect is reduced by this behavior and the source resistance modulation is more obvious when RF channel breakdown is initiated. The increase of generated hole and lower threshold for SCL cause the input capacitance of AlGaN/GaN HFET decreases with input power, which is opposite to the direction normal FETs behave.

REFERENCES

[1] Madhusudan Singh and Jasprit Singh, “Design of high electron mobility devices with composite nitride channels” *Journal of Applied Physics*, 2003, Volume 94, Issue 4, pp. 2498-2506

[2] Tomas Palacios, Siddharth Rajan, Arpan Chakraborty, Sten Heikman, Stacia Keller, Steven P.DenBaars, “Influence of the Dynamic Access Resistance in the gm and f_T Linearity of AlGaN/GaN HEMTs” *IEEE Transaction on Electron Devices,* 52, 10, 2005, pp.2117.

[3] Yuh-Renn Wu, Madhusudan Singh, Jasprit Singh, “Sources of Transconductance Collapse in III-V Nitrides-Consequences of Velocity-Field Relations and Source/Gate Design” *IEEE Transaction on Electron Devices,* 52, 6, 2005, pp.1048.

[4] S Gokden, N Balkan, B K Ridley, “Effect of non-drifting hot phonon on high-field drift velocity in GaN/AlGaN” *Semicond. Sci. Technol*. 18, 2003, pp 206-211

[5] R.J.Trew, (Invited), “SiC and GaN Transistor: Is There One Winner for Microwave Power Applications?” Proc. IEEE, Special Issue on Wide Bandgap Semiconductors, Vol. 90, pp. 1032-1047, June 2002.

[6] R.J. Trew, Y. Liu, G.L. Bilbro, W.W. Kuang, R. Vetury, and J.B. Shealy, “Nonlinear Source Resistance in High Voltage Microwave AlGaN/GaN HFET’s,” *IEEE Trans. Microwave Theory and Tech.,* vol. 54, pp. 2061-2067, May 2006

[7] Caughey, D.M., and R.E. Thomas. “Carrier Mobilities in Silicon Empirically Related to Doping and Field.” *Proc. IEEE,* 55, 2192-2193, 1967.

[8] R. J. Trew and U.K. Mishra, "Gate Breakdown in MESFETs and HEMTs," *IEEE Electron Dev. Lett*., vol. 12, pp. 524-526, Oct. 1991.

[9] T.A. Winslow and R.J. Trew, "Principles of Large-Signal MESFET Operation," *IEEE Trans. Microwave Theory Tech.*, vol. 42, pp.935-942, June 1994.

[10] W. Kuang, “”, Ph.D. dissertation, 2008

[11] W.S.Tan, P.A.Houston, P.J.Parbrook, etc, “Gate Leakage Effects and Breakdown Voltage in Metalorganic Vapor Phase Epitaxy AlGaN/GaN Heterostructure Field-Effect Transistors”, *Applied Physics Letters*, Vol.80, No.17, April 2002.

[12] Yutaka Ohno, Takeshi Nakao, Shigeru Kishimoto, etc, “Effects of Surface Passivation on Breakdown of AlGaN/GaN High-Electron-Mobility Transistors”, *Applied Physics Letters*, Vol.84, No.12, March 2004.

[13] R. J. Trew, Y.Liu, W.Kuang, H.Yin, G.L.Bilbro, *etc* "RF Breakdown and Large-Signal Modelling of AlGaN/GaN HFET's" Microwave Symposium Digest, 2006. IEEE MTT-S International, June 2006, 643 – 646.

CHAPTER 3

3.1 Physics based large signal FET model

A physics based large signal FET model [1] is used in this work to verify the physical mechanisms in AlGaN/GaN HFET devices. The model was further modified [2] to include basic gate leakage and gate breakdown mechanisms. The model calculates the intrinsic FET behavior from device structure, doping profile, and electron transport parameters. A 2D table with small signal parameters and IV results are built for the DC response. Integration of the device model in a harmonic-balance circuit simulator permits the RF operation of a power amplifier to be investigated.

To verify the physical mechanisms discussed in chapter 2 and study the impact of these effects on devices operation, the model is further modified in this work to include the nonlinear source resistance and RF channel breakdown phenomena. In this chapter the modified model is used to simulate and investigate the RF performance of devices with nonlinear source resistance, and the simulation results are compared with measured data to verify accuracy. The model is also used to investigate optimization issues associated with a device's RF performance and linearity based on the simulation results. It is shown that the model accurately predicts both DC and RF behavior of AlGaN/GaN HFET devices operating at different bias and frequencies, and excellent agreement between simulated and measured data is demonstrated.

3.2 Implementation of Nonlinear Source Resistance in the Physics FET Model

In a harmonic balance simulator the nonlinear and linear networks are separated and interfaced by means of time-frequency transformation technique, (e.g. Fourier Transforms), and the circuit response is calculated by converting the I-V results between time domain and frequency domain. Parasitic elements in the transistor's equivalent circuit model are linear items. They are considered in the frequency domain. Nonlinear component such as intrinsic FET model is considered in the time domain. To include the nonlinear source resistance calculation in the simulator, the parasitic source resistance is removed from the linear network and placed in the nonlinear network. The final IV results are calculated by comparing the current response from the intrinsic FET model and the nonlinear source resistance. A root finder is used to obtain the final solution for the nonlinear source resistance and current.

A 1-D function is formed to solve the source resistance value. Since the intrinsic FET model calculate the current response with given voltage boundary conditions, an equation is set up by comparing the current from intrinsic FET and nonlinear source resistance as follows:

$$i_{FET}(v_{gs}(i_{Rs}, Rs), v_{ds}(i_{Rs}, Rs)) - i_{Rs}(Rs) = 0 \tag{3.1}$$

Brent's method in Numerical recipes, Section 9.3 is used to find the Rs solution. The equation for $i_{Rs}(Rs)$, $v_{gs}(i_{Rs}, Rs)$, $v_{ds}(i_{Rs}, Rs)$ are:

$$i_{Rs}(Rs) = Isat \cdot (1 - (\frac{rss}{Rs})^{\beta})^{\frac{1}{\beta}} \tag{3.2}$$

$$v_{gs}(i_{Rs}, Rs) = v_{gs,ext} - i_{Rs} \cdot Rs \tag{3.3}$$

$$v_{ds}(i_{Rs}, Rs) = v_{ds,ext} - i_{Rs} \cdot Rs \tag{3.4}$$

Where $v_{gs,ext}$ and $v_{ds,ext}$ are terminal voltages across intrinsic FET with nonlinear source resistance.

Equ.(3.2) is derived from electric field dependent mobility by Caughey and Thomas [3]. The resultant expression for nonlinear source resistance is:

$$Rs = \frac{r_{ss}}{[1 - (\frac{I}{Isat})^{\beta}]^{\frac{1}{\beta}}} \tag{3.5}$$

The nonlinear drain resistance expression is in the same format. But because the electric field and carrier concentration profiles in the drain region differ from the source region, the exponential term and threshold value for the SCL effect under the gate at the drain edge are not equal to the value at source side.

Finally, any parameters that are degraded with source resistance are modified correspondingly in the model to get the correct 2D table values for RF simulation.

$$gm = \frac{gm0}{1 + gm0 \cdot Nlrss} \tag{3.6a}$$

$$gd = \frac{gd0}{1 + gd0 \cdot Nlrss} \tag{3.6b}$$

$$Cgs = \frac{Cgs0}{1 + gm0 \cdot Nlrss} \tag{3.6c}$$

The implementation of the nonlinear drain resistance is very straightforward after calculation of the source resistance. As drain resistance is easily absorbed by the large load resistance, there is no obvious degradation by SCL at the drain access region. The replacement of a nonlinear drain resistance from the linear network to the nonlinear network is achieved by subtraction of the output voltage v_{ds} from the voltage drop across the nonlinear drain resistance. The root finder routine calculates the final results for drain current, nonlinear source resistance, and nonlinear drain resistance with given terminal voltages.

3.3 Modified Physics Based Large Signal Model

The complete modified physics based FET model incorporates the basic intrinsic FET model, gate electron tunneling and surface breakdown, nonlinear source resistance and nonlinear drain resistance model, and RF channel breakdown.

A current generator in the gate-drain circuit is formulated to model the gate tunneling leakage current that results from the high field that exists at the edge of the gate contact [2]. The leakage current is a function of the donor-like surface states, electron tunneling effective mass, and the electric field magnitude at gate edge. A reverse current generator from drain to gate represents surface breakdown at the gate on the surface.

A current generator in the drain-source circuit models the RF channel breakdown in the conducting channel. Electrons generated by impact ionization enhances the drain current, which is determined by the magnitude of the channel breakdown field, the channel electric field, device temperature and the available channel electron density.

Nonlinear source resistance is modeled in the RF large signal AlGaN/GaN HFET model by inclusion of a variable source resistance at the source end with value determined as a function of current according to eqn.(3.5), as shown in Fig.3.1. The nonlinear drain resistance is added in the same way (not shown in the plot) at the output and in series with load resistance.

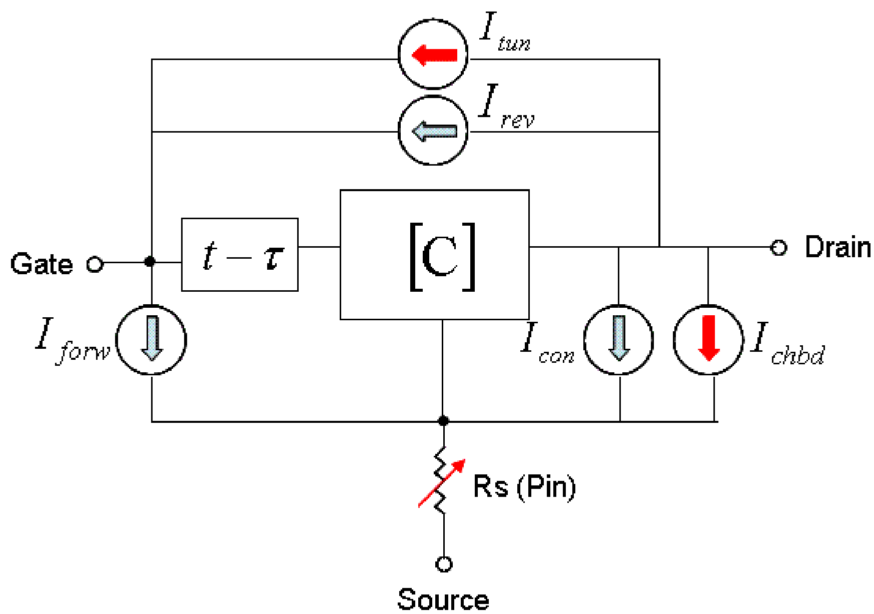

Fig. 3.1 Large-Signal RF Model including nonlinear source resistance and RF channel breakdown.

The modified model is embedded into a harmonic balance simulator to determine the device's RF performance and IMD behavior.

3.4 Verification of modified device model

To verify the accuracy of the modified physics model, comparison of the simulated and measured RF performance and dc drain current were performed for experimental devices operating at different frequencies. The gate lengths (Lg) for the calibration devices are 0.2μm, 0.2μm, and 0.8μm, corresponding to device operating frequencies at 40GHz, 10GHz, and 2.14GHz, respectively.

3.4.1 Device A (Lg = 0.8μm, f_0= 2.14GHz)

Calibration results for an AlGaN/GaN HFET class-AB power amplifier operated at 2.14 GHz are shown in Fig. 3.2. The measured and simulated DC drain currents and RF performance are shown in Fig. 3.2 (a) and (b), respectively. As indicated, the physics-based model accurately simulates the measured DC and RF performance.

The measured and simulated DC drain and gate currents are shown in Fig. 3.3(a) and (b), respectively. As indicated, excellent agreement between the measured and simulated data is obtained.

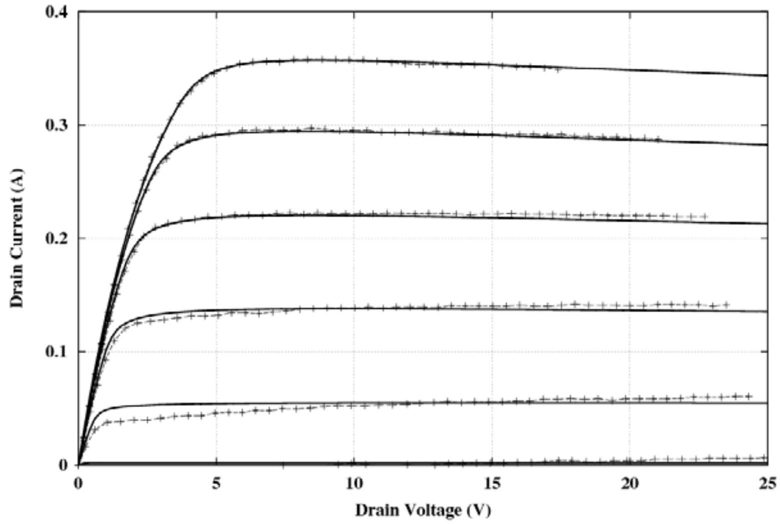

(a)

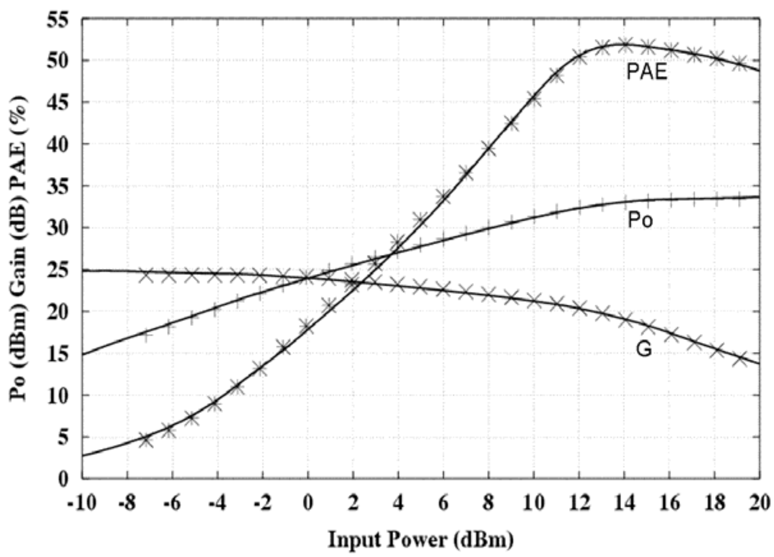

(b)

Fig. 3.2 Measured and Simulated DC (a) & RF (b) Performance for a Communications Band AlGaN/GaN HFET Amplifier (Vds=28v, F=2.14 GHz, Class A-B).

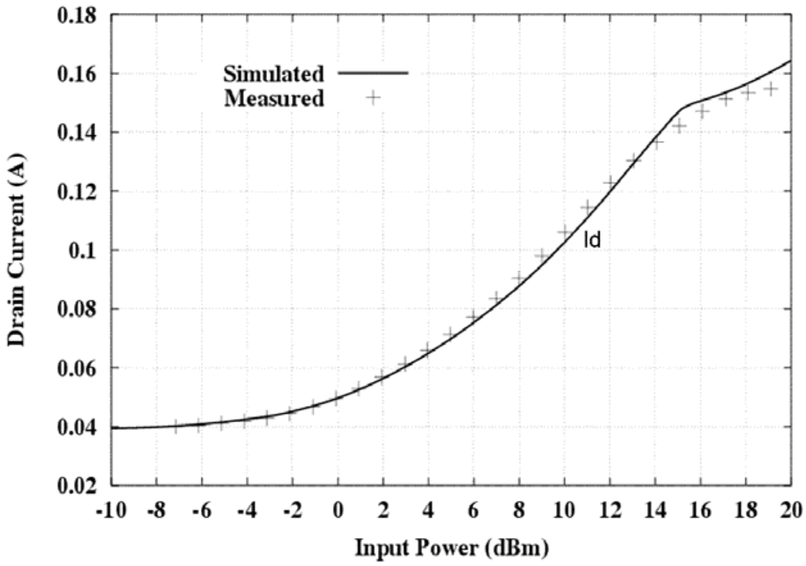

(a)

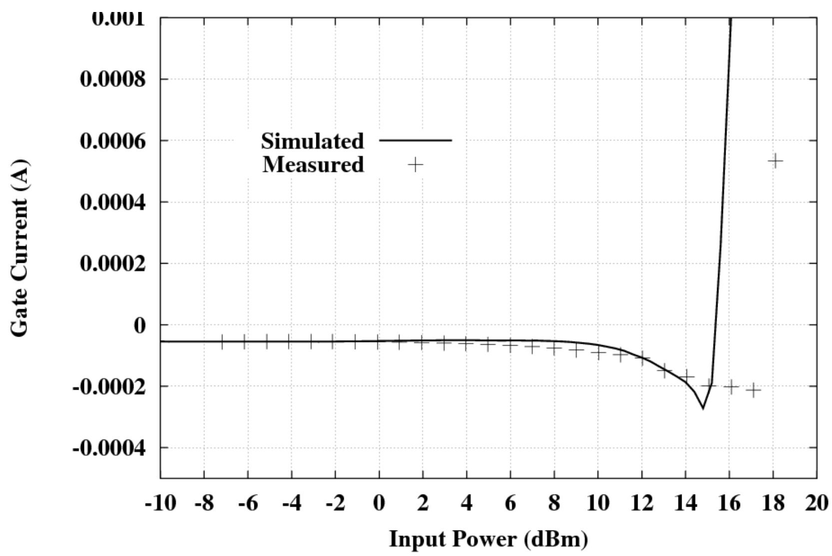

(b)

Fig. 3.3 Measured and Simulated dc Drain Current (a) and Gate current (b) for a Communications Band AlGaN/GaN HFET Amplifier (Vds=28v, F=2.14 GHz, Class A-B).

In the data shown in Figs. 3.2 and 3.3, the HFET has a gate length of 0.8μm, and a gate width of W=0.4mm. The device was biased at a drain voltage of Vds=28V. The amplifier was operated at 2.14GHz in class A-B. Ten harmonics were included in the harmonic balance routine. Simulation with more than 10 harmonics was tested for more accuracy. No obvious difference was seen. According to the simulation result, the maximum viewable harmonic distortion for this device is up to the 5^{th} order, as is shown in Fig.3.4. The accuracy of the simulation results for higher order harmonics are either limited by machine precision or tolerance due to the numerical methods that were used for the calculation.

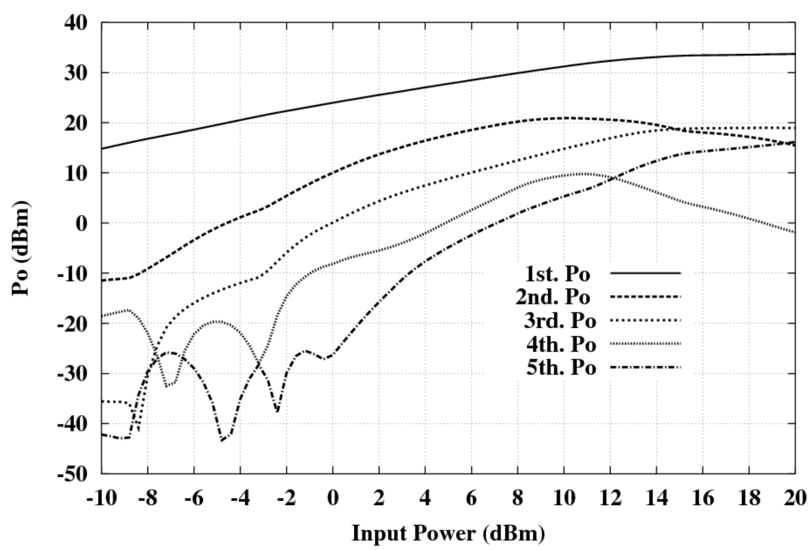

Fig. 3.4 Output power from fundamental to 5^{th} order harmonic for 2.14 GHz class-AB AlGaN/GaN HFET power amplifier.

The device performance degradation due to nonlinear source resistance influences the bell shape of the transconductance and capacitance. Fig.3.5 and Fig.3.6 show the parameter extraction results of transconductance and capacitance for the AlGaN/GaN HFET power amplifier. The terms "extrinsic" in the plots are for the intrinsic FET network including nonlinear source resistance. Two sets of simulations were performed: (1) one including a nonlinear source resistance, and (2) one using only a linear source resistance. The intrinsic values for transconductance and capacitance for both cases should be the same as shown in the figures (The extrinsic value for the linear case coincides with the intrinsic value). However, the results differ greatly between the intrinsic and extrinsic value for simulation with nonlinear source resistance. The extrinsic transconductance is degraded largely by nonlinear source resistance, especially at large Vgs, where the conduction current value is high. The bell shape of the curves is one of the impacts of nonlinear source resistance by suppression of the device's gain and introduction of nonlinearity at high current level.

As the degradation term in the denominator in eqn.(3.6) cancels each other, there is no difference in cut off frequency ($f_t = \dfrac{g_m}{2\pi C_{gs}}$) due to nonlinear source resistance. The impact of nonlinear source resistance on the device's high frequency performance is not significant.

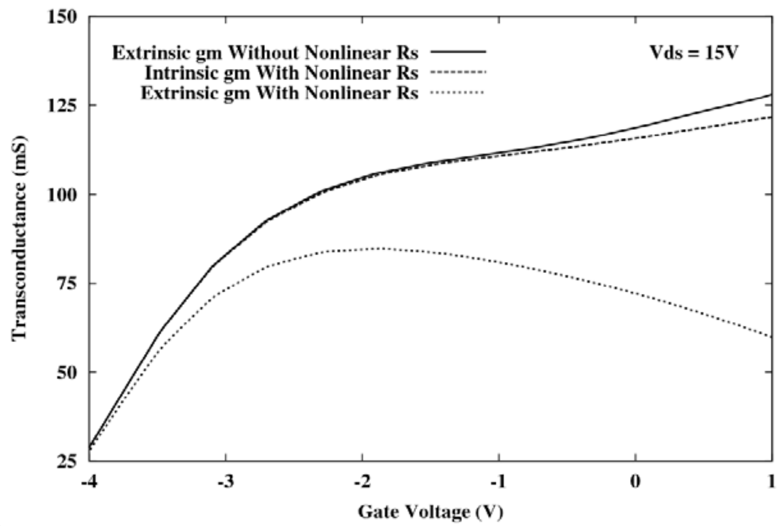

Fig. 3.5 Calibrated transconductance results for 2.14 GHz class-AB AlGaN/GaN HFET power amplifier.

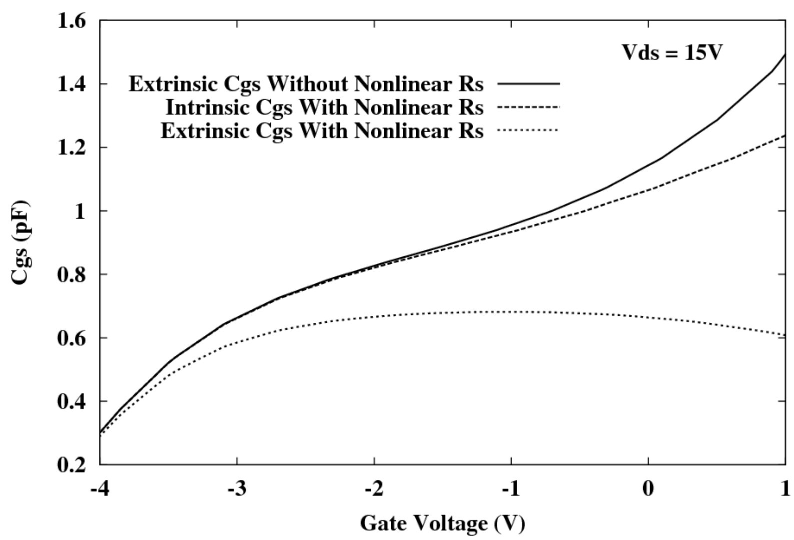

Fig. 3.6 Calibrated capacitance results for 2.14 GHz class-AB AlGaN/GaN HFET power amplifier.

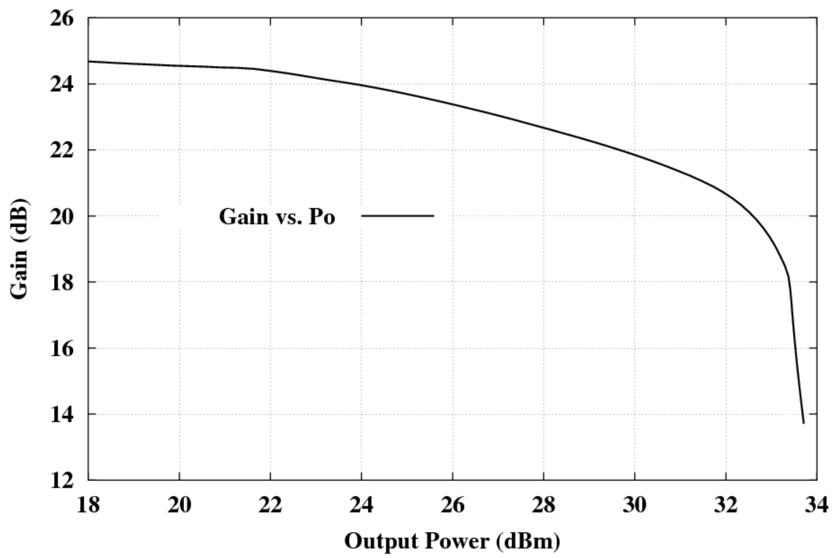

Fig. 3.7 Measured Gain vs. Pout for AlGaN/GaN HFET class A-B PA operated at 2.14 GHz.

An AlGaN/GaN HFET power amplifier exhibits gain compression even at modest drive conditions. The gain curve is flat from the beginning, then it starts to fall off at around Pin = -2dBm (Pout=22dBm) as shown in Fig.3.7. This early distortion behavior is mainly due to the effects of the nonlinear source resistance. As is shown in Fig.3.8, the DC component for nonlinear source resistance starts to increase from Pin = -2dBm.

The nonlinear source resistance is closely related to channel current. The Rs plot has the same shape as DC drain current in Fig. 3.3(a) and both curves unidirectionally increase with input power.

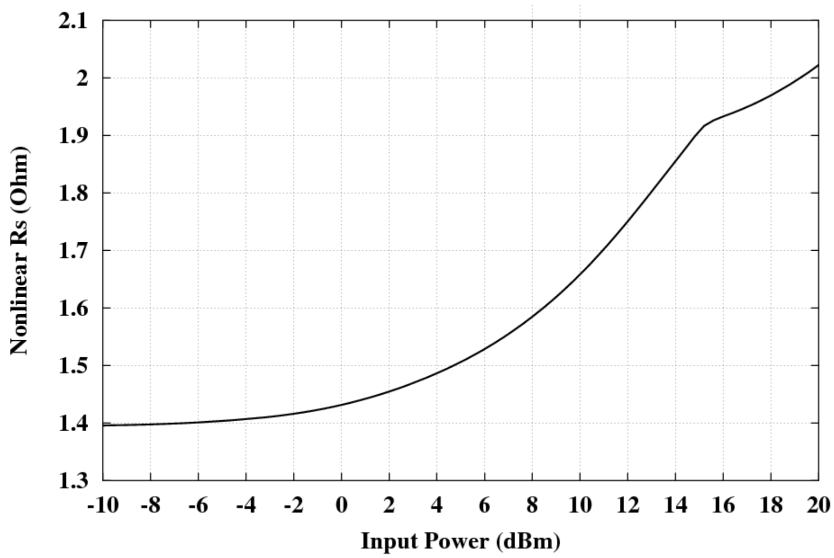

Fig. 3.8 Simulated nonlinear Rs DC component for class A-B AlGaN/GaN PA operated at 2.14 GHz.

The RF dynamic loadlines are plotted on the DC I-V characteristic plane in Fig. 3.9. Dynamic loadlines are shown for drain current at Pin = 0dBm and maxPAE@14dBm. The right axis indicates the nonlinear source resistance magnitude. The device shows RF channel breakdown at Vds = 51V. The two dynamic loadlines indicate that RF breakdown occurs twice in one cycle of operation. The nonlinear source resistance varies from linear value of 1.3 Ohm to a maximum of 2.7 Ohm in each cycle.

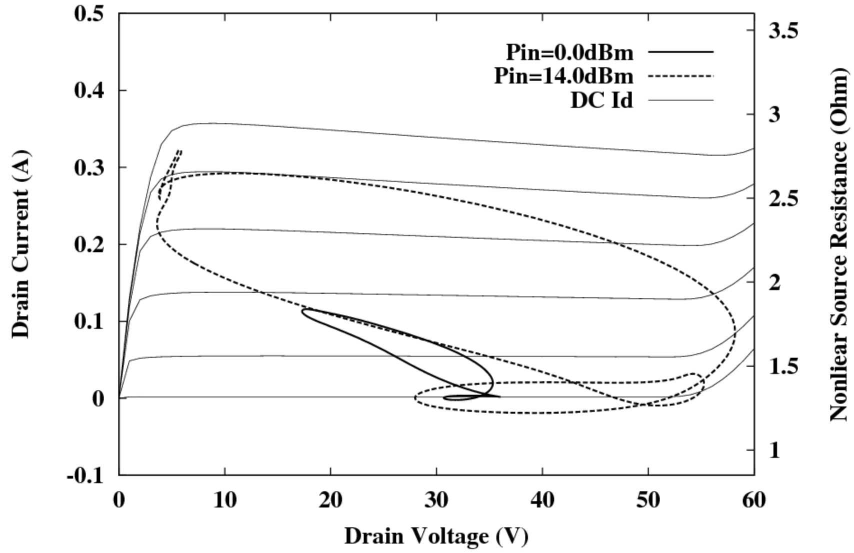

Fig. 3.9 Loadlines of a 2.14GHz class-AB AlGaN/GaN HEFT PA at Pin =0dBm and 14dBm@maxPAE.

The power amplifier's large-signal performance is limited under extremes of RF voltage and current. The nonlinear source resistance dominates in the high current portion of the RF cycle and the RF channel breakdown dominates in the high voltage portion of the RF cycle. RF waveforms for drain current, nonlinear source resistance, drain source voltage, and channel avalanche current at Pin = 0dBm&14dBm@maxPAE are shown in Fig. 3.10.

The nonlinear source resistance affects device's performance even at modest or small signal RF drive levels, as it introduces nonlinear distortion as soon as the device has an RF input signal applied. As is shown in Fig.3.10(b), the waveform for nonlinear source resistance is already distorted at an input power level of 0dBm, which comes from the half wave shape of drain current under class A-B operation.

When the drain-source RF voltage exceeds the channel breakdown voltage, which is 51V for this device, then a breakdown current generator in the drain-source circuit will begin to conduct and a breakdown current will begin to flow. As was shown in Fig.3.10(d), RF channel breakdown only occurs when the output power reaches the saturation point and it starts to limit PA's performance at large signal condition.

Fig. 3.10 Waveform plots for 2.14GHz class A-B AlGaN/GaN HFET Power Amplifier. (a) Drain current (b) Nonlinear source Resistance (c) Drain source voltage (d) Channel avalanche current

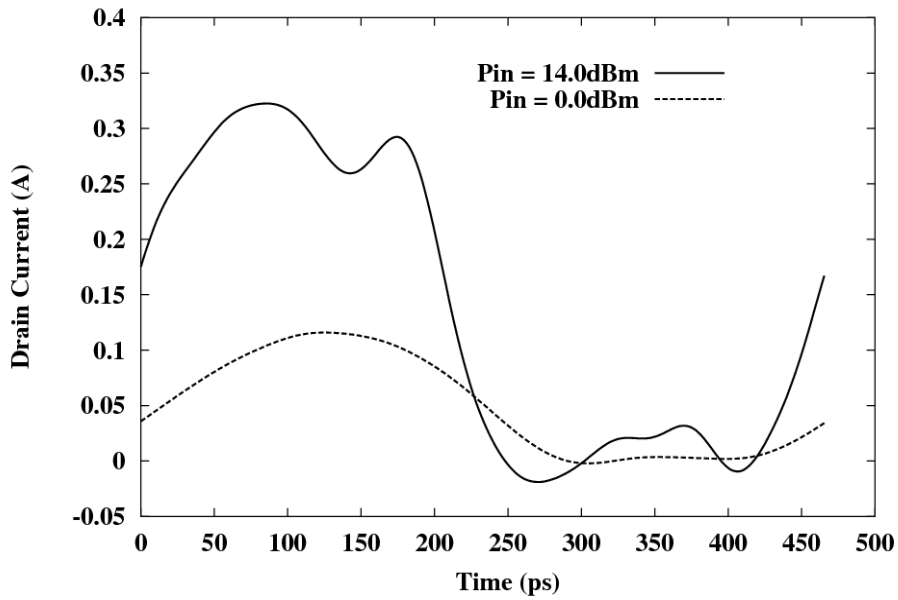

0.4
0.35
0.3
0.25
0.2
0.15
0.1
0.05
0
-0.05
0
50
100
150
200
250
300
350
400
450
500
Drain Current (A)
Time (ps)
Pin = 14.0dBm
Pin = 0.0dBm

(a)

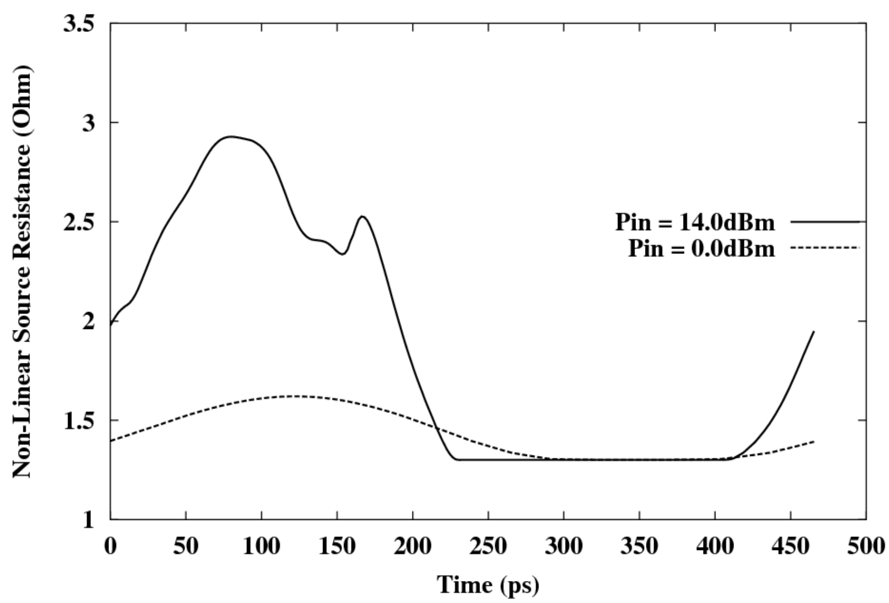

3.5
3
2.5
2
1.5
1
0
50
100
150
200
250
300
350
400
450
500
Non-Linear Source Resistance (Ohm)
Time (ps)
Pin = 14.0dBm
Pin = 0.0dBm

(b)

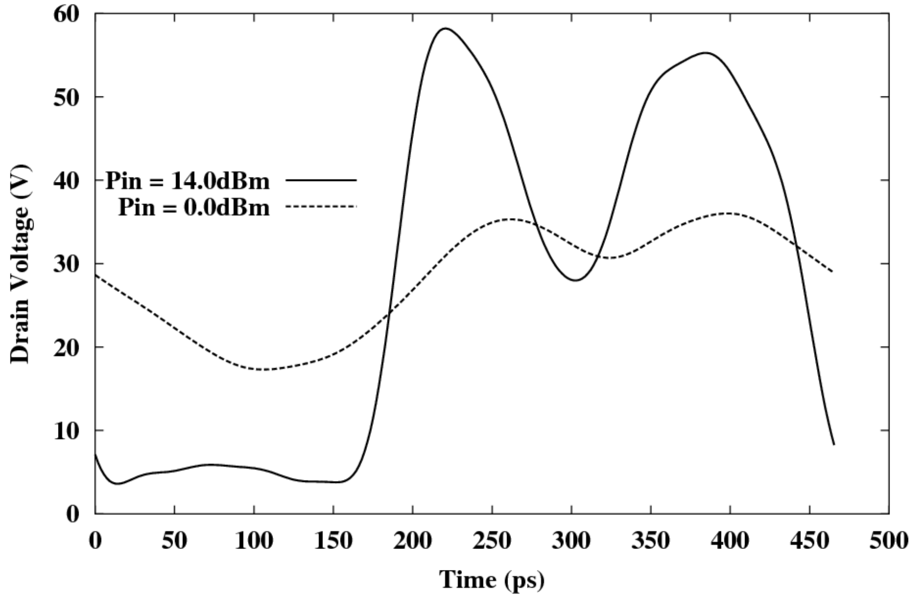

60
50
40
30
20
10
0
Drain Voltage (V)
Pin = 14.0dBm
Pin = 0.0dBm
0
50
100
150
200
250
300
350
400
450
500
Time (ps)

(c)

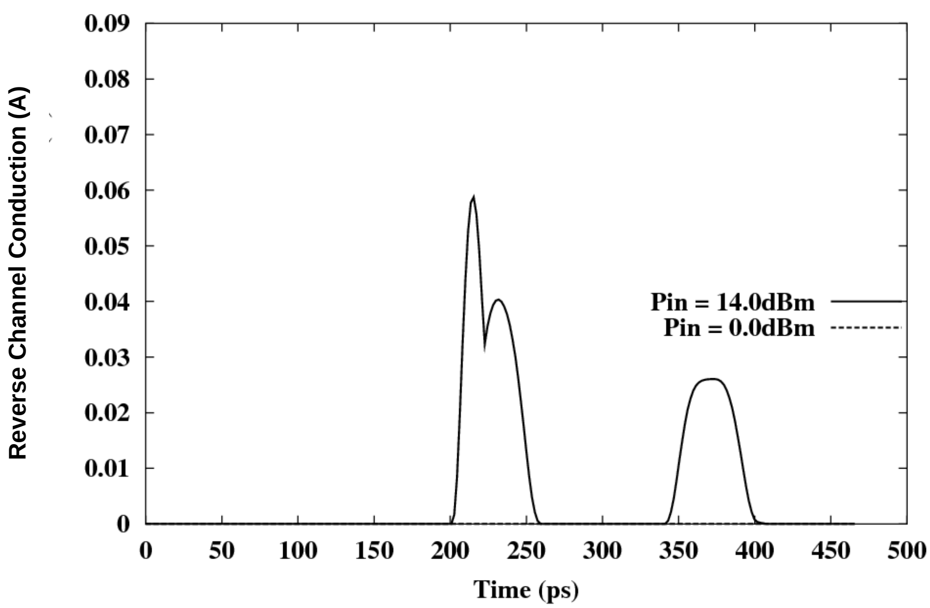

0.09
0.08
0.07
0.06
0.05
0.04
0.03
0.02
0.01
0
Reverse Channel Conduction (A)
Pin = 14.0dBm
Pin = 0.0dBm
0
50
100
150
200
250
300
350
400
450
500
Time (ps)

(d)

3.4.2 Device A Operates at 38V & 48V

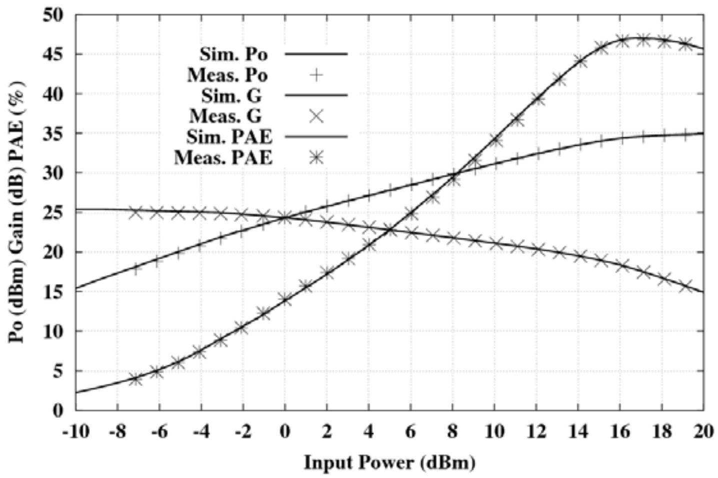

(a)

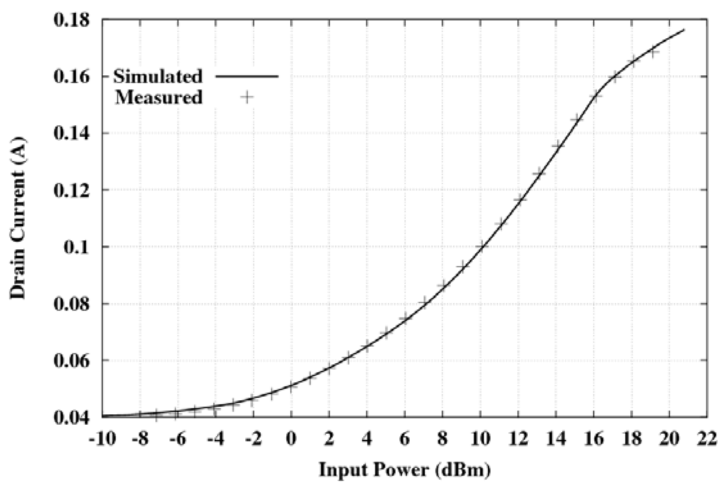

(b)

Fig.3.11 Calibrated RF results (a) and Id DC component (b) for a 2.14 GHz Class A-B AlGaN/GaN HFET PA biased at Vds = 38V.

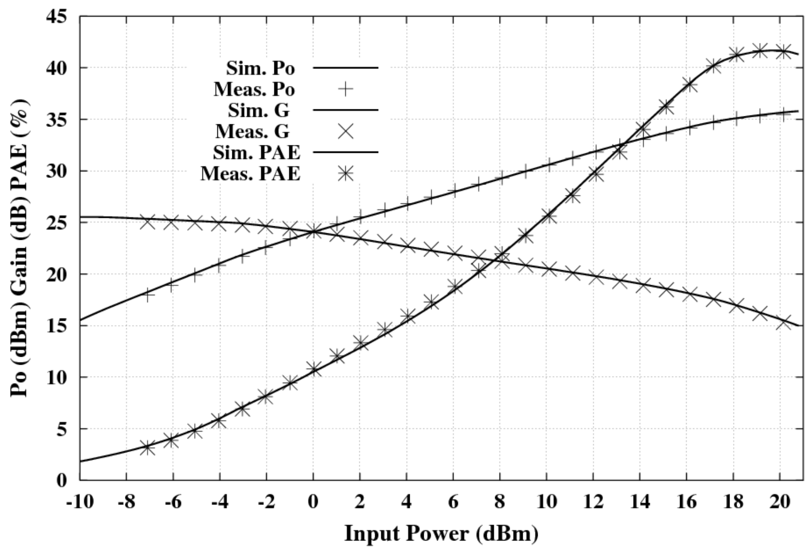

(a)

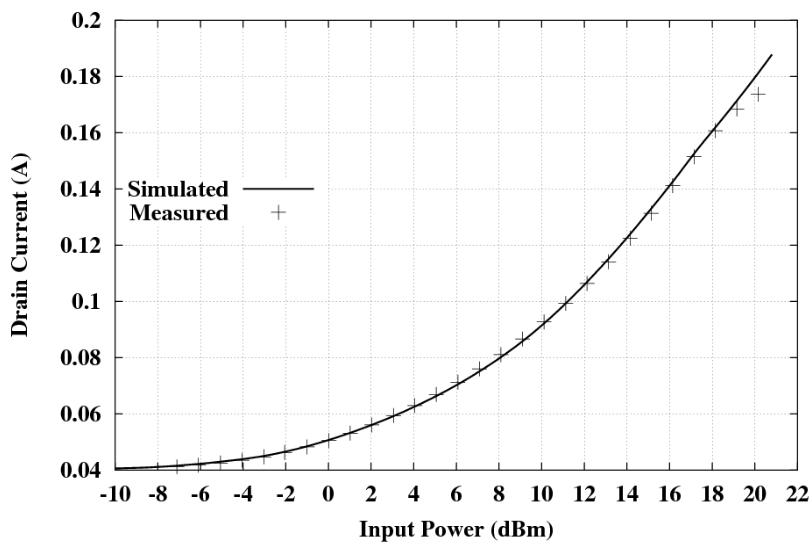

(b)

Fig. 3.12 Calibrated RF results (a) and Id DC component (b) for a 2.14 GHz Class A-B AlGaN/GaN HFET PA biased at Vds = 48V.

Fig. 3.11 and Fig. 3.12 are the measured and simulated RF results for the same 2.14 GHz AlGaN/GaN HFET amplifier operating at Vds = 38V and 48V. The results have verified the accuracy of the physics based model.

3.4.3 Device B ($Lg = 0.2\mu m$, $f_0 = 10GHz$)

Fig. 3.13 shows the calibrated RF results for a 10 GHz AlGaN/GaN HFET power amplifier. The threshold for SCL effect and RF channel breakdown voltage for this device were calibrated as 0.3A and 40V, respectively. Only three harmonics were calculated during harmonic balance simulation. The simulation results have accurately repeated the measured data.

Fig. 3.13 Calibrated RF results (a) and Id (b) & Ig (c) DC component for a 10 GHz AlGaN/GaN HFET PA.

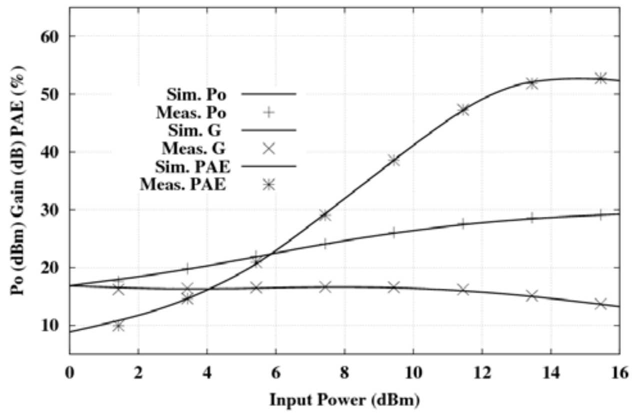

Po (dBm) Gain (dB) PAE (%)
Sim. Po
Meas. Po
Sim. G
Meas. G
Sim. PAE
Meas. PAE
Input Power (dBm)

(a)

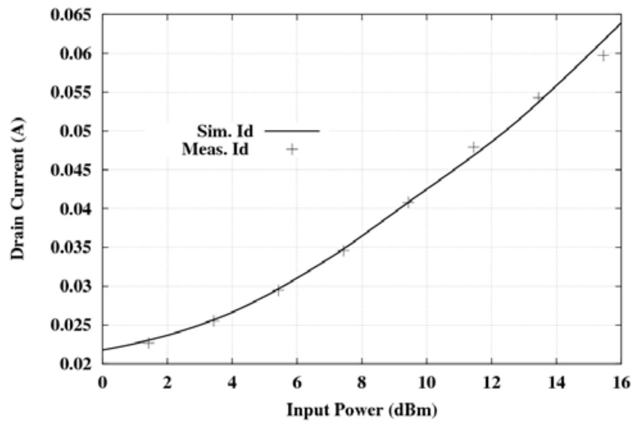

Drain Current (A)
Sim. Id
Meas. Id
Input Power (dBm)

(b)

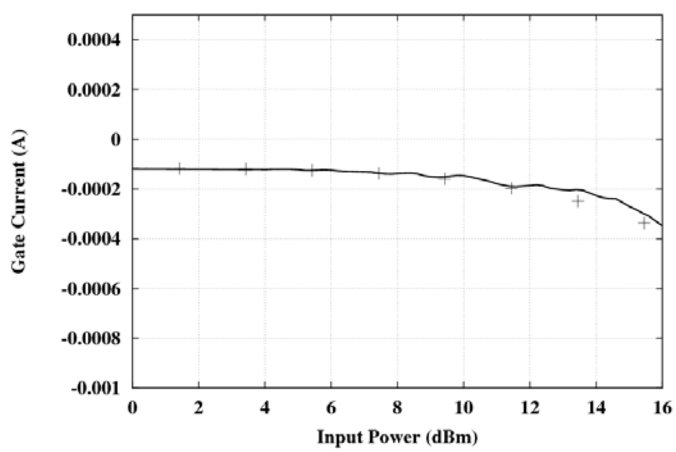

Gate Current (A)
Input Power (dBm)

(c)

3.4.4 Device C ($Lg = 0.2\mu m$, $f_0 = 40GHz$)

Fig.3.14 is the calibrated RF results for a 40 GHz AlGaN/GaN HFET power amplifier. The threshold for the SCL effect and RF channel breakdown voltage for this device were calibrated as 0.6A and 30V, respectively. Only three harmonics were calculated during harmonic balance simulation. The simulation results have accurately repeated the measured data.

Fig. 3.14 Calibrated RF results (a) and Id (b) & Ig (c) DC component for a 40 GHz AlGaN/GaN HFET PA.

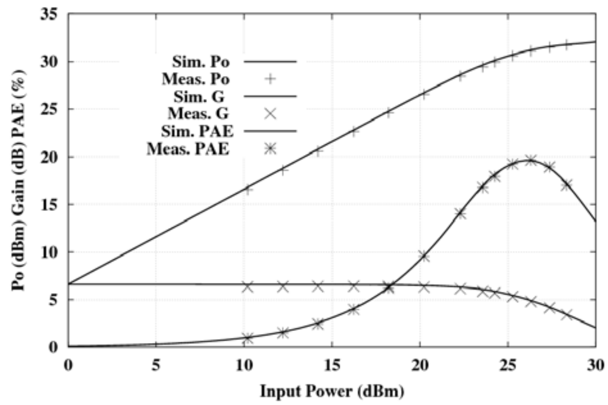
Sim. Po
Meas. Po
Sim. G
Meas. G
Sim. PAE
Meas. PAE
Po (dBm) Gain (dB) PAE (%)
Input Power (dBm)

(a)

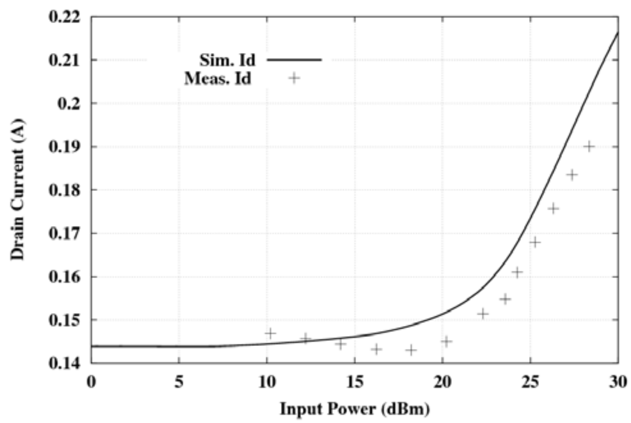
Sim. Id
Meas. Id
Drain Current (A)
Input Power (dBm)

(b)

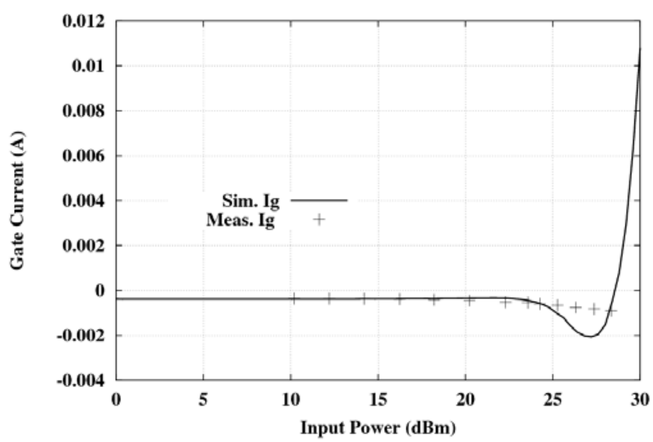
Sim. Ig
Meas. Ig
Gate Current (A)
Input Power (dBm)

(c)

3.5 Simulation results with different VBD and Isc value

An easiest way to see the impact of nonlinear source resistance and RF channel breakdown is by changing the threshold for SCL effect and breakdown voltage during simulation.

3.5.1 Simulation results with different threshold value for SCL effect

Fig. 3.15 are the RF simulation results for device A operated at Vds = 28V with fundamental frequency of 2.14 GHz. The threshold value for SCL effect was set to be 0.3A and 0.63A in the simulation. Both PAE and power gain are improved by increased Isc value from 0.30 A to 0.63 A.

The loadline simulation results shown in Fig. 3.16 explain the reason of the improvement. As the threshold value for SCL effect is increased, the amplifier could reach at a higher maximum current, which implies that device saturates at a larger output power level and better PAE could be achieved. Another advantage of increasing threshold current for SCL is nonlinearity reduction at high current region. This topic is discussed in detail in chapter 4.

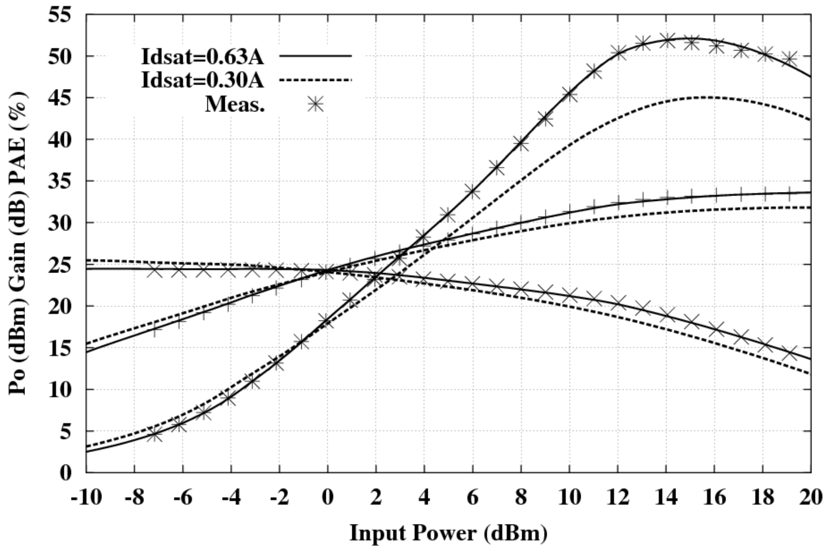

Fig. 3.15 Comparison RF simulation results for a 2.14GHz class AB AlGaN/GaN HFET PA with SCL threshold current value of 0.3A and 0.63A.

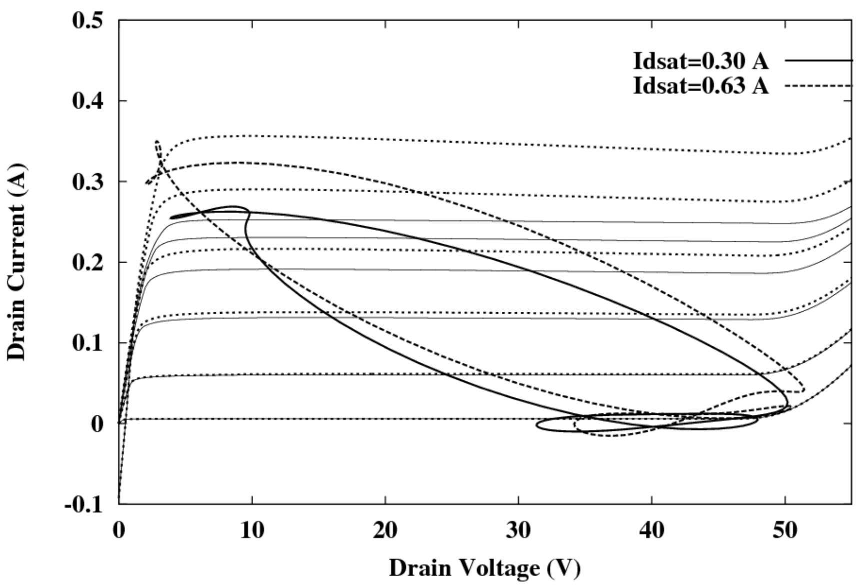

Fig.3.16 RF Loadlines for AlGaN/GaN HFET PA with SCL threshold current value of 0.3 A and 0.63 A at Pin = 14dBm@maxPAE.

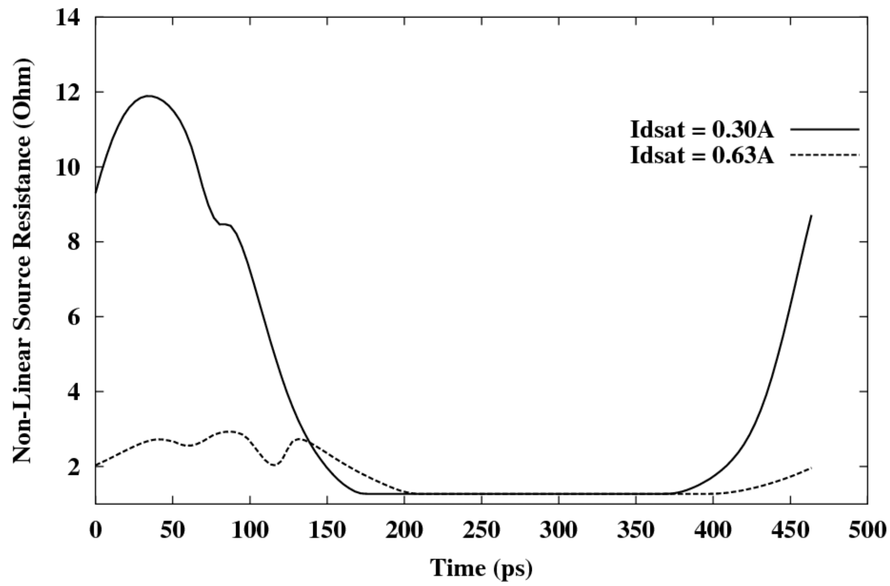

Fig.3.17 Nonlinear source resistance waveforms for a 2.14 GHz AlGaN/GaN HFET PA with SCL threshold current value of 0.3A and 0.63A, at Pin = 14dBm@maxPAE.

Fig.3.17 shows a dramatically decrease in nonlinear source resistance at Pin = 14dBm by increasing the SCL threshold current value.

3.5.2 Simulation results with different channel breakdown voltage

The limiting effects upon RF performance due to avalanche breakdown in the channel can be seen by simulation permitting the magnitude of the channel breakdown voltage to vary. Fig. 3.18 is a set of simulation of Device A with breakdown voltage being varied from 44V to 51.5V. The dynamic loadline analysis at Pin = 14dBm in Fig. 3.19 exhibits increase of maximum Vds at saturated output power, which pushes device to operate at a higher PAE and Pout as shown in Fig. 3.18.

The simulation with variable breakdown voltages for Device C operating at 40GHz is shown in Fig.3.20 and Fig. 3.21. The same improvement trend of RF performance for this device is seen by increase of channel breakdown voltage. Fig.3.22 is the reverse channel avalanche current at different breakdown voltages. As shown in the Fig.3.22, a larger breakdown voltage corresponds to less avalanche breakdown in the channel, and a smaller reverse conduction current.

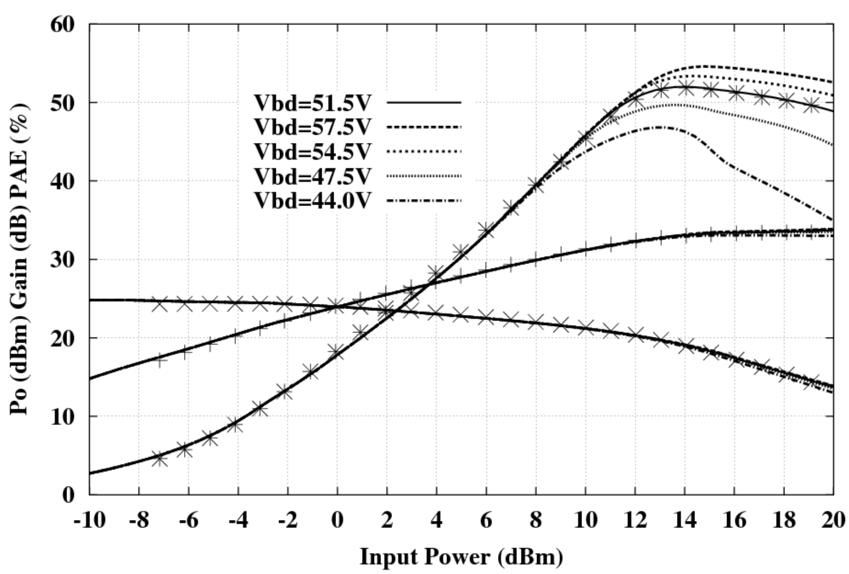

Fig. 3.18 Comparison RF simulation results for a 2.14GHz class AB AlGaN/GaN HFET PA with different channel breakdown voltages.

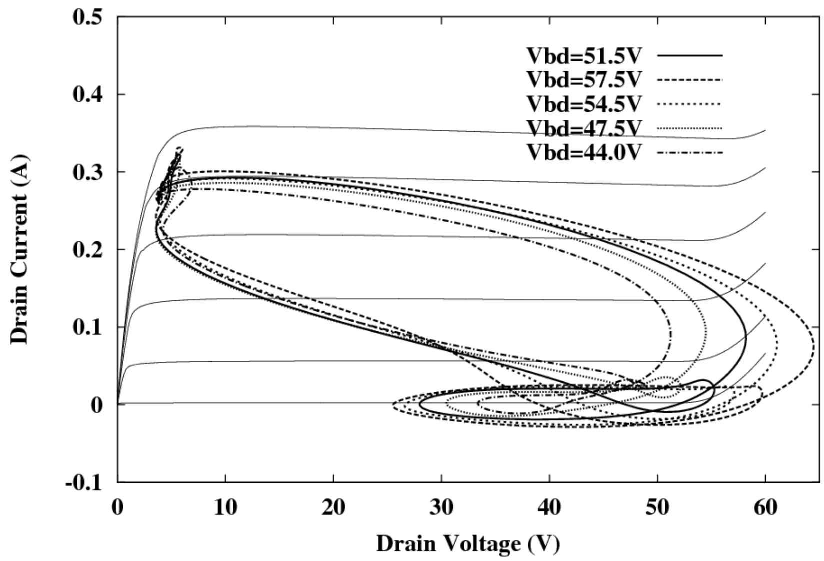

Fig. 3.19 RF Loadlines for a 2.14 GHz AlGaN/GaN HFET PA with different channel breakdown voltages at Pin = 14dBm.

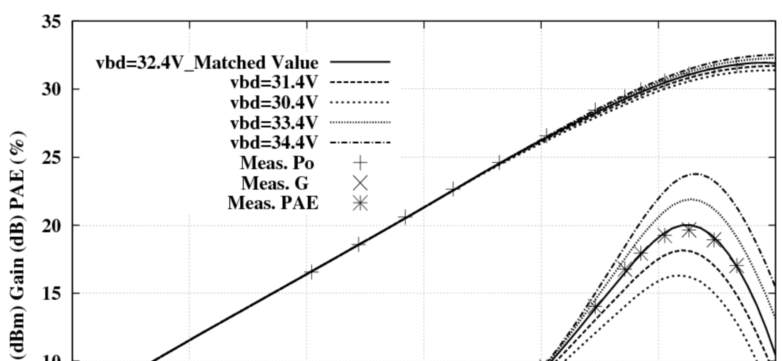

Fig. 3.20 Comparison RF simulation results for a 40GHz AlGaN/GaN HFET PA with different channel breakdown voltages.

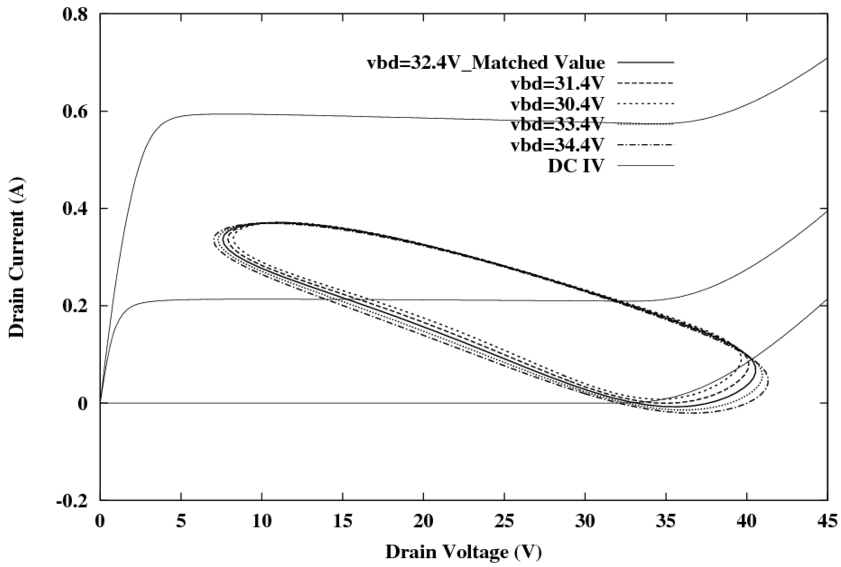

Fig. 3.21 RF Loadlines for a 40 GHz AlGaN/GaN HFET PA with different channel breakdown voltages at Pin = 26 dbm.

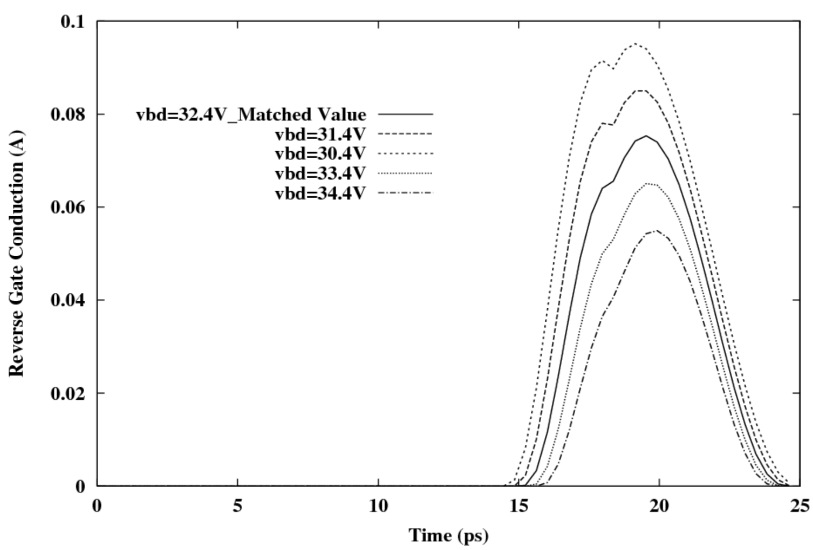

Fig. 3.22 Reverse channel conduction waveforms for a 40 GHz AlGaN/GaN HFET PA with different channel breakdown voltages, at Pin = 26dBm.

3.6 Summary

This chapter discusses in detail the incorporation of a nonlinear source resistance and RF channel breakdown in the physics based FET model. The simulation results for different AlGaN/GaN HFET devices operating at different bias, and fundamental frequency have verified the accuracy of the model. RF performance of AlGaN/GaN HFETs under large signal operation is limited by RF channel breakdown at high voltage operation and by nonlinear source resistance at high current operation. Improvement in RF operation is indicated in the simulation results by increasing the channel breakdown voltage and the threshold current level for nonlinear source resistance. The above results have verified that the two mechanisms are major factors that limit device's performance and present the possibility of improvement through the reduction of both effects.

REFERENCES

[1] M.A.Khatibzadeh and R.J.Trew,"A large-signal analytic model for the GaAs MESFET,"IEEE Trans. Microwave Theory and Techniques, vol. 36, pp.231-238, 1988

[2] T.A. Winslow and R.J. Trew, "Principles of Large-Signal MESFET Operation," *IEEE Trans. Microwave Theory Tech.*, vol. 42, pp.935-942, June 1994.

[3] Caughey, D.M., and R.E. Thomas. "Carrier Mobilities in Silicon Empirically Related to Doping and Field." *Proc. IEEE,* 55, 2192-2193, 1967.

CHAPTER 4

4.1 Overview

In this chapter the linearity performance of AlGaN/GaN HFETs is investigated for the first time with the use of a physics-based large-signal RF model for an AlGaN/GaN HFET embedded in a harmonic-balance circuit simulator [1]. The model has been modified for multi-frequency performance and the IMD spectrum is calculated. The physics-based device model for the first time permits determination of the RF and IMD performance of the device as a function of device design, bias, and circuit parameters.

The nonlinear source resistance results from the onset of space-charge limited (SCL) current within the conducting channel of the transistor. It has been demonstrated that the nonlinear source resistance modulation degrades the linearity of the device [2,3], even under modest RF drive conditions.

This chapter addresses the IMD behavior and phase distortion for a microwave power AlGaN/GaN HFET operating at 2.14GHz. IMD characteristics versus drive and nonlinear source resistance are studied. It is shown that the linearity of the amplifier can be optimized by careful selection of the gate-source spacing. An optimized Lsg spacing is determined to achieve a minimum IMD at a specified input power level.

The simulated IMD results are compared to experimental data and good agreement is obtained. The simulation results of IM3 variation at different bias condition versus space charge limit threshold are presented. Different impacts of nonlinear source resistance on IMD product were observed under small signal conditions. Both the simulation and theoretical analysis show a constant degradation of IMD with nonlinear source resistance under large signal operation. It is also shown that the nonlinear source resistance has larger impact on phase distortion than nonlinear drain resistance.

In order to achieve an accurate intermodulation simulation, the physics based large signal model was modified to run simulations under multi-tone signal generation. With the additional multi-frequency simulation capability, the large signal physics model was used to study the device linearity performance under multi tone and wide band signal condition. An improvement of intermodulation behavior was seen from the results of 4-tone simulation as the nonlinear source resistance is decreased through adjusting Lsg spacing and Isc (threshold current value for SCL effect) values. The effect of nonlinear source resistance on spectral regrowth for a WCDMA signal is also shown in this chapter. Improvement of ACPR (Adjacent Channel Power Ratio) was shown in the simulation by decreasing source resistance modulation. No obvious variation has been shown in the simulation when breakdown voltage is changed.

4.2 Nonlinearity analysis with nonlinear source resistance using polynomial model

In this section, the nonlinear distortion due to nonlinear source resistance is analyzed based upon a polynomial analysis. Under large signal operation, the onset of SCL transport induces a nonlinear source resistance in AlGaN/GaN HFET's due to high current injection [4].

Based upon polynomial analysis, it is shown that the extrinsic and third order transconductance due to nonlinear source resistance are expressed as [2]:

$$g_{mext1} = \frac{g_{mi1}}{1 + g_{mi1} r_1} \tag{4.1}$$

and

$$g_{mext3} \cong \frac{g_{mi3}}{(1 + g_{mi1} r_1)^4} - \frac{g_{mi1}^4 r_3}{(1 + g_{mi1} r_1)^4} \tag{4.2}$$

where

$$r_1 = \frac{r_{ss}}{(1 - \frac{I}{I_{sc}})^2} \tag{4.3}$$

and

$$r_3 = \frac{6 r_{ss}}{(1 - \frac{I}{I_{sc}})^4} \cdot \frac{1}{I_{sc}^2} \tag{4.4}$$

Since both r_1 and r_3 increase rapidly as current increases, the extrinsic transconductance decreases very fast because of the degradation factor $1+g_{mi1}r_1$. The third order transconductance is comprised of two components: The first part comes from the source degeneration; and the second part comes from nonlinear source resistance. As the current approaches the threshold for SCL current transport (indicated as *Isc*), the nonlinear part will dominate the third order term, and a rapid increase in g_{mext3} results. It follows that harmonic distortion due to the nonlinear source resistance increases rapidly as the device is driven into large-signal operation.

The input third order intercept point (IIP3) can be written as [5]:

$$IIP3 = \sqrt{\frac{4}{3}\left|\frac{g_{mext1}}{g_{mext3}}\right|} \tag{4.5}$$

The IIP3 is reduced due to the effect of the nonlinear source resistance. As shown in eqn.(4.2) and eqn.(4.5), the IIP3 could be improved by reducing r_{ss} or increasing the *Isc* magnitude. The former method could be realized through reducing Lsg spacing, and the latter could be realized through increasing the 2DEG concentration.

Generally, the 3rd order IMD product is determined by g_{mext3} according to the following equation [5]:

$$i_{out}(2\omega_2 - \omega_1) \cong \frac{3}{4} g_{mext3} v_{in}^3 \tag{4.6}$$

And the gain is determined by g_{mext1} and g_{mext3} as follows [6]:

$$i_{out}(\omega) = g_{mext1} v_{in} + \frac{3}{4} g_{mext3} v_{in}^3 \tag{4.7}$$

Under small signal operation, the RF gain usually shows a moderate gain compression or expansion phenomenon [6]. It starts from $g_{mext1}R_L$ and a gain compression results, when $g_{mext3}<0$, or gain expansion results, when $g_{mext3}>0$. Then a significant gain compression follows when the device is driven into large signal operation due to the large signal distortion mechanisms, which results in a negative g_{mext3}. Accordingly, the g_{mext3} changes from positive value to negative when gain expansion appears, which presents a null IMD at an intermediate signal level (large signal IMD sweet spot [7]), from eqn.(4.2). It usually occurs for a device biased into class-AB, and shows an abrupt decrease in IM3 at certain input power level. It enhances the PA linearity when the device is operated close to the sweet spot. Compared to the input back-off technique to improve the amplifier linearity, the IM3 notch bias can improve the power-added efficiency when it occurs at the 1-dB compression point. The IM3 notch is due to the compensation between the small signal and large signal distortion mechanisms. The location of the sweet spot is a function of bias, the tuning of the matching network, the device structure, and also the distortion mechanism.

The nonlinear source resistance has a great impact on IMD behavior according to eqn.(4.2). Under small signal operation conditions, depending on the bias and tuning, the nonlinear source resistance could either decrease or increase the IM3. For a device with gain compression, the original g_{mi3} is negative, and the second term in eqn.(4.2) adds to the first term, which degrades the IMD product. For a device with gain expansion, the original g_{mi3} is positive, and the second term in eqn.(4.2) subtracts from the first term, which improves the IMD product. However due to the more negative term in eqn.(4.2), the IMD sweet spot is moved from large signal to small signal level, and the PAE advantage is therefore reduced. On the other hand, for large signal conditions, the IM3 is degraded by the nonlinear source resistance regardless of the bias and tuning factors. The bias and nonlinear source resistance dependence of the IMD product will be addressed in detail in section 4.4.

In the extreme case, where the second term in eqn.(4.2) is large enough that its value dominants in the equation, the g_{mext3} remains negative regardless of the bias condition and tuning, and the null IMD point disappear due to this effect.

4.3 Nonlinearity simulation

A physics based large signal model was used to study the nonlinearity effect with source resistance modulation. The model was modified to include multi-tone simulation capability in order to predict the IMD behavior accurately. Current techniques used to analyze intermodulation performance are transient envelope analysis [8], volterra-series [9], or spectral balance [10]. As the original physics based model implemented Harmonic Balance technique to perform RF simulation, the most efficient way to add on the multi frequency simulation feature is to develop an algorithm that is based on Fourier Transform and Harmonic Balance methods. After a thorough research on the nonlinearity analysis tools for nonlinear circuit, a novel Fourier Transform method especially for closely spaced frequency generation [11] is used in the model. The new model is the first physics based large signal FET model that is able to run simulation under wide band signal generation.

4.3.1 One tone and two tone simulation for a 40GHz device

Fig. 4.1 and Fig.4.2 show the simulation results for a 40GHz device under one tone and two tone generation. Fig. 4.1 shows the variation of 1dB gain compression point under one tone generation and 3^{rd} order intermodulation term under two tone generation at Pin = 20dB, where the maximum PAE is located. Improvement of linearity can be seen from both the decrease of IM3 and increase of 1dBCP as Lsg spacing reduces.

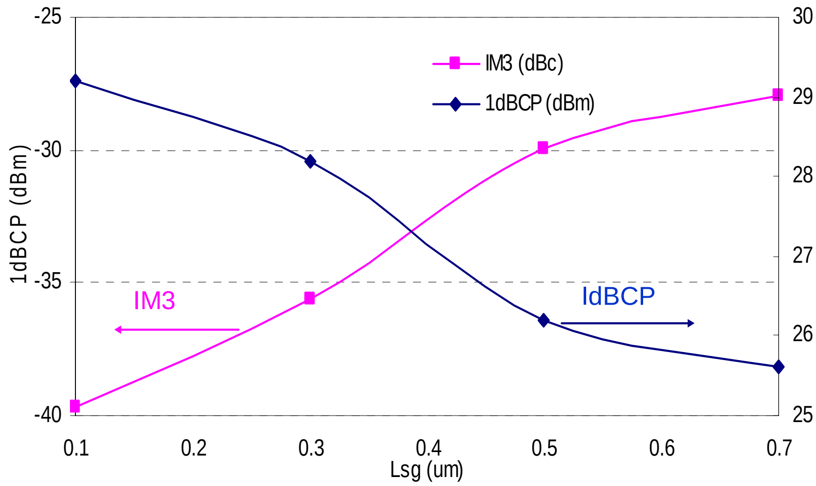

Fig. 4.1 Simulation results of 1dBCP under one tone and IM3 under two tone generation when Lsg changes from 0.1μm to 0.7μm for a 40GHz AlGaN/GaN device.

Fig. 4.2 shows the results of 1dBCP when breakdown voltage increases from 27V to 38V. It shows that breakdown mechanism has a great impact on device linearity under large signal operation conditions. Linearity is improved when there is less breakdown occurring in the conducting channel. From load line point of view, the larger breakdown voltage leaves more room for the device to operate before it reaches the saturation region.

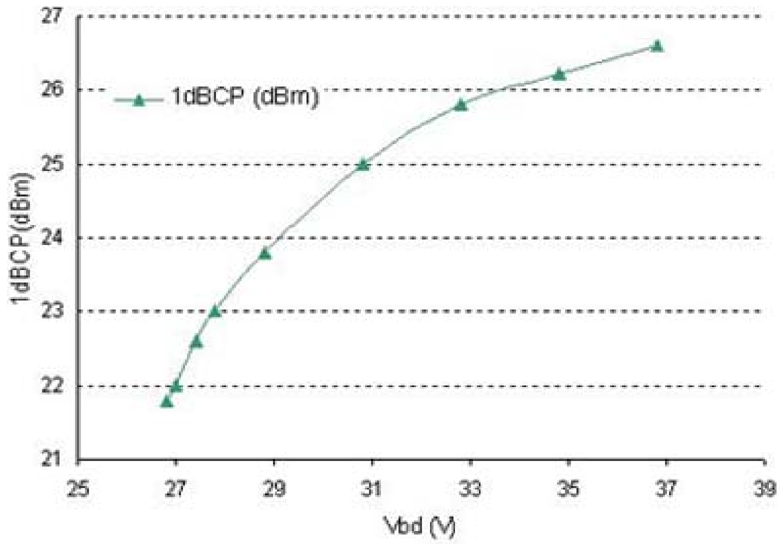

Fig. 4.2 1dBCP simulation results with breakdown voltage varied from 27V to 38V for a 40GHz AlGaN/GaN device.

4.3.2 Simulation with source resistance modulation for a 2.14GHz device

The simulations reveal the existence of a nonlinear source resistance, as shown in Fig. 4.3, which shows the real-time nonlinear source resistance for a 2.14GHz device biased at three drain voltages, Vds=28, 38, and 48V. As shown, the nonlinear source resistance increases with drain bias. The following are nonlinearity simulation results for this 2.14 GHz AlGaN/GaN device.

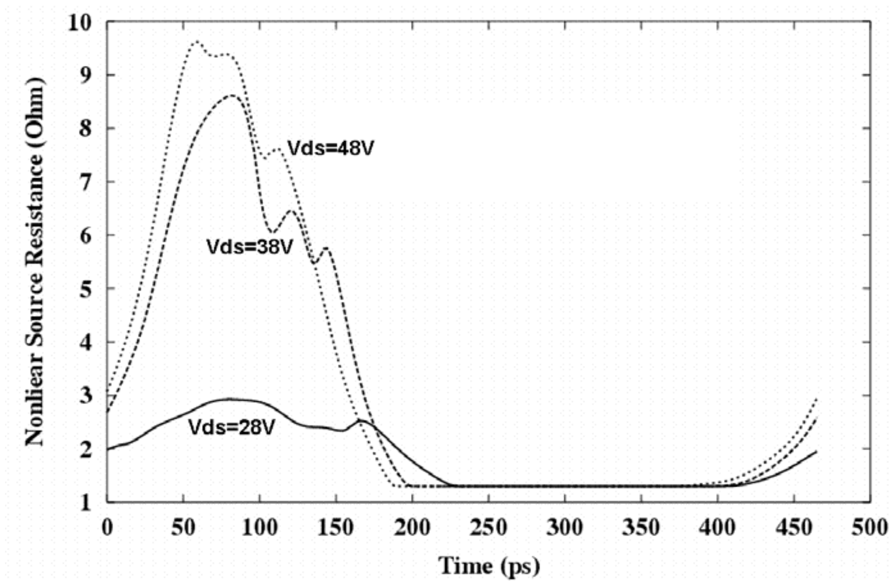

Fig. 4.3 Nonlinear source resistance real time waveforms versus drain bias, for Pin adjusted to obtain maximum power-added efficiency for a 2.14GHz AlGaN/GaN device.

The IMD behavior due to nonlinear source resistance is calculated and the results are shown in Fig. 4.4. At small and modest RF drive conditions, the device with the smaller nonlinear source resistance (i.e., Vds=28V) generates less nonlinear distortion, as expected, and improved linearity results. When the device is driven harder, tuning and other distortion mechanisms start to dominate, and the order of IM3 reverses between the device biases, with the lowest IM3 obtained with the drain bias set to Vds=48V. The exact reasons causing this reversal are investigated. Communication amplifiers are generally operated under modest drive condition and the input signal power is backed off from the 1dB compression point. At this signal level, the nonlinear source resistance is still sufficiently large to cause nonlinear distortion and limit the device linearity, as shown in Fig.4.3.

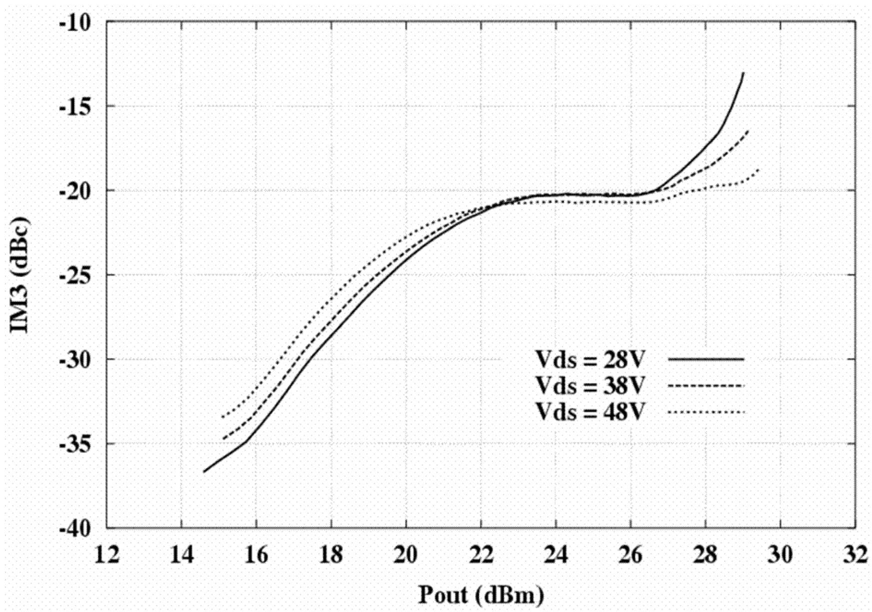

Fig. 4.4 Simulated IM3 variation for devices with different nonlinear source resistance and drain bias for a 2.14 GHz AlGaN/GaN device.

The simulated and measured IM3 versus DC current bias for the device biased at Vds=28V are shown in Fig.4.5 and Fig.4.6, respectively. The measured data in Fig.4.5 [12] is for a device with the same structure, but with an increased gate width.

Under small and modest drive conditions, the IMD is improved as current bias increases and the device is driven towards class-A operation. Under these conditions the nonlinearity is dominated by small signal distortion mechanisms. The curves tend to converge together as the device is driven harder, and the nonlinear distortion starts to be dominated by large signal operation mechanisms such as RF channel breakdown and the nonlinear source resistance.

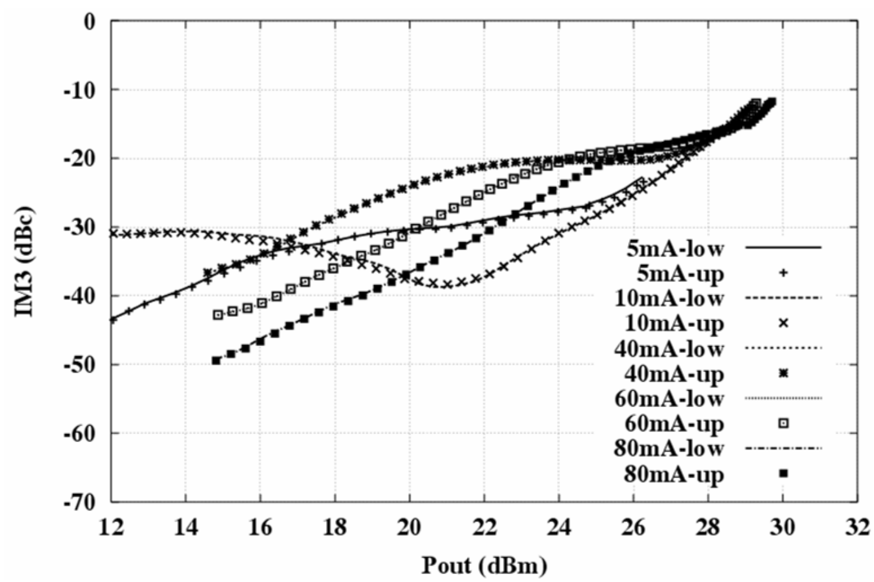

Fig. 4.5 Simulated IM3 variation versus current bias for class-AB 2.14 GHz AlGaN/GaN HFET amplifier.

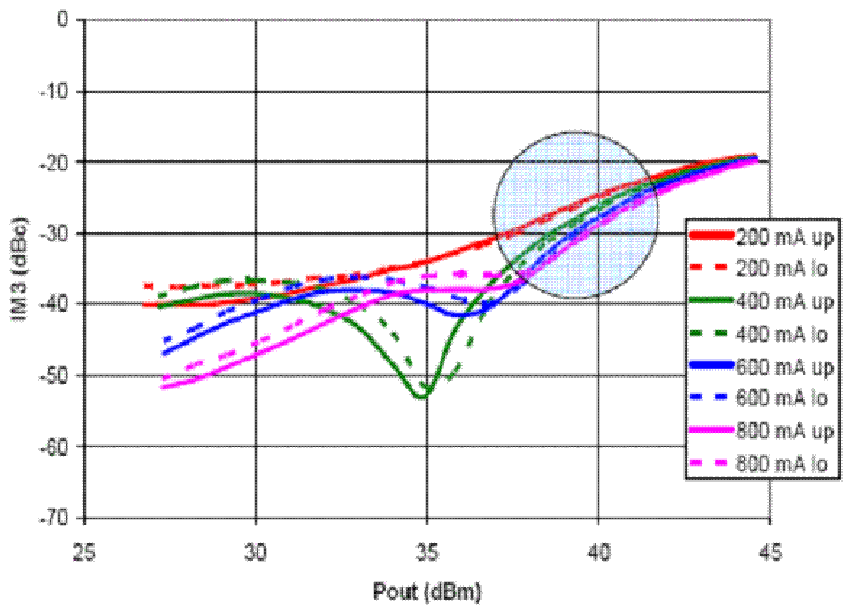

Fig. 4.6 Measured IM3 variation versus current bias for class-AB 2.14 GHz AlGaN/GaN HFET amplifier [12].

Both the measured and simulated IMD results show a notch versus input power for specified current bias, which is sometimes called the large signal IMD sweet spot [7], and usually occurs for a device biased into class-AB. It enhances the PA linearity when device is operated close to the sweet spot. Compared to the input backoff technique to improve the amplifier linearity, the IM3 notch bias can improve the power-added efficiency when it occurs at the 1-dB compression point. The IM3 notch is due to the compensation between the small signal and large signal distortion mechanisms. The location of the sweet spot is a function of bias, the tuning of the matching network, the device structure, and also the distortion mechanism.

The nonlinear source resistance can be modulated by changing Lsg spacing in the HFET. The effect is demonstrated by simulating the IM3 for the same device with various Lsg spacing values. Four Lsg values: 1.6μm, 0.8μm, 0.4μm and 0.2μm, were simulated and the results of the simulations are compared in Fig. 4.7.

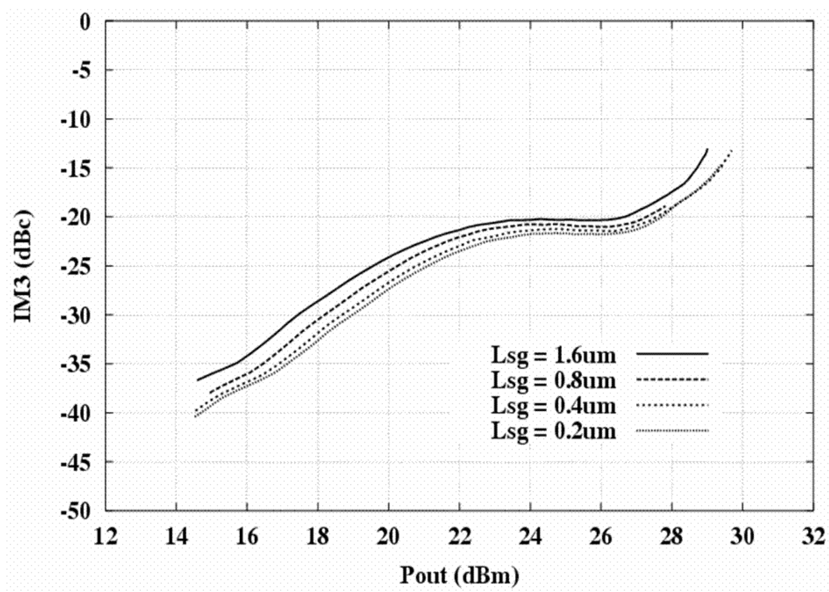

Fig. 4.7 Simulated IM3 variation versus Lsg spacing for class-AB 2.14 GHz AlGaN/GaN HFET amplifier.

The results reveal improved IMD for reduced Lsg spacing, due to a reduction in the nonlinear source resistance. However, an optimum Lsg spacing is observed to exist. This occurs due to tradeoffs between the impact of the nonlinear source resistance and the conventional nonlinearity mechanisms in the device, circuit tuning, etc. For the device under investigation the improvement in IMD is maximum for a Lsg of 0.4μm under small and modest RF drive operation. For higher drive levels the optimum Lsg is 0.8μm. The reason that the optimization saturates is because the nonlinear source resistance is decreased to a small enough level such that other nonlinear mechanisms start to dominate. Further reduction in the Lsg spacing produces limited linearity improvement.

4.3.3 Multi tone simulation

Following is a set of simulation results for a 2.14 GHz device under 4-tone signal generation using the physics base model. Fig. 4.8 shows the result when the intermodulation is simulated under four equal sinusoidal signals with output power magnitude Pout at 14dBm. The frequency spacing is 3MHz with the center frequency at 2.14 GHz. Spectrum in the adjacent shoulder region to the main channel is the major source that contributes to the spectral regrowth under wide band signal. It mainly comes from the 3rd and 5th order intermodulation terms. Higher order intermodulation terms may come into the adjacent channel when the signal is increased to a large enough level. Under wide band signal generation, linearity is the major concern for receiver and transceiver design. Power amplifier is usually chosen to operate several dBm back off from maximum PAE to guarantee a linear operation, Therefore the signal level in simulation was chosen mainly in small signal regions, where Pout = 14dBm and 19 dBm. The following simulation will show how the spectrum changes when the nonlinear source resistance varies by changing the Lsg spacing and space charge limited current value (Isc).

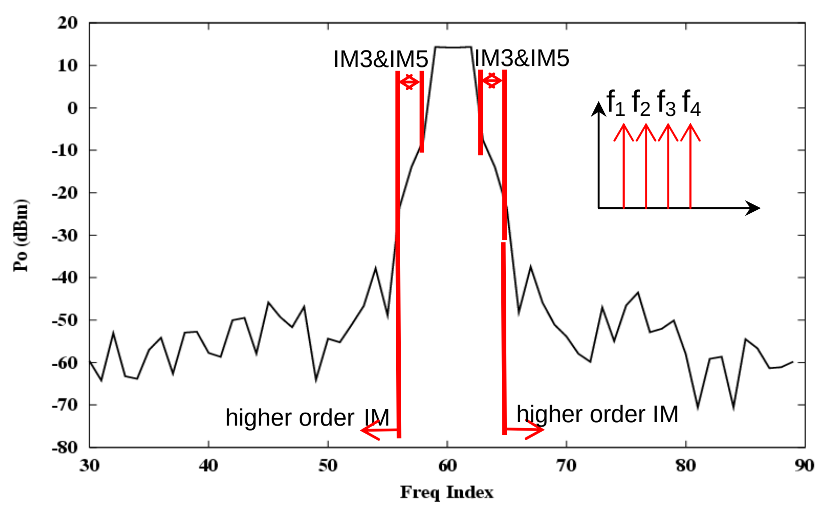

Fig. 4.8 Spectrum simulation results under four equal sinusoidal signals when Pout = 14 dBm.

Fig. 4.9 shows the multitone simulation results when the space charge limited current threshold value increases from 0.40 A to infinity. The spectrum in adjacent channel is 18 dBc when Isc = 0.4 A, and increases to 24dBc when the source resistance becomes pure linear, which is the case when Isc is close to infinity. The simulation results demonstrate an improvement in spectral regrowth when the nonlinear source resistance effect is decreased. It shows a 6dB improvement on the spectrum density in the adjacent channel by increasing Isc value.

Fig. 4.10 is a set of simulation for the same device with Lsg varying from 0.25um to 1.6um at Pout = 19 dBm. The space charge limited current threshold value (Isc) in the simulation is set to be 0.56A. Power density in adjacent channel is about 18dBc when Lsg =1.6um and increased to 24dBc when Lsg = 0.25um. In this simulation, the nonlinear source resistance is reduced through decreasing the linear resistance at small signal (rss), rather than by increasing the space charge limited current threshold value in the previous case. And the spectral regrowth is improved by about 6dB when rss decreases from 1.3 Ohm to 0.2 Ohm.

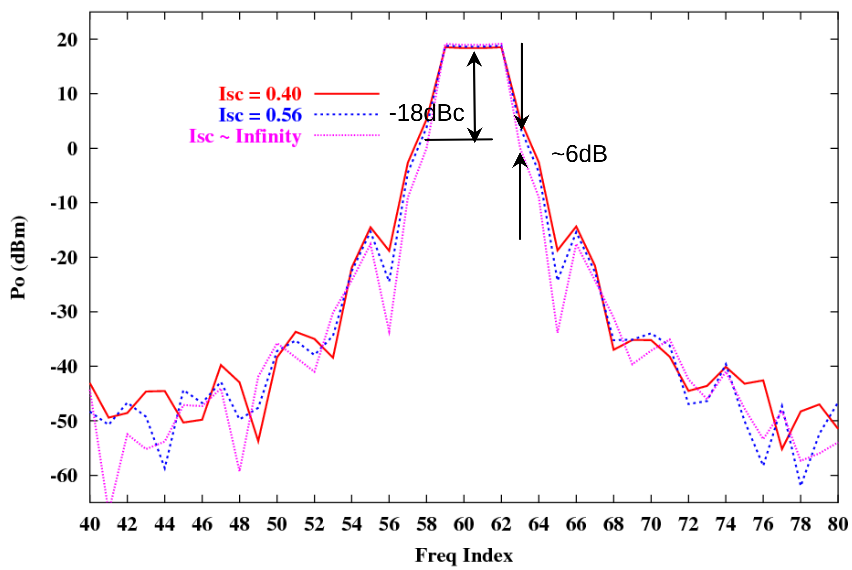

Fig. 4.9 Spectrum simulation results with different Isc value under four equal sinusoidal signals when Pout = 19 dBm.

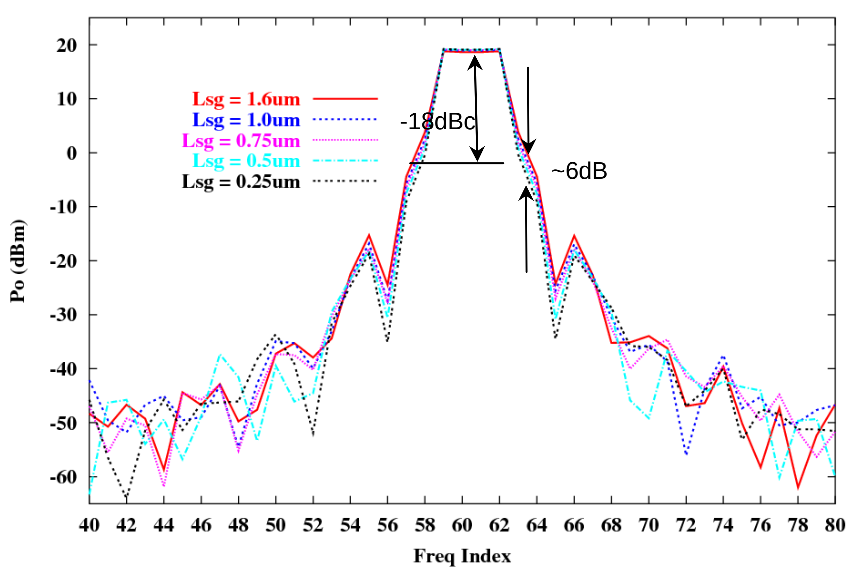

Fig. 4.10 Spectrum simulation results with different Lsg spacing under four equal sinusoidal signals when Pout = 19 dBm.

As a comparison, Fig. 4.11 shows a set of simulation with variable Lsg spacing for 4-tone signal when Pout = 14 dBm. Power density in adjacent channel when Lsg = 1.6 um is about 24 dBc, and it is improved by about 5 dB by decreasing the Lsg spacing to 0.25um. As the effect of source resistance modulation is smaller at smaller power level, the improvement on spectral regrowth by limiting the source resistance is less obvious than that in previous case.

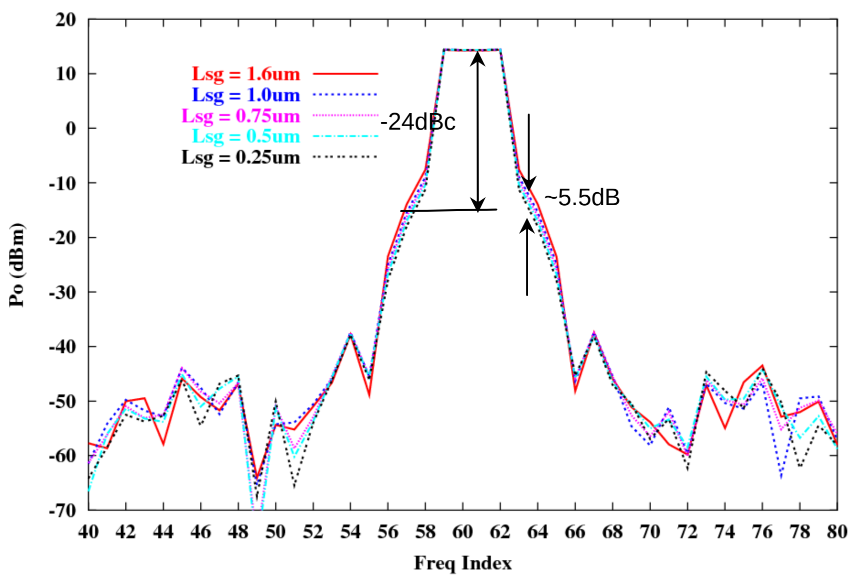

Fig. 4.11 Spectrum simulation results with different Lsg spacing under four equal sinusoidal signals when Pout = 14 dBm.

4.4 IMD with nonlinear source resistance

As discussed in 4.2, the nonlinear source resistance has a different effect on the IMD product depending on the original sign of g_{mi3}. To further understand this behavior, several sets of simulations were performed with different bias current and space charge limited threshold current. Fig. 4.12 shows a set of simulation of IM3 versus Isc at different bias conditions. For comparison, the simulation results with only a linear source resistance were also added. This case is shown with Isc ~ infinity.

In case A, the device is biased for class A operation with Id =80mA. The original g_{mext3} term at the small signal condition is negative, and neither gain expansion nor the IMD sweet spot appears in the plot. The decrease in the threshold value for space charge limited current enhances the nonlinear source resistance effect. Therefore, the addition of the second negative term and the first term in eqn. (4.2) degrades the IMD product when the Isc value decreases, as was shown in Fig. 4.12a.

Fig. 4.12 Simulated IM3 variation versus Isc at different bias current for a 2.14 GHz AlGaN/GaN device. (a) Id = 80mA (b) Id = 40mA (c) Id = 10mA (d) Id = 5mA

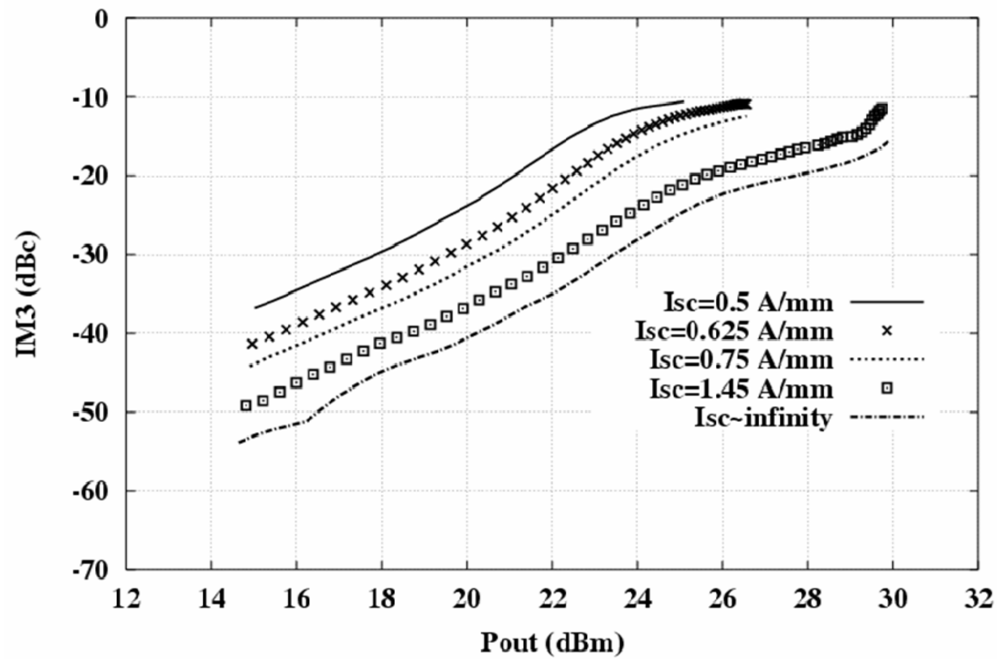

IM3 (dBc)
Pout (dBm)
Isc=0.5 A/mm
Isc=0.625 A/mm
Isc=0.75 A/mm
Isc=1.45 A/mm
Isc~infinity

(A)

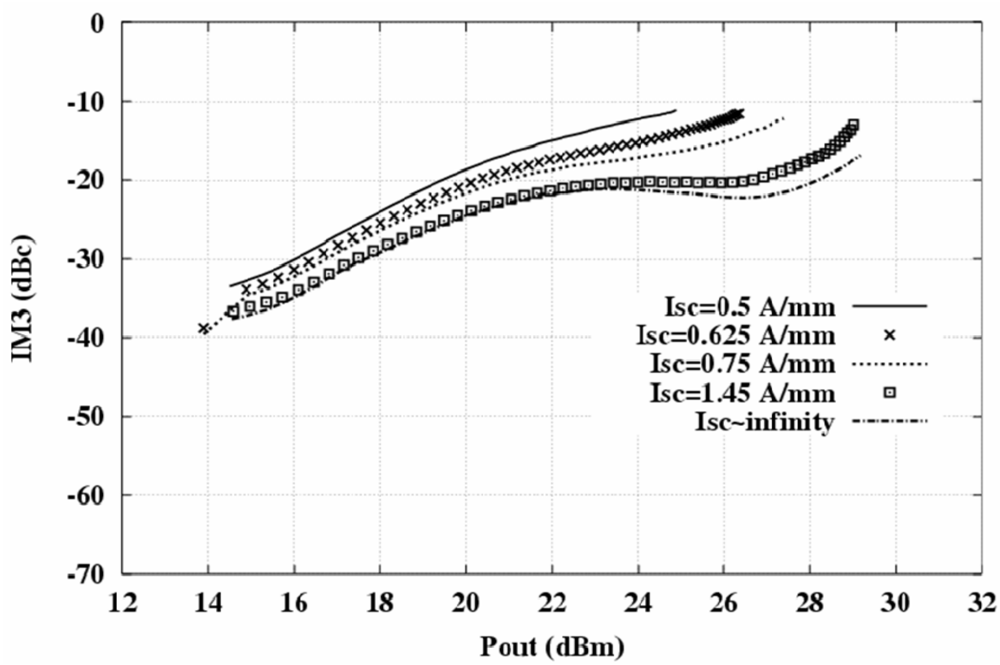

IM3 (dBc)
Pout (dBm)
Isc=0.5 A/mm
Isc=0.625 A/mm
Isc=0.75 A/mm
Isc=1.45 A/mm
Isc~infinity

(B)

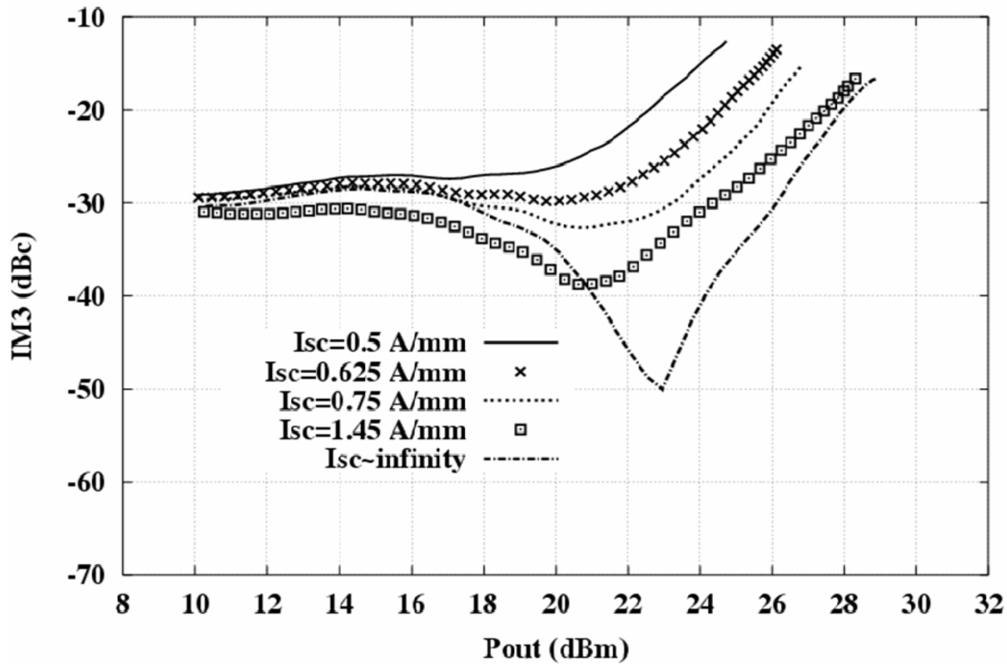
-10
-20
-30
-40
-50
-60
-70
IM3 (dBc)
8
10
12
14
16
18
20
22
24
26
28
30
32
Pout (dBm)
Isc=0.5 A/mm
Isc=0.625 A/mm
Isc=0.75 A/mm
Isc=1.45 A/mm
Isc~infinity

(C)

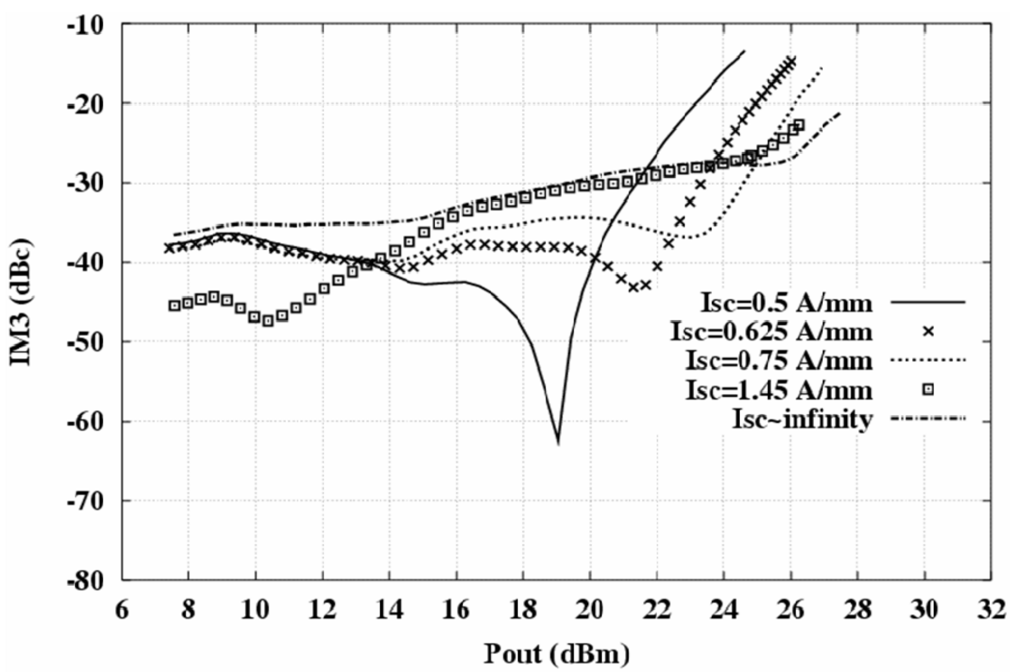
-10
-20
-30
-40
-50
-60
-70
-80
IM3 (dBc)
6
8
10
12
14
16
18
20
22
24
26
28
30
32
Pout (dBm)
Isc=0.5 A/mm
Isc=0.625 A/mm
Isc=0.75 A/mm
Isc=1.45 A/mm
Isc~infinity

(D)

Case B corresponds to the device biased for class AB with Id = 40mA. When only a linear source resistance is included, the original g_{mext3} shows a slightly positive value, with mild degradation under large signal conditions. Inclusion of the nonlinear source resistance increases the degradation of the IMD behavior. Further reduction of Isc increases the magnitude of the second term in eqn. (4.2) and the g_{mext3} becomes negative. The dip in IM3 shown in Fig. 4.12b then disappears.

Case C is for a device biased near pinch off, with Id = 10mA. The IM3 shows a deep notch at Pout=23dBm for the curve without inclusion of the nonlinear resistance effect, and a positive g_{mext3} at small signal conditions results. Setting the Isc=1.45A/mm, the nonlinear source resistance reduces the g_{mext3} value by subtracting the two terms in eqn.(4.2). An improvement in IM3 is shown in the plot at small signal conditions. Further decrease in the Isc magnitude produces a more negative g_{mext3} with a corresponding degraded IMD product. The IM3 minimum disappears when Isc=0.75A/mm and the curves show degraded IM3 for Isc = 0.625 and 0.5 A/mm.

In Case D, the nonlinear source resistance produces non-uniform results. When Isc ~ infinity, two gradual IM3 valleys are present. The nonlinear source resistance with Isc = 1.45A/mm improves the IMD behavior and introduce a small signal sweet spot. When Isc decreases below 0.75A/mm, IM3 is constantly decreased, and two IM3 minimums are presented both at small signal and large signal conditions. To explain this behavior, a more accurate expression for eqn.(4.6) is introduced:

$$i_{out}(2\omega_2 - \omega_1) \cong \frac{3}{4} g_{mext3} v_{in}^3 + \frac{25}{8} g_{mext5} v_{in}^5 \quad (4.8)$$

The relationship of the nonlinear source resistance and g_{mext5} is:

$$g_{mext5} \cong \frac{g_{mi3}}{(1 + g_{mi1} r_1)^6} - \frac{g_{mi1}^6 r_3}{(1 + g_{mi1} r_1)^6} \quad (4.9)$$

The variation of g_{mext5} versus nonlinear source resistance is similar to g_{mext3}.

For the curve without nonlinear source resistance, $g_{mext3}<0$, $g_{mext5}>0$, and g_{mext5} gradually dominates in eqn.(4.8) as input power increases. This creates a wide valley with improved IM performance at small signal levels by the interaction between g_{mext5} and g_{mext3}, and a second valley at large signal conditions by the interaction between g_{mext5} and the large signal distortion mechanisms. No IM3 notch is observed. Inclusion of the nonlinear source resistance increases the g_{mext3} according to eqn.(4.2), which enhances the interaction between g_{mext3} and g_{mext5}, and a small signal sweet spot at Pout = 10dbm is produced. The g_{mext5} term then dominates at large signal operation, and the curve demonstrates a reduced IM3 when the nonlinear source resistance is included. Further decrease of the Isc magnitude reduces the g_{mext5}, but the term remains positive and dominates the response, thereby introducing the two IM3 minimuma. The first IM3 minimum is due to the interaction between g_{mext5} and g_{mext3}, and the second is due to the compensation between small signal (g_{mext5}) distortion and the nonlinear source resistance distortion. As was shown in the plot, the IMD is improved from Isc=0.75A/mm to 0.5A/mm with a deeper IM3 notch, but appears at a smaller input power, which agrees with the analysis shown before.

Since the IM3 is mainly determined by a negative g_{mext3} at large signal levels, the IM3 is always degraded with an increase of the nonlinear source resistance, as was shown in Fig.4.12. Therefore, under large signal conditions, increased nonlinear source resistance magnitude always degrades the IMD.

4.5 Phase distortion with nonlinear source resistance

Linearity is a crucial factor in today's third-generation (3G) systems, where a multicarrier signal with variable envelope amplitude is amplified at the base station and in personal communication devices. The transmission of these signals encounters both amplitude and phase distortion. Experiment has shown that these signals are much more susceptible to AM-PM conversion than constant envelope signals [13]. Distortion shown in the final signal as spectral regrowth is usually characterized by ACPR and EVM specification. It has been shown in previous work that nonlinear source resistance distorts the amplitude of AlGaN/GaN HFET power devices due to extrinsic transconductance degradation [2,3]. As mobile communication systems have transitioned from TDMA to CDMA, it is especially important to study the AM-PM conversion for AlGaN/GaN HFET devices, which have attracted much recent attention for power amplifier applications. In this section, the effect of nonlinear source resistance upon AM_PM conversion is investigated. Several cases are reported: (1) a linear device with linear Rs, (2) a linear device with nonlinear Rs, and (3) a nonlinear device with nonlinear Rs.

4.5.1 Model generation

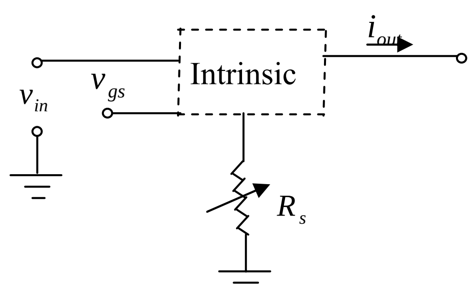

Fig. 4.13 Equivalent circuit for phase distortion analysis

The device equivalent circuit is shown in Fig.4.13

Assume the signal is described by the following:

$$v_{in} = A\cos(\omega t + \theta + \beta) \tag{4.10}$$

$$v_{gs} = B\cos(\omega t + \theta) \tag{4.11}$$

Where v_{gs} and v_{in} are the input signals before and after Rs distortion. The term β represents the extra phase distortion introduced by Rs.

Also,

$$i_{out} = C\cos(\omega t + \theta + \varphi) \tag{4.12}$$

Where φ represents the AM-PM characteristic for the intrinsic FET, and $G_{mi} = \frac{C}{B}$, represents the AM-AM characteristic for the intrinsic FET.

Substitute (4.10), (4.11), and (4.12) into

$$v_{in} = v_{gs} - i_{out} \cdot R_s \tag{4.13}$$

and after rearranging the equation, the resulting extra phase variation, β, is expressed as,

$$\beta = -\arctan\frac{G_{mi}R_s\sin\varphi}{1 - G_{mi}R_s\cos\varphi} \tag{4.14}$$

The AM_PM conversion for the extrinsic FET is,

$$\varphi' = \varphi - \beta = \varphi + \arctan\frac{G_{mi}R_s\sin\varphi}{1 - G_{mi}R_s\cos\varphi} \tag{4.15}$$

It follows that:

$$\varphi' = \arctan \frac{\sin\varphi}{\cos\varphi - G_{mi}R_s} \tag{4.16}$$

The effect of Rs upon AM_PM conversion depends upon the Rs value, the intrinsic device's AM-AM conversion and the AM-PM conversion. In the case when $\varphi = 0$, Rs would have no effect regardless of its value.

4.5.2 Simulation results

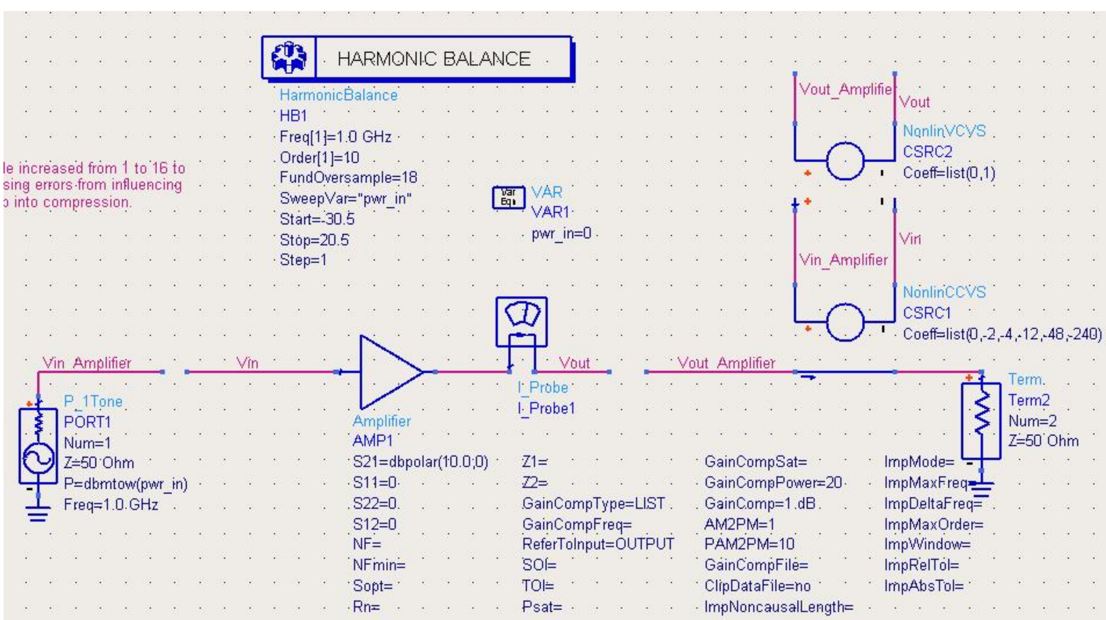

Fig. 4.14 AM-PM simulation circuit with nonlinear source resistance in Agilent ADS.

To verify the analytical equation for phase distortion, the AM-PM conversion was simulated in Agilent ADS using a behavioral power amplifier (PA) model. Fig. 4.14 shows the simulated circuit in Agilent ADS. A current controlled voltage source component is used to represent the nonlinear source resistance as shown in Fig. 4.14.

In order to see the verification result, the source resistance was set to a constant value, Rs=2 Ω, in the simulation. The phase derivation values shown by eqn. (4.14) for both the linear device (without amplitude distortion) and the nonlinear device (with amplitude distortion) cases are shown in Fig. 4.15. The solid line is the calculated results from above equations. The circle line is the simulated results from ADS. The left side figure shows the AM-PM conversion results, defined as φ' in eqn. (4.16), and the right side figure is the extra phase distortion β caused by Rs according to eqn. (4.14).

The analytic model is in excellent agreement with the ADS simulation results for AM-PM distortion and the extra phase variation. Several observations were made from this model:

i. For a linear system without AM-PM and AM-AM conversion but a constant phase shift φ, the **linear** source resistance only introduces an extra constant phase shift β, determined by eqn. (4.14), with no impact upon system linearity. The final phase of the output signal is determined by eqn.(4.16)

ii. For the nonlinear system with only AM-AM distortion, but without AM-PM conversion, the linear source resistance Rs introduces AM-PM conversion into the system through the intrinsic device's AM-AM distortion. The final phase distortion is determined by eqn. (4.16).

iii. For a linear system without AM-PM and AM-AM conversion but with a constant phase shift φ, the **nonlinear** source resistance Rs transforms it into a nonlinear system, and introduces phase distortion into the system, as determined by eqn. (4.14).

iv. For a nonlinear system with both AM-AM and AM-PM conversion, the nonlinear source resistance Rs introduces an extra phase variation β in addition to the original phase distortion φ, where β and the final phase distortion φ' are determined by eqn. (4.14) and eqn. (4.16) respectively.

The analytical model shows that the nonlinear Rs introduces amplitude distortion, as previously reported [2,3], and also introduces phase distortion. The nonlinearity of Rs transforms a pure linear system into a nonlinear system by introducing both AM-AM conversion and AM-PM conversion.

The results in Fig. 4.15 indicate how AM-AM distortion impacts AM-PM distortion. Eqn. (4.14) shows that device gain (Gm) amplifies the effect of nonlinear source resistance upon phase distortion through the term GmRs. Therefore less phase

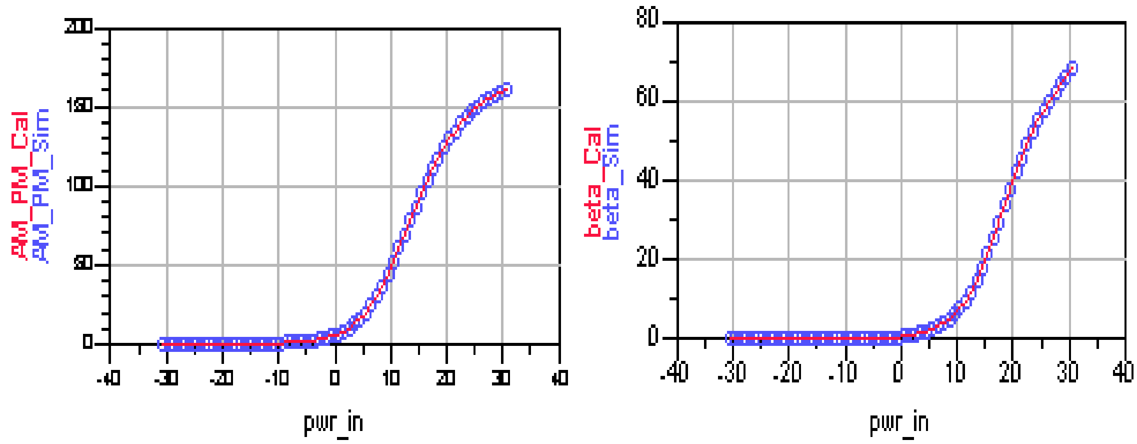

(a)

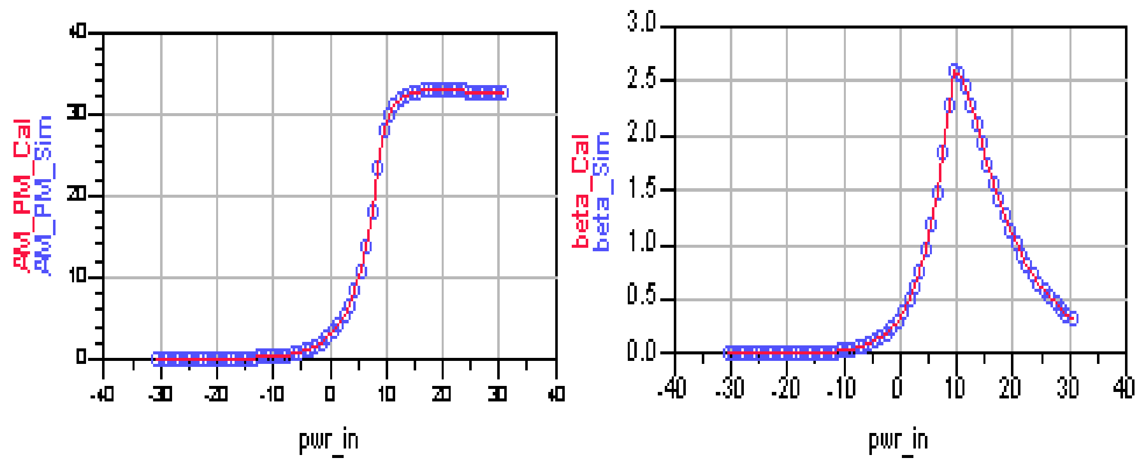

(b)

Fig. 4.15 Comparison AM_PM conversion and phase variation due to Rs from the Agilent ADS simulation and the analytical model. (a). Power amplifier without AM_AM conversion and a linear source resistance Rs = 2 Ohm. (b) Power amplifier with 1dB gain compression at Pin=20 dBm and a linear source resistance Rs = 2 Ohm.

distortion due to nonlinear Rs is expected for a device with gain compression. As input power increases, dc drain current also increases along with the magnitude of nonlinear source resistance. For devices without AM-AM conversion, β starts from zero, and then unilaterally increases with input power. For devices with AM-AM conversion, as power increases, β reaches at a maximum value and then decreases. The decrease of β with increasing RF signal drive is caused by gain compression.

The nonlinear source resistance in the simulation is modeled as a current controlled voltage source with the voltage expressed as a polynomial.

The simulation results for phase distortion with nonlinear source resistance are shown in Fig.4.16. The results with only a linear resistance are also included for comparison. The circle line is the result with a nonlinear source resistance, $Rs = 2 + 4I_d + 12I_d^2 + 48I_d^3 + 240I_d^4$ Ohm. The solid line is the result with a linear Rs=2 Ohm.

Fig. 4.16 Simulation Results of AM-PM conversion for PA with nonlinear source resistance. (a) Power amplifier without AM_AM conversion. (b) Power amplifier with 2dB gain compression at Pin=30 dBm. (c) Power amplifier with 2dB gain compression at Pin=20 dBm.

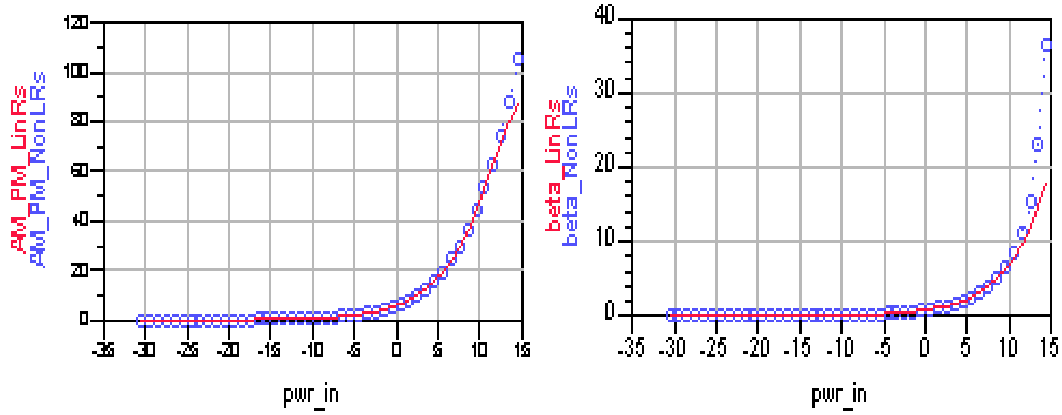
AM_PM_LinRs
AM_PM_NonLRs
pwr_in
beta_LinRs
beta_NonLRs
pwr_in

(a)

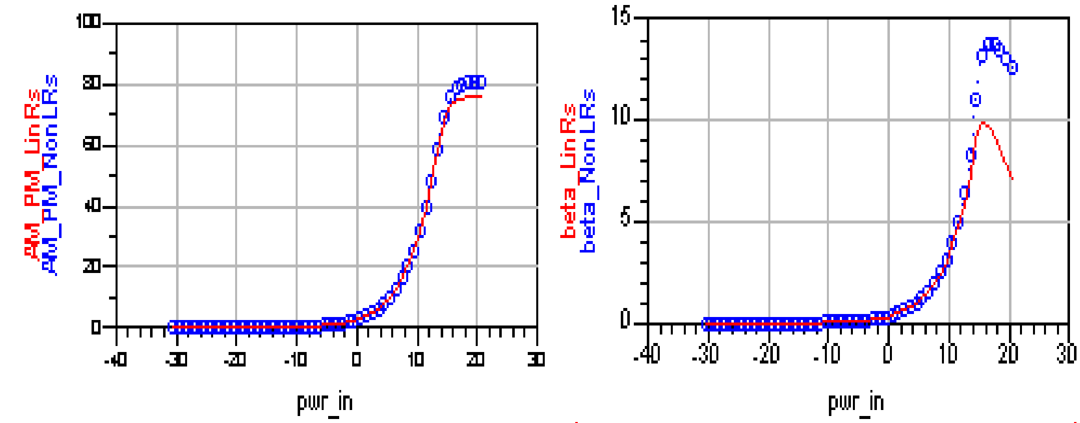
AM_PM_LinRs
AM_PM_NonLRs
pwr_in
beta_LinRs
beta_NonLRs
pwr_in

(b)

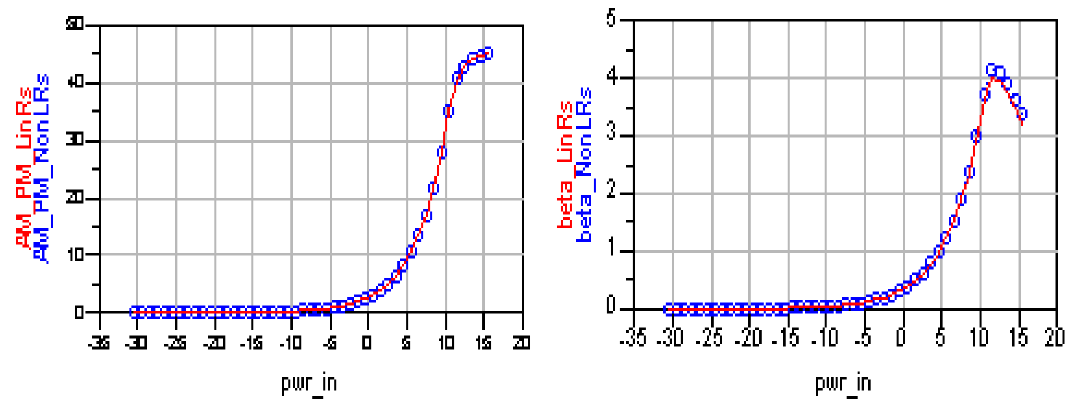
AM_PM_LinRs
AM_PM_NonLRs
pwr_in
beta_LinRs
beta_NonLRs
pwr_in

(c)

As mentioned previously, the effect of the nonlinear source resistance upon phase distortion is more obvious for a PA without AM-AM distortion than for those with AM-AM distortion, since the decrease of Gm at large input power level suppresses the GmRs term in eqn. (4.14). An effective method to decrease AM-PM conversion due to a nonlinear Rs is to reduce and limit device gain. Fig. 4.16(b) and Fig. 4.16(c) show phase distortion results for two PA with different linearity. Power amplifier in (b) has less gain compression than PA in (c), and shows more phase variation due to nonlinear source resistance. Linearization techniques such as source degeneration, improve linearity by limiting PA gain, and also improve phase distortion as explained in the above analysis.

4.5.3 Phase distortion analysis using physics base model

In this section some simulation results using physics based model are presented to study the phase distortion under source and drain resistance modulation. Fig. 4.17 shows the phase distortion results for a 2.14 GHz AlGaN/GaN HFET device with and without nonlinear resistance. The phase distortion in the simulation is defined as the output current phase changing value refered to the original phase shift at small signal level, which in this case is when Pin = -10 dBm. The minima appearing in the curve are due to the convergence problem of the numeric solver. They are not part of the device behavior.

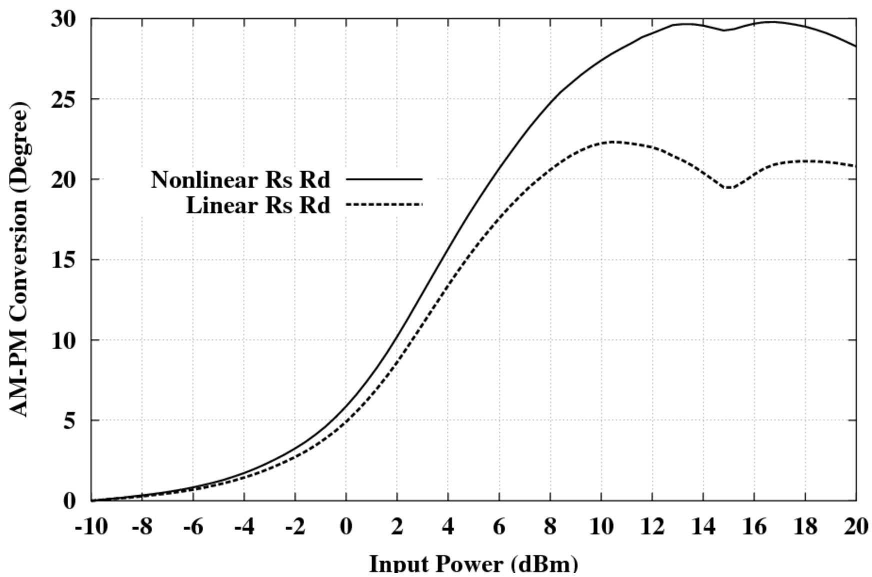

Fig. 4.17 Phase Distortion simulation results for a 2.14 GHz AlGaN/GaN HFET device.

The phase distortion starts from 0 degree and increases to a maximum of 30 degree when Pin reaches the maximum output power. A dramatic decrease of phase distortion is seen from the simulation when the nonlinear resistances are replaced by linear ones. The maximum phase distortion decreases by about 10 degree from the nonlinear resistance case. This simulation shows the nonlinear resistance has a great impact on phase distortion.

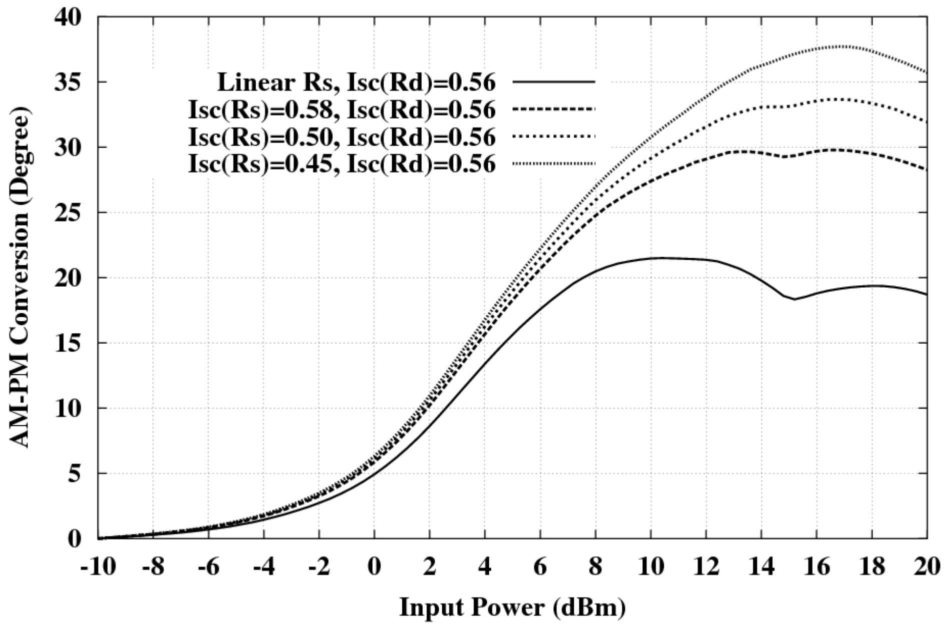

Fig. 4.18 Phase distortion simulation results for a 2.14 GHz AlGaN/GaN HFET device when Isc (Rs) varies from 0.45 A to infinity, Isc(Rd) = 0.56A.

The following simulation results separate the effect of nonlinear source resistance from nonlinear drain resistance by only changing one resistance modulation at a time and leaving the other one to be constant. Fig.4.18 is a set of simulation when only the nonlinear source resistance modulation is changed by adjusting Isc(Rs), the threshold for space charge limited current at source access region, while leaving the threshold for SCL current at drain access region to be a constant, Isc(Rd) = 0.56A. The phase distortion increases as nonlinear source resistance modulation increases by

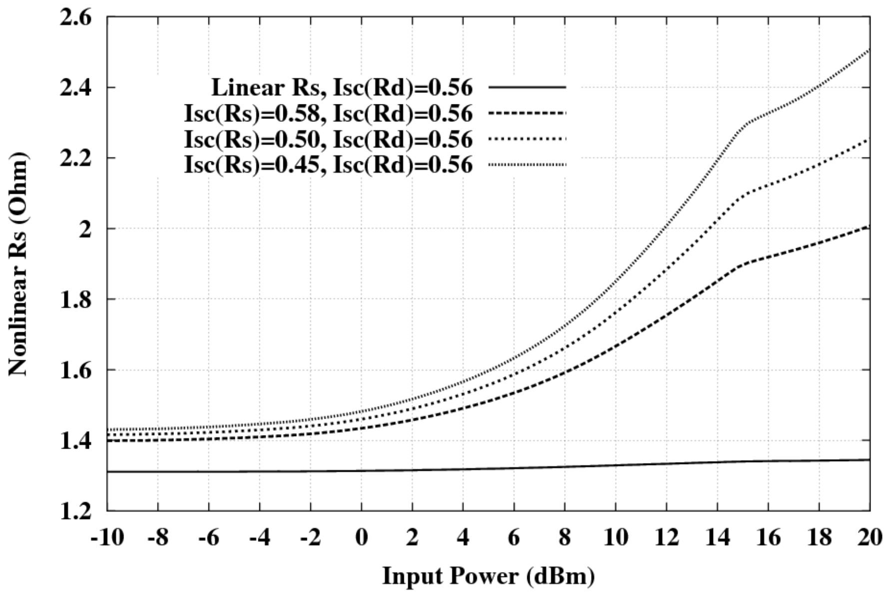

(a)

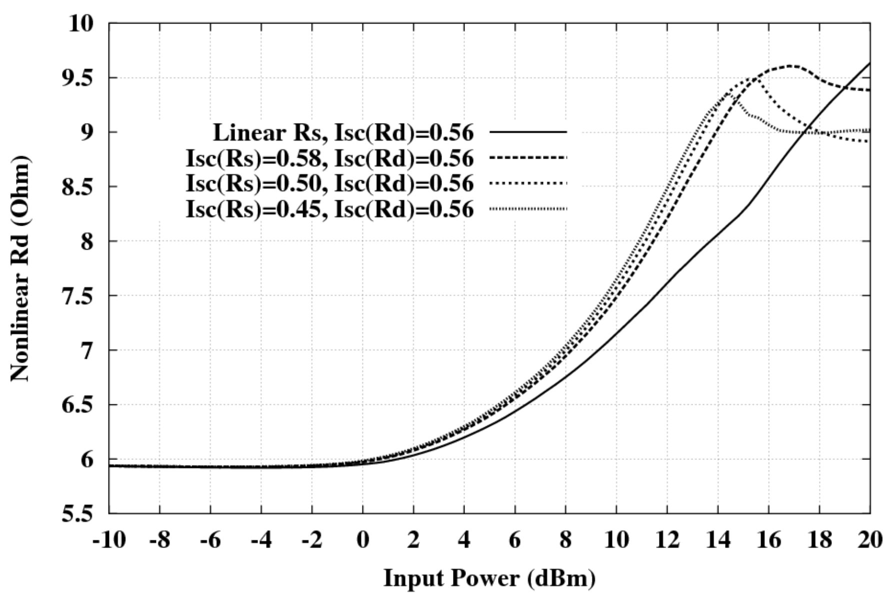

(b)

Fig. 4.19 Nonlinear source and drain resistance versus Pin when Isc(Rs) changes from 0.45A to infinity. (a) Nonlinear Rs (b) Nonlinear Rd decreasing the Isc(Rs) value. A decrease of 20 degree of the maximum phase distortion is reached when only a linear Rs is used, which is the case when Isc(Rs) value approaches infinity.

Fig. 4.19 shows the variation of nonlinear source resistance and nonlinear drain resistance as Isc(Rs) changes. We can see that the increase of phase distortion mainly comes from the increase of nonlinear source resistance. The changing of drain resistance modulation is small enough to be neglected.

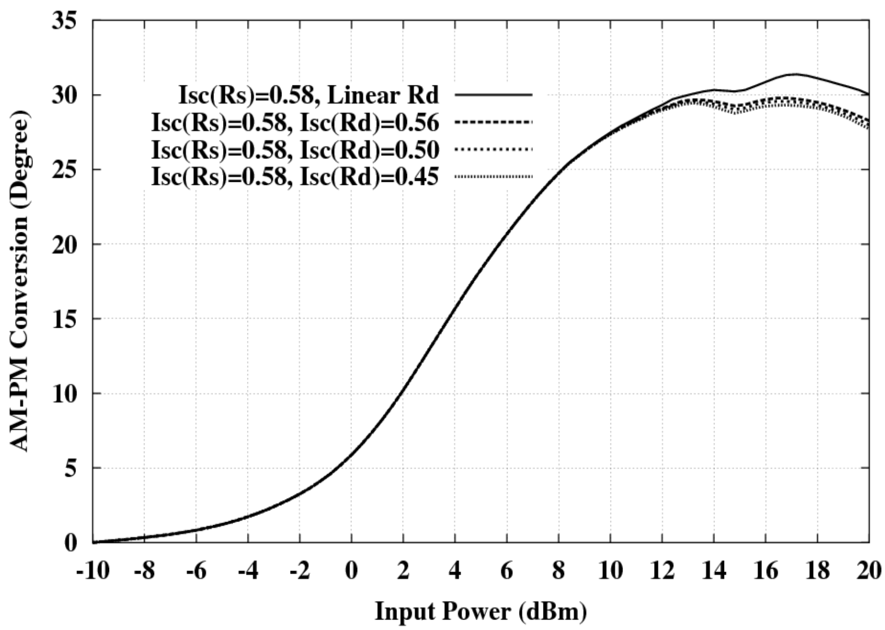

Fig. 4.20 Phase distortion simulation results for a 2.14 GHz AlGaN/GaN HFET device when Isc (Rd) varies from 0.45 A to infinity, Isc(Rs) = 0.58A.

Fig. 4.20 is a set of phase distortion simulation when only the nonlinear drain resistance modulation is changed by adjusting Isc(Rd) value from 0.45 A to infinity, while leaving the Isc(Rs) value to be a constant, Isc(Rs) = 0.58A.

Compared to Fig. 4.18, Fig. 4.20 shows a much less phase distortion variation. It shows that nonlinear source resistance has a greater impact on phase distortion than nonlinear drain resistance. The result is not hard to understand, as the operation nature of FET device determines that the device output current depends only on the input voltage. Nonlinear drain resistance only affects the output voltage, while the nonlinear source resistance at the input port affects the output current by forming a feedback loop from the output to input. The effect of nonlinear source resistance is further amplified by a factor of Gm, as was shown is the analysis in section 4.5.1. It also proves that it is very important to limit the nonlinear source resistance modulation in order to optimize the device performance.

Noted that the phase distortion in this set of simulation actually increases when the drain resistance modulation decreases by increasing the Isc(Rd) value. The reason can be explained as followings. Fig. 4.21 shows the changing of nonlinear source resistance modulation and nonlinear drain resistance modulation as Isc(Rd) varies. From the simulation results, we can see that the byproduct of increasing the Isc(Rd) value is the increase of nonlinear source resistance. Even though the variation of

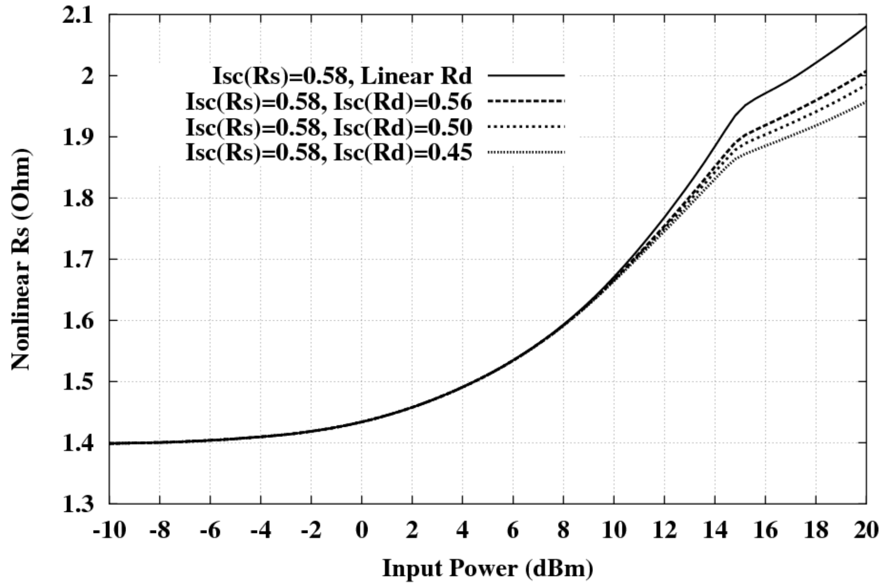

(a)

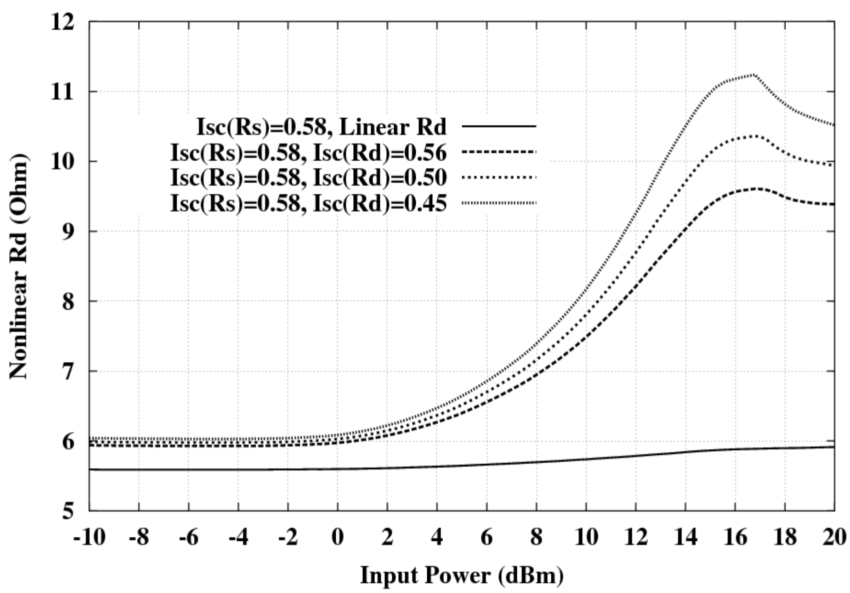

(b)

Fig. 4.21 Nonlinear source and drain resistance versus Pin when Isc(Rd) changes from 0.45A to infinity. (a) Nonlinear Rs (b) Nonlinear Rd nonlinear source resistance is not as large as that in previous case when Isc(Rs), it is the origin that causes the phase distortion, which also proves that the increase of phase distortion is mainly due to the increase of nonlinear source resistance.

The impact of breakdown mechanism on phase distortion is also studied. Fig. 4.22 is a set of simulation results showing the change of phase distortion when breakdown voltage varies from 45V to 60V. Not much phase distortion improvement has been seen in the simulation when breakdown voltage increases. The breakdown mechanism has very little impact on phase distortion.

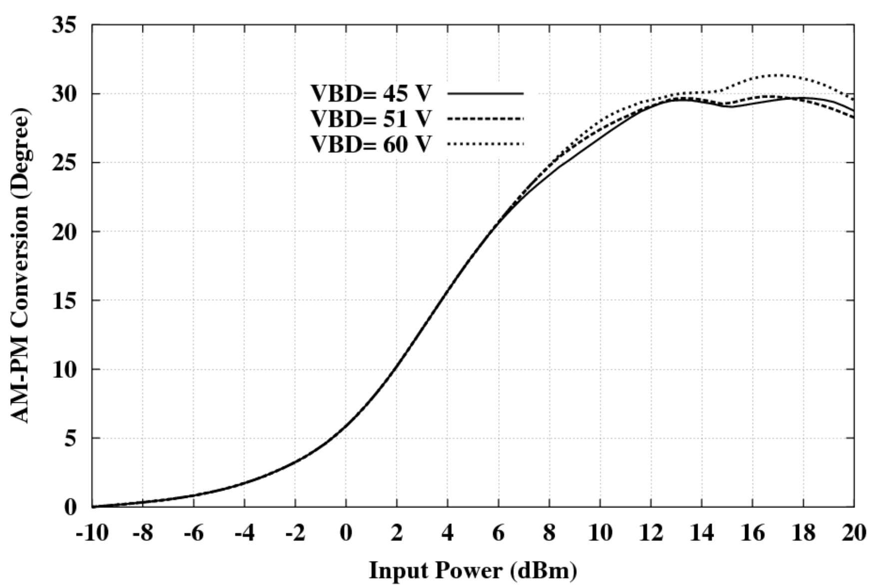

Fig. 4.22 Phase distortion simulation results for a 2.14 GHz AlGaN/GaN HFET device when breakdown voltage varies from 45V to 60V.

Power amplifiers are usually chosen to be operated at small to medium signal level to ensure a linear performance for input generation with variable envelope. In such cases breakdown is not yet happening in the device. Only if when device is overdriven into deep saturation, breakdown mechanism can have a great impact on device performance. And breakdown affects the nonlinearity mainly through amplitude distortion. Therefore for generations with variable envelope such as WCDMA signal, breakdown has not much impact on the output spectral regrowth. We will further prove this scenario in the following section.

4.6 Spectral regrowth simulation

The inherent nonlinearity of PA is the major factor that causes nonlinear distortion when signal is transmitted. A common form of nonlinear distortion appearing in a wide band signal transmission is spectral regrowth characterized by ACPR (Adjacent Channel Power Ratio), where the adjacent channel is polluted during transmission. Prediction of spectral regrowth is usually done through time domain analysis [14] or calculation from analytical equation, in which the PA are represented by a closed-form expression obtained from its AM-AM and AM-PM characteristics [15, 16]. The AM-AM and AM-PM conversion are derived from measurements of complex gain versus input power for a one tone signal setup and obtained from some simulation techniques, i.e. harmonic balance or periodic-steady-state simulation. These analyses herein assume that the AM-AM and AM-PM characteristic are sufficient to represent the device operation. The accuracy of these methods is often limited by the complexity expression of amplifier's transfer function. Up to seventh-order nonlinearities in Volterra expression has been seen in the calculation [15]. Although these methods do provide some valuable insight in to the connection between spectral regrowth and PA nonlinearity, no information based on device physics has been given.

In this section the physics based model is used to exploit the nonlinearity behavior of a 2.14GHz AlGaN/GaN device under wide band signal. As the output response is calculated from power amplifier's physics based model, the results of spectral regrowth are directly related to device's physical mechanism and structure. It provides a useful tool for RF engineers and researchers to understand the specific nonlinear process that leads to spectral regrowth, and opens up the opportunity for device optimizations in terms of geometry and structure design.

Adjacent channel power ratio or adjacent channel leakage ration is the ratio of power in the transmitted channel to the power in the side band channel. It characterizes the interference produced by mixing products between the individual frequency components of the spectrum, and deteriorates as amplifier is driven into saturation. Typical requirement for ACPR specification in 3GPP (3rd Generation Partnership Project) system is from 45 to 50 dB.

The original physics based model apply harmonic balance (HB) simulator to convert the voltage and current waveform response between time-domain and frequency-domain. An important feature of HB is that frequency component of the output for one tone generation consists of integer multiples of the fundamental frequency. Since the originality of spectral regrowth comes from intermodulation of odd-order nonlinearity, the spectrum is composed of closely spaced mixing products. The amount of time sample needed for harmonic balance to calculate spectral regrowth is nearly impossible to realize. Several techniques in terms of Fourier transform have been developed to minimize the time sample number [17-19]. Among these techniques, a modified multitone harmonic balance algorithm introduced by Vuk Borich [11] is applied in the large signal model. It efficiently reduces the time sample by shifting the higher order mixing products to the lower order harmonics, when a certain condition is satisfied for the relationship between center frequency, frequency components and sampling rate. The shifting of the center frequency is usually very small, and considered to be negligible enough to cause very little change in result. Detail derivation and explanation of the algorithm can be referred to Ref. [11].

The following ACPR simulation utilizes one carrier of the first test model TM1 specified in 3G system specification [20] with 64 active user channels. I, Q data files for WCDMA signal are generated from Agilent ADS software, and imported into physics based model to do the simulation. Fig. 4.23 shows the input and output spectrums for the calibrated AlGaN/GaN HFET device biased at 8mA. The input spectrum is plotted in Agilent ADS with centered frequency at 2.14GHz, and modulation bandwidth of 3.84MHz.

The total number of frequency used in the HB simulator is 2999 with band limit of 1000. Tone spacing is set to be 0.015MHz. The first 999 frequency components are from 0.015MHz to 14.985MHz, which is not the spectrum we are interested in. And the rest components from 1000 to 2999 are frequency range from 2.125GHz to 2.155GHz, where most of the signal is being transmitted. Without modifying the algorithm the time sample needed to calculate the frequency response is 2.155GHz / 0.015 MHz = 143666, which is very time consuming and will need a lot of computing resource to calculate the spectrum we don't really need. The application of the new algorithm greatly reduces the time sample and is very efficient.

P1, P2, P3 labels in the output spectrum plot represent the integrated power density in the main channel and 5MHz offset adjacent channel. The P1, P2 and P3 results are used to calculate ACPR and denoted as (the frequency range is referred to the center frequency):

P1 = Integrated power of output spectrum for main channel from -1.92MHz to 1.92MHz

P2 = Integrated power of output spectrum for lower side band from -6.92MHz to -3.08MHz

P3 = Integrated power of output spectrum for upper side band from 3.08MHz to 6.92MHz

The ACPR result can be calculated as:

ACPR _Low5 = P2-P1 = 10.56 dBm – (-20.80 dBm) = 31.36 dB

ACPR_Up5 = P3-P1 = 10.56 dBm – (-20.66 dBm) = 31.22 dB

Following are several simulations for different bias and nonlinear source resistance. The tone spacing is set to be 0.0075MHz in order to achieve more detail calculated spectrum. Fig. 4.24 and Fig. 4.25 are simulation results when device is biased at 21 mA and 35 mA respectively.

<u>Biased at 21mA:</u>

ACPR _Low5 = P2-P1 = 17.71 dBm – (- 14.79 dBm) = 32.50 dB

ACPR_Up5 = P3-P1 = 17.71 dBm – (- 14.86 dBm) = 32.57 dB

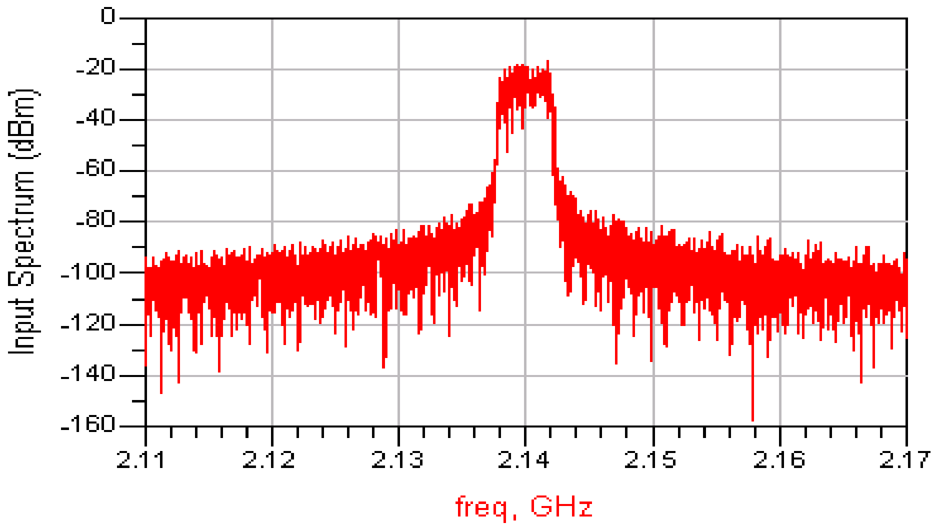

(a)

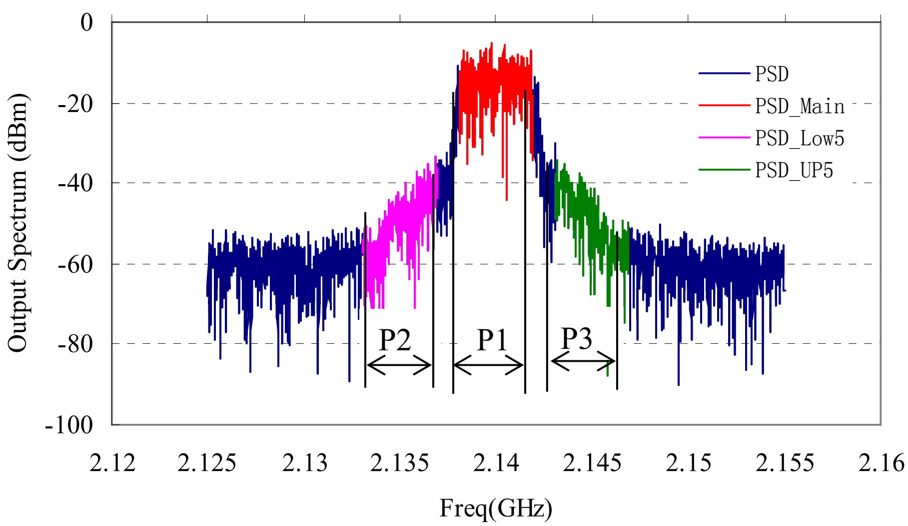

(b)

Fig. 4.23 Input and output spectrum for an AlGaN/GaN HFET device biased at 8mA with test model TM1 WCDMA signal.

Biased at 35mA:

ACPR _Low5 = P2-P1 = 19.86 dBm – (- 11.49 dBm) = 31.35 dB

ACPR_Up5 = P3-P1 = 19.86 dBm – (- 11.58 dBm) = 31.44 dB

Fig. 4.26 and Fig. 4.27 are simulation results for the same device without source resistance modulation (SRM) and biased at 21mA and 35 mA respectively.

ACPR results for device with only linear source resistance when biased at 21mA:

ACPR _Low5 = P2-P1 = 18.00 dBm – (- 16.93 dBm) = 34.92 dB

ACPR_Up5 = P3-P1 = 18.00 dBm – (- 16.74 dBm) = 34.74 dB

ACPR results for device with only linear source resistance when biased at 35mA:

ACPR _Low5 = P2-P1 = 20.06 dBm – (- 16.08 dBm) = 36.14 dB

ACPR_Up5 = P3-P1 = 20.06 dBm – (- 15.58 dBm) = 35.63 dB

Table 4.1 summarizes the above ACPR results with different simulation setup. The impact of SRM on ACPR increases when device's current bias increases. The decreasing of ACPR from 32dB to 31dB when current bias increases from 21mA to 35mA with nonlinear source resistance is due to the impact of SRM on nonlinearity. SRM is removed by replacing the nonlinear resistance with a pure linear one. Without the effect of nonlinear source resistance, ACPR is improved form 34dB to 36dB. By removing the SRM, an approximate of 2dB improvement on ACPR is seen when device is biased at 21mA. And about 5dB improvement is seen when device is biased at 35mA.

Table 4.1. ACPR calculation results from the physics based model for an AlGaN/GaN HFET device with TM1 WCDMA signal.

	21mA	35mA
With SRM	32 dB	31 dB
Without SRM	34 dB	36 dB

Simulation was also done when breakdown voltage varies to see the impact of breakdown mechanism on ACPR. Device is operated far before saturation, therefore breakdown has negligible impact on linearity. Secondly, breakdown mechanism does not cause much AM-PM conversion, a major distortion factor that leads to spectral regrowth. As what we expected, the simulation does not show much difference in ACPR results when breakdown voltage changes.

Both simulation and theoretic analysis show that nonlinear source resistance has a great impact on spectral regrowth. It is beneficial to optimize device design to minimize nonlinear source resistance in order to improve PA's linear performance under wide band signal. The optimization on device structure to minimize SRM will be able to reduce the analog manufacturing complexity and relieve engineers from the burden of designing linearization circuitry.

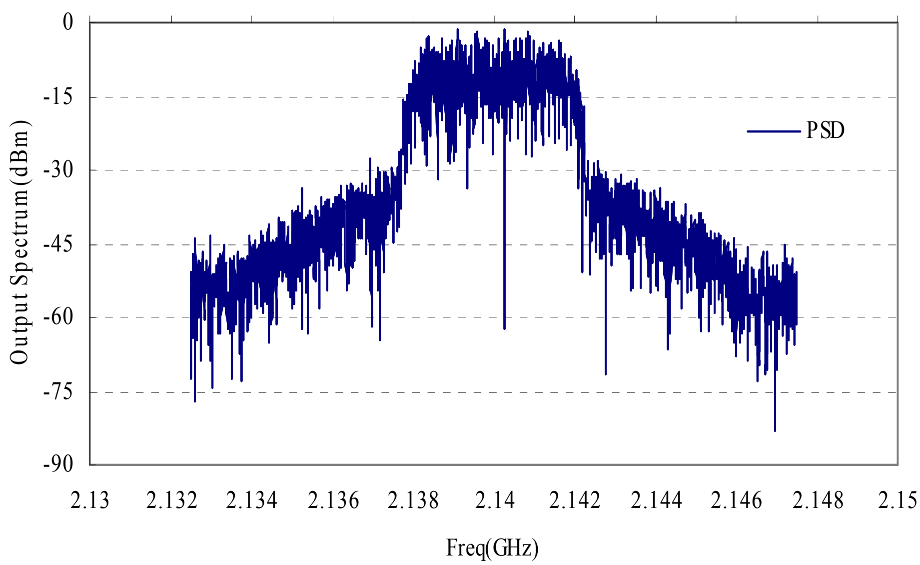

Fig. 4.24 Output spectrum for an AlGaN/GaN HFET device with test model TM1 WCDMA signal, when biased at 21mA including SRM.

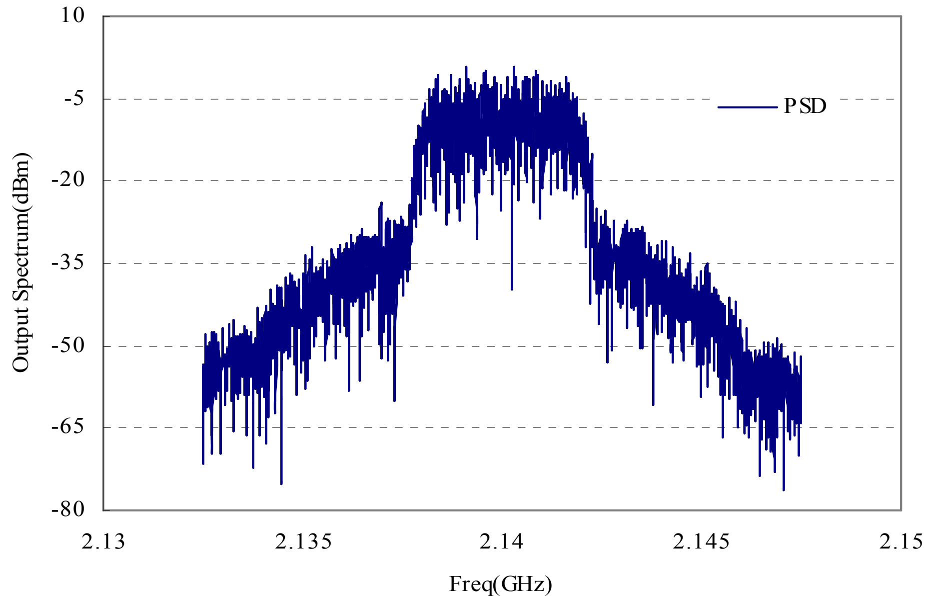

Fig. 4.25 Output spectrum for an AlGaN/GaN device with WCDMA signal, when biased at 35mA including SRM.

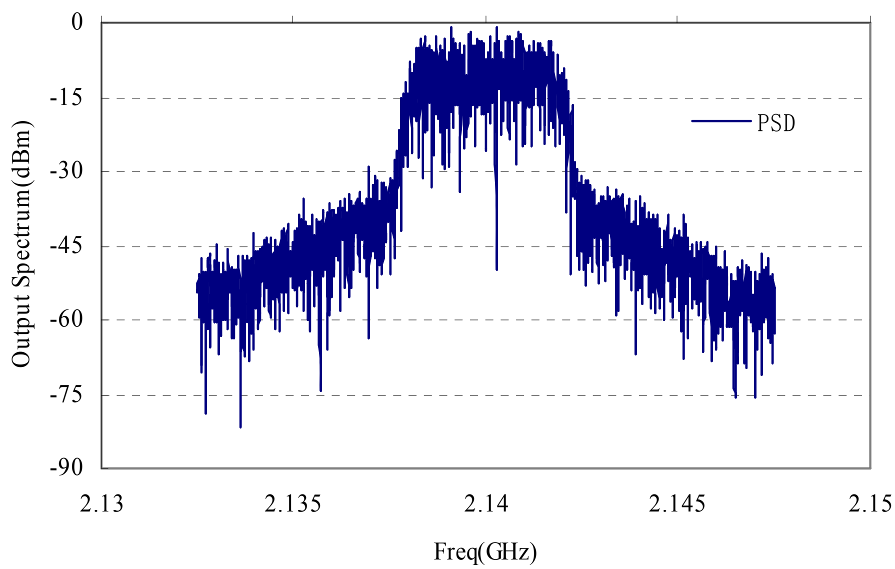

Fig. 4.26 Output spectrum for an AlGaN/GaN device without SRM, when biased at 21mA.

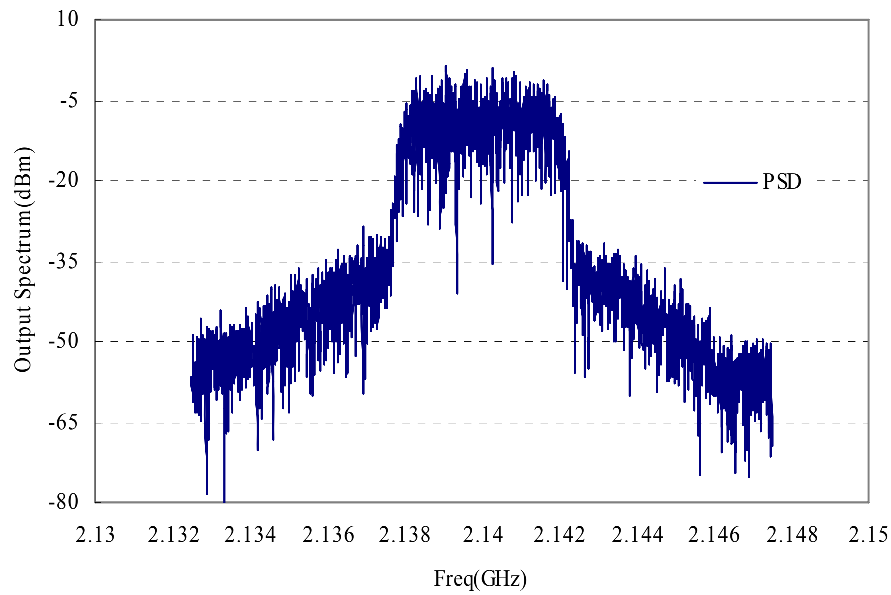

Fig. 4.27 Output spectrum for an AlGaN/GaN device without SRM, when biased at 35mA.

4.7 Summary

AlGaN/GaN HFET's have great potential to produce RF output power more than an order of magnitude greater than traditional FETs. However AlGaN/GaN HFETs currently suffer from physical effects that limit linearity. In particular, a nonlinear source resistance induced by the onset of SCL current transport seriously limits the device linearity under modest and large signal RF operation. A physics based large signal model embedded in a harmonic balance simulator is used to investigate the IMD behavior of AlGaN/GaN HFETs as a function of bias and gate-source spacing. The simulated RF performance is in excellent agreement with experimental data. IMD simulation reveals improvement in linearity by up to 5-6 dB by reducing the Lsg spacing. An optimum source-gate spacing is found to exist, and reduction of Lsg below this value produces no further improvement. The optimum value for Lsg spacing depends on the input power level and the nonlinear distortion mechanism. Detail analysis of the simulation results shows different impacts of nonlinear source resistance on IMD behavior under small signal operation, and a degradation impact on IM3 under large signal operation. The effect of nonlinear source resistance upon power amplifier phase distortion is studied. An analytic model is developed and verified with Agilent ADS simulation results. The nonlinear source resistance transforms a pure linear system into nonlinear system through both amplitude distortion and phase distortion. The analysis shows that the nonlinear source resistance adds an extra phase variation to the original nonlinear system. Device amplifies this effect through the GmRs term, which indicates that an effective method to improve linearity is to suppress and limit device gain. Simulation using the physics model verifies the great impact of nonlinear source resistance on AM-PM conversion. The phase distortion variation shows a large improvement of 15 degree with different SRM when device reaches the maximum output power. Almost double of source resistance has been seen in the simulation when power increases, which is the major factor that cause nonlinearity. Not much impact on AM-PM conversion has been seen with nonlinear drain resistance and breakdown mechanism. The implementation of an efficient HB algorithm makes the physics model be able to simulate PA response with wide band signal within an acceptable time sample range. The calculated ACPR shows about 5dB improvement when nonlinear source resistance is replaced with a linear one. The simulation results show the effect of SRM on spectral regrowth, offering an opportunity for engineers to optimize device design in terms of minimizing nonlinear source resistance.

REFERENCES

[1] T.A. Winslow and R.J. Trew, "Principles of Large-Signal MESFET Operation," *IEEE Trans. Microwave Theory Tech.*, vol. 42, pp.935-942, June 1994.

[2] Yueying Liu, Robert J Trew, Griff Bilbro, etc,"Linearity Limitations of AlGaN/GaN HFET's," *IEEE Wireless and Microwave Technology Conference*, December 2006

[3] Yueying Liu, Robert J Trew, Griff Bilbro,"RF Linearity and Nonlinear Source Resistance in AlGaN/GaN HFET's," *IEEE Wireless and Microwave Technology Conference*, June 2007

[4] R.J. Trew, Y. Liu, G.L. Bilbro, W.W. Kuang, R. Vetury, and J.B. Shealy, "Nonlinear Source Resistance in High Voltage Microwave AlGaN/GaN HFET's," *IEEE Trans. Microwave Theory and Tech.,* vol. 54, pp. 2061-2067, May 2006

[5] Stephen A. Maas, *Nonlinear Microwave and RF Circuits, Second Edition*, Norwood: Artech House, Inc. 2003.

[6] Muhammad Taher Abuelma'atti, "Prediction of Gain Expansion and Intermodulation Performance of Nonlinear Amplifiers," *ETRI Journal,* vol. 29, No.1, February 2007.

[7] Nuno Borges de Carvalho, Jose Carlos Pedro, “Large and small signal IMD behavior of microwave power amplifier,” *IEEE Trans. Microwave Theory & Tech.,* vol. 47, no. 12, pp. 2364-2373, November 1999.

[8] E. Ngoya and R. Larcheveque, "Envelope Transient Analysis: A New Method for the Transient and Steady State Analysis of Microwave Communication Circuits and Systems," *IEEE MTT-S Int. Microwave Symp. Dig.,* pp. 1365-1368, 1996.

[9] Stephen A. Maas, "Volterra Analysis of Spectral Regrowth," *IEEE Microwave Guided W. Lett.,* vol 7, July 1997.

[10] Nuno Borges de Carvalho and Jose Carlos Pedro, “Multitone Frequency-Domain Simulation of Nonlinear Circuits in Large- and Small-Signal Regimes,” *IEEE Trans. Microwave Theory & Tech.,* vol. 46, pp. 2016-2024, December 1998.

[11] Vuk Borich, Jack East, and George Haddad, “An Efficient Fourier Transform Algorithm for Multitone Harmonic Balance,” *IEEE Trans. Microwave Theory &Tech,* vol. 47, no.2, pp. 182-188, Feb. 1999.

[12] Matthew Poulton, “Design techniques for high linearity, high efficiency GaN PA architectures,” *2006 IEEE Compound Semiconductor IC Symposium*, November 2006.

[13] J. Staudinger, “Effects of AM/AM and AM/PM Distortion on Spectral Regrowth in 3GPP W-CDMA BS Power Amplification”, *Microwave Journal*, November 2002

[14] S. W. Chen, W. Panton, and R. Gilmore, “Effects of nonlinear distortion on CDMA communication systems,” *IEEE Trans. Microwave Theory Tech.*, vol. 44, pp. 2743–2749, Dec. 1996.

[15] G. Tong Zhou, J. Stevenson Kenney, “Predicting Spectral Regrowth of Nonlinear Power Amplifiers,” *IEEE Trans. Communications*, vol. 50, pp. 718–722, May. 2002.

[16] L. Sundström, “Fast and Accurate ACLR Estimation Method,” *2004 IEEE Radio and Wireless Conference,* 19-22 Sept. 2004, pp 183 – 186.

[17] J. Angel Garcia, M. L. De la Fuente, J. M. Zamanillo, etc, “Intermodulation Distortion Analysis of FET Mixers under Multitone Excitation,” *2000 European Microwave Conference,* Oct. 2000, pp 1 – 4.

[18] V.Rizzoli, C. Cecchetti, and A. Lipparini, “A general-purpose Program for the Analysis of Nonlinear Microwave Circuits under Multitone Excitation by Multidimensional Fourier Transform,” *Proc. 17th European Microwave Conf.,* Sept. 1987, pp 635 – 640.

[19] R. Gilmore, “Nonlinear Circuit Design Using the Modified Harmonic Balance

Algorithm," *IEEE Trans. Microwave Theory Tech.,* Vol. MTT-34, pp. 1294-1307, Dec. 1986.

[20] 3GPP Specification TS 25.141, Base Station Conformance Testing (FDD).

CHAPTER 5

5.1 Conclusion

In this work a modified physics based large signal FET model was developed to include the nonlinear source resistance effect and RF channel breakdown. Both effects were found to be the main factors that limit device's RF performance at large signal condition. Especially nonlinear source resistance is becoming significant even at modest signal condition. The modified model has been verified by comparing with the measured data. The impact of these physical mechanisms on devices RF performance is shown in simulation by changing the breakdown voltage and threshold current value for SCL effect.

Both channel breakdown and gate breakdown exist in AlGaN/GaN HFET devices. The conducting channel is separated from the gate surface by AlGaN buffer layer. The higher critical field for gate breakdown determines that RF channel breakdown dominates the breakdown process and contributes most in limiting AlGaN/GaN HFET devices performance.

It has been proved in the work that the nonlinear source resistance limits the device's gain and linearity by suppressing the extrinsic transcondutance, the maximum drain current, and affecting the bell shape of gm and Cgs. Nonlinear source resistance originates from space-charge limited current (SCL) effects when the conduction current reaches the threshold current value. The lack of background doping and high current operation make this effect very important to AlGaN/GaN power amplifier. The nonlinear source resistance value is doubled or tripled even at modest power drive condition. It limits devices gain, output power, and also linearity performance.

The physics based model was improved by adding multi-tone and wide band signal simulation capability. With this feature, detail analysis of the impact of nonlinear source resistance on the device's linearity has been performed. Nonlinearity parameters including IMD, AM-PM conversion, and ACPR are calculated.

Nonlinear source resistance impacts the device's linearity performance through both amplitude and phase distortion mechanisms. Theoretical analysis of phase distortion has shown that nonlinear source resistance introduces AM-PM conversion by adding an extra phase variation at the output.

For the calibrated 2.14GHz class-AB amplifier, both RF performance and linearity, including IMD behavior and ACPR parameter, were improved by minimization of nonlinear source resistance effect either through decreasing the Lgs spacing or increasing the threshold current level for SCL effect.

5.2 Future work

As reliability has been a major issue for AlGaN/GaN HFET power amplifier, Researchers have put much effort in improving device reliability in order to move them into the commercial sector. The physics based model provides a good opportunity to study the physical mechanism and help save the cost and time to optimize device design for better reliability performance. Therefore it is beneficial to complete the physics based model by adding the surface hopping conduction mechanism based on the gate tunneling model that already exists.

The current physics based model was based on MESFET behavior. Specific model that describes the hetero-junction structure and physical features for AlGaN/GaN HFET devices are yet to be set up. Some features such as 2DEG and polarization field coming from AlGaN/GaN materials polarization charges need to be included in order to completely describe the device. The calculated electric field and potential distribution in the channel from the new model should be more accurate than the current model, which would provide more insight into the device operation principles.

APPENDICES

APPENDIX A

Derivation of Power Amplifier Extrinsic Transconductance With Source Resistance Modulation

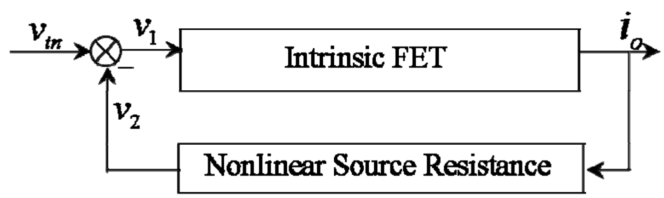

Fig. A.1 Transfer Function Flow Chart of HFET with Nonlinear Source Resistance.

i_o and v_2 can be expressed in polynomial format:

$$i_o = g_{mi1} v_1 + g_{mi2} v_1^2 + g_{mi3} v_1^3 + \ldots \qquad \text{(A.1)}$$

$$v_2 = r_1 i_o + r_2 i_o^2 + r_3 i_o^3 + \ldots \qquad \text{(A.2)}$$

and v_1 follows that:

$$v_1 = v_{in} - v_2 \qquad \text{(A.3)}$$

Where

$$g_{mi1} = \frac{\partial i_o}{\partial V_{gs}}, g_{mi2} = \frac{1}{2}\frac{\partial^2 i_o}{\partial V_{gs}{}^2}, g_{mi3} = \frac{1}{6}\frac{\partial^3 i_o}{\partial V_{gs}{}^3}, \ldots$$

And

$$r_1 = \frac{\partial v_r}{\partial i_r}, r_2 = \frac{1}{2}\frac{\partial^2 v_r}{\partial {i_r}^2}, r_3 = \frac{1}{6}\frac{\partial^3 v_r}{\partial {i_r}^3}, ... \tag{A.4}$$

Where v_r and i_r are voltage and current across the nonlinear source resistance, and

$$Rs = \frac{v_r}{i_r} = \frac{r_{ss}}{1 - \frac{I}{I_{sc}}}$$

And $r_1 = \frac{r_{ss}}{(1-\frac{I}{I_{sc}})^2}, r_2 = \frac{2r_{ss}}{(1-\frac{I}{I_{sc}})^3}\cdot\frac{1}{I_{sc}}, r_3 = \frac{6r_{ss}}{(1-\frac{I}{I_{sc}})^4}\cdot\frac{1}{I_{sc}^2}, ...$

The final expression for i_o is:

$$i_o = g_{mext1}v_{in} + g_{mext2}v_{in}^2 + g_{mext3}v_{in}^3 + ... \tag{A.5}$$

Substituting (A.3) and (A.4) into (A.2),

$$\begin{aligned} i_o &= g_{mi1}(v_{in} - v_2) + g_{mi2}(v_{in} - v_2)^2 + g_{mi3}(v_{in} - v_2)^3 + ... \\ &= g_{mi1}(v_{in} - r_1 i_o - r_2 i_o^2 - r_3 i_o^3 - ...) + g_{mi2}(v_{in} - r_1 i_o - r_2 i_o^2 - r_3 i_o^3 - ...)^2 \\ &\quad + g_{mi3}(v_{in} - r_1 i_o - r_2 i_o^2 - r_3 i_o^3 - ...)^3 + ... \end{aligned} \tag{A.6}$$

Compare items in (A.5) and (A.6) with same order:

1st order:

$$g_{mext1}v_{in} = g_{mi1}(v_{in} - v_2) = g_{mi1}(v_{in} - r_1 g_{mext1} v_{in})$$

$$g_{mext1} = g_{mi1} - g_{mi1} r_1 g_{mext1} \quad \Rightarrow \quad g_{mext1} = \frac{g_{mi1}}{1 + g_{mi1} r_1} \tag{A.7}$$

2nd order:

$$g_{mext2} v_{in}^2 = g_{mi1}(v_{in} - v_2) + g_{mi2}(v_{in} - v_2)^2 \quad \Rightarrow$$

$$g_{mext2} v_{in}^2 = g_{mi1}(v_{in} - r_1 g_{mext1} v_{in} - r_1 g_{mext2} v_{in}^2 - r_2 g_{mext1}^2 v_{in}^2)$$

$$+ g_{mi2}(v_{in} - r_1 g_{mext1} v_{in} - r_1 g_{mext2} v_{in}^2 - r_2 g_{mext1}^2 v_{in}^2)^2$$

It follows that:

$$g_{mext2} = g_{mi2} - g_{mi1} r_1 g_{mext2} - g_{mi1} r_2 g_{mext1}^2 + g_{mi2} r_1^2 g_{mext1}^2 - 2 g_{mi2} r_1 g_{mext1}$$

$\Rightarrow$

$$g_{mext2} = \frac{g_{mi2} r_1^2 g_{mext1}^2}{1 + g_{mi1} r_1} - \frac{g_{mi1} r_2 g_{mext1}^2}{1 + g_{mi1} r_1} + \frac{g_{mi2}}{1 + g_{mi1} r_1} - \frac{2 g_{mi2} r_1 g_{mext1}}{1 + g_{mi1} r_1}$$

$$= \frac{g_{mi2} r_1^2 g_{mi1}^2}{(1 + g_{mi1} r_1)^3} - \frac{g_{mi1}^3 r_2}{(1 + g_{mi1} r_1)^3} + \frac{g_{mi2}}{1 + g_{mi1} r_1} - \frac{2 g_{mi1} r_1 g_{mi2}}{(1 + g_{mi1} r_1)^2}$$

$$= \frac{g_{mi1}^2 g_{mi2} r_1^2 - g_{mi1}^3 r_2 + g_{mi2} + 2 g_{mi1} g_{mi2} r_1 + g_{mi1}^2 g_{mi2} r_1^2}{(1 + g_{mi1} r_1)^3}$$

$$- \frac{2 g_{mi1} g_{mi2} r_1 + 2 g_{mi1}^2 g_{mi2} r_1^2}{(1 + g_{mi1} r_1)^3}$$

$$= \frac{- g_{mi1}^3 r_2 + g_{mi2}}{(1 + g_{mi1} r_1)^3}$$

$$= \frac{g_{mi2}}{(1 + g_{mi1} r_1)^3} - \frac{g_{mi1}^3 r_2}{(1 + g_{mi1} r_1)^3}$$

And g_{mext2} can be written as:

$$g_{mext2} = \frac{g_{mi2}}{(1 + g_{mi1} r_1)^3} - \frac{g_{mi1}^3 r_2}{(1 + g_{mi1} r_1)^3} \tag{A.8}$$

3rd order:

$$g_{mext3}v_{in}^3 = g_{mi1}(v_{in} - v_2) + g_{mi2}(v_{in} - v_2)^2 + g_{mi3}(v_{in} - v_2)^3$$

$\Rightarrow$

$$g_{mext3}v_{in}^3 = g_{mi1}[v_{in} - r_1(g_{mext1}v_{in} + g_{mext2}v_{in}^2 + g_{mext3}v_{in}^3)$$

$$- r_2(g_{mext1}v_{in} + g_{mext2}v_{in}^2)^2 - r_3 g_{mext1}^3 v_{in}^3] + g_{mi2}[(1 - r_1 g_{mext1})v_{in}$$

$$- (r_1 g_{mext2} + r_2 g_{mext1}^2)v_{in}^2]^2 + g_{mi3}(v_{in} - r_1 g_{mext1} v_{in})^3$$

$\Rightarrow$

$$g_{mext3}v_{in}^3 = g_{mi1}(-r_1 g_{mext3} - 2r_2 g_{mext1} g_{mext2} - r_3 g_{mext1}^3)v_{in}^3$$

$$- 2g_{mi2}(1 - r_1 g_{mext1})(r_1 g_{mext2} + r_2 g_{mext1}^2)v_{in}^3 + g_{mi3}(1 - r_1 g_{mext1})^3 v_{in}^3$$

$\Rightarrow$

$$g_{mext3} = -g_{mi1}g_{mext3}r_1 - 2g_{mi1}g_{mext1}g_{mext2}r_2 - g_{mi1}g_{mext1}^3 r_3 - 2g_{mi2}g_{mext2}r_1$$

$$+ 2g_{mi2}g_{mext1}g_{mext2}r_1^2 - 2g_{mi2}g_{mext1}^2 r_2 + 2g_{mi2}g_{mext1}^3 r_1 r_2 + g_{mi3}$$

$$- g_{mi3}g_{mext1}^3 r_1^3 + 3g_{mi3}g_{mext1}^2 r_1^2 - 3g_{mi3}g_{mext1}r_1$$

$\Rightarrow$

$$g_{mext3} = \frac{g_{mi3} - 3g_{mi3}g_{mext1}r_1 + (3g_{mi3}r_1^2 - 2g_{mi2}r_2)g_{mext1}^2 - 2g_{mi2}g_{mext2}r_1}{1 + g_{mi1}r_1}$$

$$- \frac{(g_{mi1}r_3 + g_{mi3}r_1^3 - 2g_{mi2}r_1 r_2)g_{mext1}^3 + 2(g_{mi2}r_1^2 - g_{mi1}r_2)g_{mext1}g_{mext2}}{1 + g_{mi1}r_1}$$

Substitute g_{mext1} and g_{mext2} into above equation:

$\Rightarrow$

$$g_{mext3} = \frac{g_{mi3}}{1+g_{mi1}r_1} - \frac{3g_{mi1}g_{mi3}r_1}{(1+g_{mi1}r_1)^2} + \frac{3g_{mi1}^2 g_{mi3}r_1^2 - 2g_{mi1}^2 g_{mi2}r_2}{(1+g_{mi1}r_1)^3}$$

$$- \frac{2g_{mi2}r_1(g_{mi2} - g_{mi1}^3 r_2)}{(1+g_{mi1}r_1)^4} - \frac{(g_{mi1}r_3 + g_{mi3}r_1^3 - 2g_{mi2}r_1r_2)g_{mi1}^3}{(1+g_{mi1}r_1)^4}$$

$$+ \frac{2(g_{mi2}r_1^2 - g_{mi1}r_2)g_{mi1}(g_{mi2} - g_{mi1}^3 r_2)}{(1+g_{mi1}r_1)^5}$$

$\Rightarrow$

$$g_{mext3} = \frac{g_{mi3}}{(1+g_{mi1}r_1)^4} - \frac{g_{mi1}^4 r_3}{(1+g_{mi1}r_1)^4} + \frac{2g_{mi1}^5 r_2^2 - 2g_{mi2}^2 r_1 - 4g_{mi1}^2 g_{mi2} r_2}{(1+g_{mi1}r_1)^5}$$

If we assume the 2nd order interaction term is very small, then:

$$g_{mext3} = \frac{g_{mi3}}{(1+g_{mi1}r_1)^4} - \frac{g_{mi1}^4 r_3}{(1+g_{mi1}r_1)^4} \tag{A.9}$$

Therefore the extrinsic transconductance for up to 3rd order are:

$$g_{mext1} = \frac{g_{mi1}}{1+g_{mi1}r_1}$$

$$g_{mext2} = \frac{g_{mi2}}{(1+g_{mi1}r_1)^3} - \frac{g_{mi1}^3 r_2}{(1+g_{mi1}r_1)^3}$$

$$g_{mext3} \cong \frac{g_{mi3}}{(1+g_{mi1}r_1)^4} - \frac{g_{mi1}^4 r_3}{(1+g_{mi1}r_1)^4}$$

APPENDIX B

Power Amplifier Phase Distortion With

Source Resistance Modulation

v_{gs}, v_i, and i_{out} in Fig. 4.13 can be expressed as:

$$v_{in} = A\cos(\omega t + \theta + \beta) \tag{B.1}$$

$$v_{gs} = B\cos(\omega t + \theta) \tag{B.2}$$

$$i_{out} = C\cos(\omega t + \theta + \varphi) \tag{B.3}$$

Substitute (B.2) and (B.3) into

$$v_{in} = v_{gs} - i_{out} \cdot R_s \tag{B.4}$$

Rearrange (B.4) as:

$$v_{in} = B\cos(\omega t + \theta) - C\cos(\omega t + \theta + \varphi) \cdot R_s$$

$$= B\cos(\omega t + \theta) - R_s C\cos(\omega t + \theta)\cos\varphi + R_s C\sin(\omega t + \theta)\sin\varphi$$

$$= (B - R_s C\cos\varphi)\cos(\omega t + \theta) + R_s C\sin\varphi\sin(\omega t + \theta)$$

$$= A\cos(\omega t + \theta + \beta)$$

Compare the above result with v_{in} in (B.1), it follows that:

$$A = \sqrt{R_s{}^2 C^2 \sin^2\varphi + (B - R_s C\cos\varphi)^2} = \sqrt{R_s{}^2 C^2 + B^2 - 2R_s BC\cos\varphi} \tag{B.5}$$

$$\beta = \arctan\frac{-R_s C\sin\varphi}{B - R_s C\cos\varphi} = -\arctan\frac{G_{mi} R_s \sin\varphi}{1 - G_{mi} R_s \cos\varphi}$$

Where

$G_{mi} = \frac{C}{B}$, represents the AM-AM characteristic for the intrinsic FET.

It is straight forward that:

$$\tan\beta = -\frac{G_{mi} R_s \sin\varphi}{1 - G_{mi} R_s \cos\varphi} \tag{B.6}$$

The extrinsic phase distortion is $\varphi' = \varphi - \beta$, and it can be expressed as:

$$\tan(\varphi - \beta) = \frac{\sin\varphi\cos\beta - \cos\varphi\sin\beta}{\cos\varphi\cos\beta + \sin\varphi\sin\beta} = \frac{\sin\varphi - \cos\varphi\tan\beta}{\cos\varphi + \sin\varphi\tan\beta} \tag{B.7}$$

Substitute (B.6) into (B.7):

$$\tan(\varphi - \beta) = \frac{\sin\varphi}{\cos\varphi + R_s G_{mi}} \tag{B.8}$$

Therefore

$$\varphi' = \arctan\frac{\sin\varphi}{\cos\varphi - G_{mi} R_s} \tag{B.9}$$